INFORMATION TO USERS

This manuscript has been reproduced from the microfilm master. UMI films the text directly from the original or copy submitted. Thus, some thesis and dissertation copies are in typewriter face, while others may be from any type of computer printer.

The quality of this reproduction is dependent upon the quality of the copy submitted. Broken or indistinct print, colored or poor quality illustrations and photographs, print bleedthrough, substandard margins, and improper alignment can adversely affect reproduction.

In the unlikely event that the author did not send UMI a complete manuscript and there are missing pages, these will be noted. Also, if unauthorized copyright material had to be removed, a note will indicate the deletion.

Oversize materials (e.g., maps, drawings, charts) are reproduced by sectioning the original, beginning at the upper left-hand corner and continuing from left to right in equal sections with small overlaps.

Photographs included in the original manuscript have been reproduced xerographically in this copy. Higher quality 6" x 9" black and white photographic prints are available for any photographs or illustrations appearing in this copy for an additional charge. Contact UMI directly to order.

Bell & Howell Information and Learning
300 North Zeeb Road, Ann Arbor, MI 48106-1346 USA

UMI®
800-521-0600

In-situ cure monitoring and characterization of Graphite/Epoxy composites using fiber optics and ultrasonics

Jianyin Chen

A Thesis

in

The Department

of

Mechanical Engineering

Submitted in Partial Fulfillment of the Requirements

for the Degree of Doctor of Philosophy at

Concordia University

Montreal, Quebec, CANADA

February 1998

ABSTRACT

In-Situ Cure Monitoring and Characterization of Graphite/Epoxy Composites Using Fiber Optics and Ultrasonics

Jianyin Chen, Ph.D.
Concordia University, 1998

Advanced composites can be fabricated by laminating multiple plies into the desired shape, and then cured in an autoclave with simultaneous application of proper heat and pressure. The knowledge of the cure process is very important in order to obtain fully cured and high-quality composites. *In-situ* sensors capable of monitoring the change of physical and chemical properties during the cure process are therefore desirable. The major aspects of research in this thesis are as follows:

The chemical kinetic and rheological properties of AS4/3501-6 Graphite/Epoxy composites are characterized by using Differential Scanning Calorimetry and Dynamic Mechanical Analyzer. This indicates that at 176°C, the cure reaction is almost fully completed after 60 minutes, and increasing cure temperature results in a noticeable decrease in loss tan δ and a profound increase in the T_g. Ultrasonic characterization shows that the moduli of 3501-6 epoxy increase with increasing cure temperature, whereas the moduli of AS4/3501-6 composite reach their maximum around 176°C. Also, the moduli of the composite increase with increasing cure time, whereas the moduli of the epoxy, after being cured at 176°C for 80 minutes, exhibit no change.

A state-of-the-art fiber-optic and ultrasonic cure processing monitoring system is developed, which consists of ultrasonic transducers with clad buffer rods, Extrinsic Fabry-Perot Interferometric fiber-optic sensors, and a special autoclave feedthrough. This system is workable in an autoclave at high temperature and gas pressure, has high ultrasonic signal to spurious noise ratio, and is suited for longitudinal and/or shear wave measurement. The

development of properties of the curing AS4/3501-6 composite is monitored by using *in-situ* fiber-optic and/or ultrasonic sensors, indicating that (1) both sensors can sense the gelation period; (2) the ultrasonic sensor is able to determine the end-of-cure, while the fiber-optic sensor is not; (3) during the cool-down period the development of thermal mismatch strains between the mold plates and the composite panel, prior to and after the detachment, can be detected by the fiber-optic sensor.

ACKNOWLEDGEMENTS

I would first like to express my sincere gratitude to my thesis supervisor, Dr. S. V. Hoa, for his interest and support which made my Ph.D. study at the Concordia Center for Composites possible. It was he who brought me into the cutting edge of composite materials and processing. His close supervision, numerous discussions and critical comments made my thesis research a success.

My special gratitude is expressed to my thesis co-supervisor Dr. C.-K. Jen at Industrial Materials Institute, National Research Council of Canada (IMI, NRC) for his guidance in every stage of my thesis research at IMI. His valuable suggestions and consistent encouragement have been crucial for my successful research. I will always be indebted to him for what I have learned from him, not only concerning science and research but also in regards to dedication and perseverance.

My special appreciation is also given to Dr. J.-P. Monchalin at IMI. It was he who provided me this wonderful opportunity to access facilities at IMI. The experience I have obtained there has constituted important and indispensable parts of my industrial R & D background, which will be greatly beneficial to my future career.

My special thanks are also paid to my Chinese supervisors Dr. Wei-Zang Chien at Shanghai University of Technology, Shanghai and Dr. Qian Huang at State Educational Committee of China, Beijing for their constant guidance and encouragement during my Ph.D. study in China. It was they who taught me solid state mechanics, which was very helpful to my later study at Concordia. It was also they who made great efforts to send me to Canada. Even when I was studying at Concordia, they still gave me a lot of research advice and personal help. I will be forever grateful for their kindness.

Many thanks are given to Dr. H. Wang at IMI for his fruitful discussions concerning fiber-optic experiments; Drs. M. Viens and D. Levesque at IMI for their useful discussions concerning ultrasonic anisotropic and attenuation characterization; Mr. H. Herbert at IMI for his laboratory technical assistance; Dr. X. Xiao at the Concordia Center for Composites for her teaching in operating the DMA instrument; Ms. D. Banu at the Center for Building Studies of Concordia University for her assistance in DSC measurements; Dr. N.N. Hsu at the Ultrasonics Group, National Institute of Standards and Technology, Gaithersburg, MD, for providing the PVDF line-focus-beam transducer; and FISO Technologies Inc., Quebec City, PQ, for loaning the WFS-100 fiber-optic sensor system, respectively.

I would like to thank my colleagues and friends, Dr. G.-L. Qian, Dr. X.-X. Xia, Ms. L. Li, Mr. P. Ouellette, Dr. M. El-Karmalawy, Dr. M. Xia (Concordia University), Mr. L. Wen and Mr. B. Wen (McGill University) for their cooperation and friendship during the course of my experimental research.

Finally, I am deeply indebted to my wife Ms. Lijie Mei for her love, patience and sacrifice throughout my experimental research.

This research was partially supported by the National Sciences and Engineering Research Council of Canada (NSERC) from an operating and a strategy (STR0192858) grant, and a Concordia Graduate Student Fellowship. Special appreciation is given to IMI, NRC where part of the thesis research has been carried out.

DEDICATION

To My Parents

TABLE OF CONTENTS

LIST OF FIGURES

LIST OF TABLES

Chapter 1

INTRODUCTION

As Graphite/Epoxy (Gr/Ep) composite materials are increasingly being used as engineering materials in aircraft, buildings, containers, and other structures, the high costs associated with manual fabrication techniques such as laying up the prepregs make the resulting structural components expensive. Even though advantages such as high strength over weight ratio and geometrically tailored mechanical properties outweigh these high costs for many critical applications, a reduction in the cost of manufacturing is always desired and would expand their further applications [1-4]. Moreover, as structural designs become more complex and material requirements for improved performance increase, *in-situ* process monitoring and control during fabrication is highly desirable.

The mechanical properties of composites are largely dependent upon the chemical and rheological events taking place during the manufacturing process [5-9]. Although materials suppliers provide a standard recommended cure procedure for their particular prepregs, fabrication still requires a certain degree of 'trial and error' to produce high-quality composites, owing to the varying geometries of the structures and thermal properties of autoclaves and pressing tools. Information such as temperature, pressure, viscosity, degree of cure, resin flow, void and the formation of residual stresses inside the material itself needs to be quantified as a function of time and position within the laminate during the cure.

1.1 Fabrication and cure processing of polymer composites

In most load-bearing engineering applications, advanced composites are used in the form of laminates which consist of individual layers of various composite materials or laminae. Reinforcing fibers are typically graphite and glass [1-2,10-12]. Composite materials can be built by stacking plies of reinforcing layers at varying angles through the thickness of the material. When heat and pressure are applied, the composite is consolidated to produce a laminated structure of low density containing a volume fraction of fiber of about 60% [10-12].

A variety of techniques can be used to fabricate composites [2,10,13-15]. For example, composites can be molded by hot press or vacuum bag autoclave techniques to produce components of the required shape. Resin can be also injected into a preform of reinforcement held in a mold, as in resin transfer molding. In addition, pultrusion or filament winding can be used to fabricate tubes of hollow cross-section.

Autoclave molding is used extensively, especially by the aerospace industry, to produce high-quality laminates of higher density and lower void content than those produced by many other techniques [3, 5-7]. Typically, a component, once laid up on a mold, is enclosed in a flexible bag tailored approximately to the desired shape. This whole assembly is then laid in an autoclave, a pressure vessel designed to contain gas at elevated temperature. The bag is firstly evacuated, to remove trapped air and vapors from the composite, and then the chamber is pressurized to provide additional consolidation during the cure [7,16].

During the heating cycle the viscosity of the composite resin changes [7,17]. As the temperature rises, an initial fall is recorded followed by an increase as chemically induced crosslinking occurs. The time and temperature at which the consolidating pressure is applied are critical to ensure adequate inter-fiber flow of resin. The resin and hardener often react exothermically. Care must be taken to ensure the optimal process conditions, which are designed to avoid excessive temperature rise, especially in thick sections. Such deviations from the optimum cure schedule can lead to laminates with

undesirable levels of built-in stresses, due to differences in fiber and matrix thermal expansion coefficients as the composite is cooled down after the cure [7,18-21].

Indeed, the curing process is complex involving the control of many varying parameters and careful optimization to ensure a correct, uniform state of cure and consolidation throughout a component. Improvements in the composite cure cycle can shorten fabrication time, reduce its operational cost and enhance the quality of the end product. Current practice relies on temperature and pressure sensors to establish process conditions. This approach often requires much effort in adjusting different parameters to arrive at a desired cure cycle. It is a time-consuming and costly procedure for the fabrication of advanced composites, whose performance requirements are becoming increasingly stringent. Analytic models developed for autoclave curing could provide information on the "optimal" processing conditions [5,6,18-24]; however, their application is limited to certain geometrical shapes. Furthermore, these models often require extensive material data which are difficult to measure. Therefore, the development of sensors for monitoring cure state, to determine the degree of cure of a thermoset resin throughout the composite matrix, may lead to an optimal process procedure. The knowledge of the process and time when the resin is fully crosslinked may further enable the use of adaptive cure control to improve the composite qualities and to reduce manufacturing costs.

1.2 Sensor development and cure monitoring

Currently, very few sensors and techniques have successfully monitored and provided crucial information such as the end-of-cure during the entire cure cycle of composites in an autoclave. Traditional thermal analysis, like the Differential Scanning Calorimetry (DSC) or Dynamic Mechanical Analyzer (DMA), can be used to characterize the extent of cure chemistry and viscoelasticity of composite resins. It is understood that DSC measures heat flow in a polymer as a function of temperature or time [17, 25-26]. This technique may be used to determine degree of cure and characteristic temperatures for polymer melting, crystallization and glass transition, and to study cure kinetics and

monitor the onset of gelation[1] and vitrification[2] in the composite resin. However, it is not practical for direct usage as a real-time sensor in an autoclave during composite processing. DMA is a method which can measure the degree of a polymer responding to an applied periodic stress as a function of temperature [27-30]. It is normally employed to measure key rheological parameters such as loss tangent, storage and loss moduli, viscosity, and glass transition temperature. This approach cannot be used for *in-situ* cure monitoring because it is, in nature, destructive. In addition, both methods impose constraints in sample geometry and dimensions which prevent them from being effective when applied to composite manufacturing.

On the other hand, dielectrometric analysis, which measures the permittivity and loss factor of the composites [24,31-36], has been successfully used to determine the time at which viscosity is minimum, and the time at which the cure is completed. Dielectric measurements for cure monitoring are normally carried out with sinusoidal excitations at specific radio frequencies. By applying a step-change voltage across the material, the resulting current waveform is obtained. The frequency-dependent dielectric properties can therefore be derived from the Fourier transform of the current waveform [24]. The drawbacks of dielectric analysis include its empirical nature and inadequate correlation between dielectric properties and other material characteristics such as mechanical properties [36]. Furthermore, dielectric sensors are intrusive, and remain part of the composite structure at the completion of cure.

---

[1] Gelation corresponds to a transition from linear or branched molecules to an infinite network of chains. At gel point, a three-dimensional network of chains with a particular infinite molecular weight (gel) is formed. After gelation, more molecular chains will be incorporated into the cross-linked network at the expense of the soluble portion (sol) [24].

[2] Vitrification represents a transition from a rubbery to a glass state. As curing proceeds, the glass transition temperature of the growing chains increases as the network molecular weight increases. Should the cure temperature at any point becomes lower than the glass transition temperature of the growing polymer chains, chain mobility becomes severely restricted, and further conversion to the network structure is limited. The resin is said to be vitrified, and its glass transition temperature coincides with the maximum cure temperature achieved [24].

Recently, increasing interest in 'smart' composites has led to the development of embedded waveguide sensor technology, by which cure properties and characteristics are monitored either intrinsically (*i.e.* the measurement directly modulates the signal in the waveguide) or extrinsically (the waveguide acts as a medium for transporting energy to and from a discrete sensing point) [37]. Several techniques have been developed for *in-situ* monitoring of cure states, cure kinetics, resin viscosity and residual stress build-up during the manufacture of composite laminates [38-47]. For example, fiber-optic sensing for cure *via* refractive index was developed because of the fact that the refractive index of uncured resin increased as the crosslinking reaction took place, and this could have a profound effect on the signal of the optical fiber sensor [41]. Another approach used Extrinsic Fabry-Perot Interferometeric (EFPI) fiber-optic sensors to monitor the state of cure of composite material by detecting local strain changes caused by process-induced strains [40], the phase lag caused by local dynamic excitation [42], or the refractive index caused by the degree of cure [44]. After the cure, the sensor may still be operated as a conventional EFPI strain sensor. In addition, Fourier Transform Infrared (FTIR) spectroscopy has been demonstrated for cure measurement [45]. In this approach, an FTIR spectrometer was used to analyze the output of a fluoride or chalcogenide infrared fiber embedded in the curing epoxy matrix [45].

Normally, a prerequisite for any *in-situ* sensor is that it must not be detrimental to the operational requirements of the structure. Optical fiber-based measurement techniques are suitable for *in-situ* cure monitoring, because they can be incorporated into the component during the manufacturing process, for example, in prepregs. Meanwhile, the dimensions and orientation of the optical fibers within the prepregs can be selected to have a minimal impact on mechanical properties of the composites [48]. Furthermore, fiber-optic sensors may be a practical way for *in-situ* monitoring of polymers and composites processing, because the light path can be extended outside of the instrument. Light is carried from the instrument to the point of measurement through optical fibers. The sensors at the end of the fiber experience the process conditions, whereas the instrument is located some distance away in a more protected area. This arrangement allows direct measurements even under extreme processing conditions (*e.g.*, high

temperatures and pressures) [24]. Furthermore, the advantage of fiber-optic sensor technology, compared with other cure monitoring techniques such as dielectric analysis, is its low susceptibility to electromagnetic interference and electrical insulation [38, 43]. Techniques based on embedded fiber-optic sensors have been shown to possess a clear potential for further monitoring the structural integrity of the composite during part qualification and throughout its service life.

However, using fiber-optic sensors to monitor the state of cure is expensive, and the sensors may not be repairable or reusable. Moreover, due to the fragility of the fiber optic sensors, when they are fed through an autoclave, damage often occurs to the sensors [49]. As a compromise, the curing process is sometime studied in a platen-heated press in lieu of an autoclave [49]. Thus whether the experimental results can be applied to a practical autoclave processing environment is questionable.

Recently ultrasonic techniques have shown great promise for effective *in-situ*, real-time cure monitoring of composite materials [50-61]. Ultrasonic waves as a means to monitor and characterize the curing of polymers was described by Sofer and Hauser in 1952 [50]. Significant changes in attenuation and velocity of longitudinal ultrasonic waves took place when the thermosetting resins gelled and cured. Ultrasonic attenuation can be related to the viscosity of the material, a critical physical parameter in the control of the curing composites. Papadakis [51] used ultrasonic methods to measure the elastic moduli of polymers during the solidification process. Lindrose [52] found that the shear and bulk relaxation moduli changed during the cure. Rokhlin *et al.* [53] studied the real-time frequency dependence of attenuation and velocity of ultrasonic waves during the curing of epoxy resin. He also investigated temperature effects on the velocity and attenuation of longitudinal waves at different stages of the cure reaction of thermosetting resins. Green *et al.* [54] monitored cure processing by using resonant ultrasound spectroscopy. In his investigation, differences in amplitude, frequency and damping were related to the degree of curing of the composite; however, the determination of 'end-of-cure' was not reported. Achenbach *et al.* [43] used a fiber-optic ultrasonic system to monitor the curing of an epoxy resin, in which ultrasound was generated using a high-

power optical fiber to deliver high-energy optical pulses, and detected by local fiber optic ultrasound sensors embedded in the curing epoxy resin. A model consisting of springs and dashpots was proposed by Hahn [62] to explain the experimental data on wave speed and attenuation of ultrasonic waves during the cure.

When compared with other sensors like dielectric and fiber optic sensors, the ultrasonic approach has at least two advantages. Firstly, the ultrasonic sensor is not embedded into the composite part. This makes the sensor both reusable and very unlikely to affect the part due to its presence. Secondly, it produces a measurement which is an average over the thickness of the part, while other techniques generally produce a measure of the state-of-cure in a very small area near the sensor. However, the difficulties of ultrasonic techniques are due to the facts that: (1) the commonly used broadband and high-efficiency piezoelectric ultrasonic transducers (UTs) can only be operated continuously at a temperature of less than 60°C. This limitation presents difficulties when applying the techniques in actual processing environments which have, such as for AS4/3501-6 Gr/Ep composite curing, a temperature of 176°C; (2) the gel type ultrasonic couplant is degraded when operated at high temperature [48].

The introduction of an ultrasonic buffer rod between UT and monitored material could be a good alternative to avoid exposing the UT to adverse conditions [63-66]. However, one concern with a long buffer rod is the presence of spurious signals due to wave diffraction and the finite rod diameter. These signals always arrive later than directly transmitted or reflected echoes. Such echoes are unwanted because of their possible interference with the desired signals from the sample. Jen and his co-workers [67-71] have studied many kinds of ultrasonic buffer rods. They recently found that clad metallic buffer rods [72-74] fabricated by a thermal spray method have excellent waveguide performance, making many on-line processing monitoring applications feasible [75-77]. This provides a great opportunity to do *in-situ* ultrasonic cure monitoring at high temperature in an autoclave.

1.3 Objective of the present work

In the case of advanced composite components, a recent estimate indicates that approximately 80% [38] of the finished cost is taken up in the fabrication process, thus this area is clearly targeted for cost reduction.

The objectives of the experimental research in this thesis are to characterize the processed AS4/3501-6 Gr/Ep composites by using thermal and ultrasonic analyses, and try to correlate the material properties (degree of cure, glass transition temperature, damping factor and moduli, *etc.*) to the process parameters (cure temperature and cure time, *etc.*) in order to seek the most sensitive parameters which may be used later for controlling material processing.

Furthermore, *in-situ* cure monitoring of composite process in an autoclave will be studied using EFPI fiber-optic and/or ultrasonic sensors. The suitability of these sensors for *in-situ* cure monitoring will be also evaluated. This experimental research will be carried out to explore how the properties of Gr/Ep composites develop as the cure process progresses. This helps to understand the cure process and to achieve the goal of controlling it.

1.4 Contents of the thesis

Hercules AS4/3501-6 prepregs are selected for our present study, because of their usefulness in the aerospace industry and the availability of many published material data. Therefore, it is possible to make comparison with other researchers' work.

It is understood that the ultimate mechanical properties of the composites are largely dependent upon chemical and rheological events taking place during the manufacturing process. In Chapter 2, thermal analysis will be used to characterize the chemical and rheological behavior of uncured and processed Hercules 3501-6 epoxies and AS4/3501-6 composite panels. From isothermal DSC measurements, the kinetic equations, *e.g.* the development of the degree of cure with respect to cure temperature and time, can be obtained, while from dynamic DSC measurements, the final degree of cure

of the epoxies and composites processed by different cure conditions can be evaluated. Moreover, DMA tests will be carried out to characterize the viscoelastic properties of the processed epoxies and composites by measuring their complex modulus E*, loss tan δ and glass transition temperature T_g. These thermal rheological evaluations will clearly reveal profound effects of the cure conditions on material properties.

The evaluation of mechanical properties of composites fabricated by different cure processes is of importance because the curing parameters may have significant effects on the status-of-cure of the ensuing composite. Numerous efforts have already been made to characterize these effects. For example, Springer *et al.* [78] attempted to correlate the longitudinal and shear moduli of T300/976 laminates with their degrees of cure, which ranged from 0.6 to 0.96. Unfortunately, because of the large error bar introduced in their measurements, the observation of the corresponding relations in their experimental scatter data was difficult.

Ultrasonic techniques can be used for characterizing the elastic properties of a composite by measuring the phase or group velocities of elastic waves which propagate in various directions [79-97]. For composites which are anisotropic materials, one usually deals with a laminated thin plate structure. This means that in-plane properties are difficult to obtain, although through-thickness properties can be readily measured. One approach is to obtain large samples of cube-shaped material, and measure the ultrasonic wave speeds in specific directions [98]. Analytical formulas, derived from the solutions of Christoffel's equation [85], are then used to recover all elastic constants of the composite. This technique can be very accurate, especially for measuring shear properties, but requires a relatively large and thick specimen, and is destructive in nature. Alternatively, plate waves of known modes may be generated in a composite to obtain a measure of the in-plane properties [92,93]. A third approach relies upon mode conversion and multiple incidence angles to generate and receive the desired waves [79, 82-84]. In this thesis research, the water immersion method to measure elastic constants of the composite is preferred, because of the availability of ultrasonic facilities at our laboratory. Group velocities of quasi-longitudinal (QL) and quasi-shear (QS) waves can be directly

measured and converted into the corresponding phase velocities. Elastic constants can then be restructured from Christoffel's equation by using the algorithm reported in [82]. Furthermore, the Line-Focus-Beam (LFB) method [99-101] is also proposed to evaluate the in-plane properties of the materials.

In addition, two of the most important ultrasonic parameters, the attenuation and velocity dispersion of ultrasonic waves, can also be used to characterize the viscoelastic properties of composites. Ultrasonic attenuation refers to the loss of the energy of the wave when it propagates through the medium, and velocity dispersion is the dependence of velocity upon the product of the frequency of the wave and the thickness of the composite. The ultrasonic attenuation may come from scattering by inhomogeneities in the medium (*e.g.* the presence of fibers in the epoxy matrix), and/or absorption in the epoxy matrix [102-107]. They are generally frequency-dependent and directly related to dispersion by the Kramers-Kronig relations [108,109]. Since the degree of cure of the composites is associated with their viscosity, the ultrasonic velocities and attenuation may be linked to the cure status. We anticipate that a quantitative evaluation of ultrasonic dispersion and attenuation may provide information on the state of cure of the materials.

The experimental work described in Chapter 3 is based on the study of Hercules 3501-6 epoxies and AS4/3501-6 Gr/Ep composites. Ultrasonic measurements will be performed on these samples in order to evaluate their engineering elastic moduli, through-thickness longitudinal wave dispersion, and through-thickness longitudinal wave attenuation. A sensitivity study will be carried out in an attempt to determine the ultrasonic parameters which are sensitive to cure processing. Such measures may thereafter be taken as controlling parameters during the course of material fabrication.

However, the above methods may provide only limited assurance to the quality of the fabricated composite laminates. The utilization of a non-destructive evaluation technique for real-time monitoring of the state-of-cure is highly desirable. The idea of being able to monitor a combination of both physical and chemical events taking place at

various locations inside an actual composite part during its manufacturing presents opportunities for increases in both quality control and component reliability.

We want to select a sensor, as an integral part of the manufacturing process, which can directly measure engineering parameters such as crosslinking reaction. Normally, the monitoring will provide the global property changes due to effects of cure temperature, time and pressure. Also characterization of mechanical property development during cure reveals information concerning the strength or stiffness of the composites. For instance, although a chemical characterization, such as DSC measurement of the composites, can assess the chemical or thermal stability of the materials, it does not accurately reflect the development of mechanical properties during the cure. Significant changes in the moduli may occur during the later stages of the cure, when the degree of cure is fully developed as indicated by DSC.

Two kinds of sensors will be used for *in-situ* monitoring of the development of the cure process: EFPI fiber-optic and ultrasonic sensors.

The EFPI fiber-optic sensors from FISO Technologies, Inc., Quebec City, PQ, are investigated in Chapter 4 as a potential candidate for *in-situ* cure monitoring of Gr/Ep composites in an autoclave. The merits of such fiber-optic strain gages are small size and high spatial resolution. These merits make the EFPI a suitable candidate for cure monitoring, because an embedded EFPI sensor may directly detect the evolution of process-induced strain in the material. In Gr/Ep composites, strains are caused by two sources: the chemical shrinkage of the epoxy during cure, and the thermal expansion or contraction of the fiber and matrix during the heat-up or cool-down. Therefore, the detected strain evolution could provide a non-destructive and real-time indication of the state of cure in the composite. Also, due to their small diameters, the fiber-optic strain gages can be embedded at different locations, between selected layers and along preferred directions in the laminate, so that quasi-distributed sensing may be achieved. Furthermore, the embedded sensors can be subsequently used as integrated sensors to monitor the load and health conditions of the structure when it is in service.

The ultrasonic technique provides mechanical property characterization of the material and is suitable for *in-situ*, non-destructive process monitoring. Variations in ultrasonic velocity (or time delay), attenuation and shear reflection coefficient may be correlated to variations in the elastic modulus, loss modulus, and viscosity of the curing composites.

In Chapter 5, *in-situ* cure monitoring will be carried out using ultrasonics. The ultrasonic sensing system is composed of high-performance 5 MHz broadband longitudinal or shear piezoelectric UTs, couplants, a novel clad buffer rod which is an ultrasonic waveguide, and an air cooling system. The air cooling system is to cool down the UTs to 60°C or less. A special feed-through will be fabricated to incorporate the electrical wires and cooling pipes into an autoclave, so that ultrasonic monitoring may be performed inside the autoclave. Because of the high performance of the present ultrasonic measurement system, a high signal-to-noise ratio (S/N) of ultrasonic longitudinal and shear signals can be obtained. The results obtained from the ultrasonic time-delay, attenuation and shear reflection coefficient should exhibit global information concerning the development of the composite material properties starting from gelation, *via* cure reaction, to cool-down stages. Also, simultaneous *in-situ* fiber-optic and ultrasonic cure monitoring will be performed to investigate the build-up of residual stresses during processing.

In Chapter 6, conclusions will be drawn based on thermal and ultrasonic characterization of the processed composites, and *in-situ* fiber-optic and ultrasonic process monitoring of the curing composites. Because much development is still required to transfer our current technology from the laboratory bench to the factory environment, future experimental research work will be proposed.

Chapter 2

THERMAL CHARACTERIZATION OF PROCESSED GRAPHITE/EPOXY COMPOSITES

One of the most important properties of polymer composites is their thermal behavior, in which some physical parameters of the materials are determined as a function of temperature. The knowledge of this behavior is essential not only for the selection of proper fabrication and processing conditions, but also for the characterization of the composite properties, and for the selection of appropriate end uses.

Differential Scanning Calorimetry (DSC) and Dynamic Mechanical Analyzer (DMA) tests are selected for this experimental research. DSC is used to determine some characteristic behavior such as the degree of cure α_{DOC}, and to study cure kinetics and monitor the onset of gelation and vitrification in the composite resin by measuring heat flow in the composite as a function of temperature or time. DMA is employed to measure key rheological parameters such as storage modulus E', loss modulus E", loss tan δ (=E"/E') and glass transition temperature T_g, by determining how the composite sample responds to an applied periodic stress as a function of temperature or frequency.

2.1 Fabrication and cure processing of AS4/3501-6 composites

2.1.1 Description of the materials

AS4/3501-6 Gr/Ep prepreg tape is selected for this study, in which the reinforcements are Hercules continuous type AS4 carbon filaments, surface-treated to increase the composite shear and transverse tensile strength, while Hercules 3501-6 epoxy is the composite matrix resin developed to operate in a temperature of up to 176°C [110].

The epoxy content of the prepregs is around 35 wt.%, and their cure state is B-staged[1]. This partial cure provides some measure of physical integrity at room temperature, to facilitate handling. The general properties of this type of prepreg tape are summarized in Table 2-1 [110], while a brief description of Hercules 3501-6 epoxy is given in Table 2-2 [17].

Table 2-1 Typical characteristics of AS4/3501-6 Gr/Ep prepregs [110]

Fiber areal weight	150 g/m^2
Standard width	30.5 cm
Resin content, % by weight	35±3%
Gel time at 177°C	6-12 min.
Volatile content, % by weight	1% max
Shelf life at room temperature	10 days
Shelf life at - 18°C	12 months
Cured-ply thickness	0.13 mm

Table 2-2 Composition of Hercules 3501-6 epoxy
(amounts given are in parts per hundred resin) [17]

Epoxide No.1 (H)	100
Curing agent (DDS)	44
Epoxide No.2 (H)	16
Epoxide No.3 (H)	15
BF_3	2

[1] B-stage represents a partially cured and usually vitrified system prior to the gel point, while A-stage represents the initial uncured state characterized by low viscosity, allowing good flow and impregnation of the resin into the reinforcing fiber bundles, and C-Stage the crosslinking state characterized by insolubility and infusibility [24].

2.1.2 Vacuum bagging

All tested composite samples are fabricated by using vacuum bagging and autoclave processing. A typical assembly of a laminate and associated materials for autoclave processing is depicted by Figure 2-1. The region of space containing the laminate is separated from the interior of an autoclave by a membrane, known as the bag, which is closed around periphery of the laminate by a sealing tape. This closed space is connected to the outside of the autoclave by the bag vacuum line. On the inside of the bag is a porous membrane which ensures a continuous gas path for volatiles to escape in applied vacuum and to achieve a uniform distribution of the vacuum over the whole area. The prepreg laminae lie on the aluminum (Al) plate and are covered by a porous release layer. Excess resin exuded from the laminate can be taken up by the absorbing bleeder material.

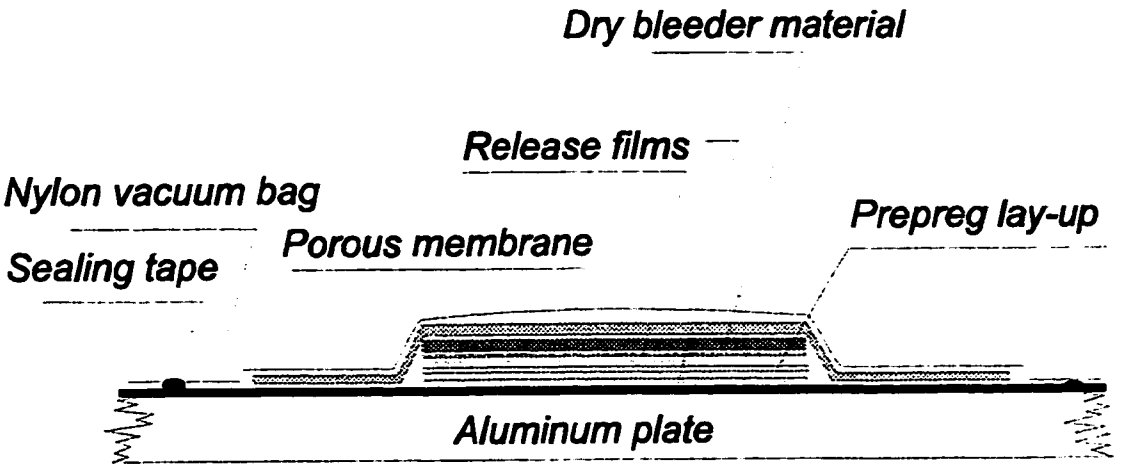

Figure 2-1 Schematic of the autoclave molding assembly

Essentially, the fabrication of AS4/3501-1 Gr/Ep laminate plates can be simplified into a few steps [16]: (1) spray the plate surface of the Al mold with the mold releasing agent; (2) place the stack of prepregs on the plate without covering up the vacuum connection; (3) completely encircle the prepreg stack with bagging adhesive; (4) place a peel-ply and a sheet of Teflon film with regularly spaced pinholes on top of the prepreg stack, preventing bleeder sheets from sticking to the laminate and serving to allow excess

resin to be squeezed out; (5) place the proper number of bleeder sheets; (6) place a continuous vent cloth on top of the layup, extend the cloth over the vacuum line attachment, and make sure the vacuum line is covered completely by the vent cloth; (7) place nylon bagging film over the entire plate, seal it against the bagging adhesive, and allow enough material to permit it to conform to all contours without being punctured; (8) place the plate in an autoclave (Figure 2-2) and attach the vacuum line; (9) turn on the vacuum pump, check for leaks, maintain a vacuum of 25 to 28 mmHg for 20 minutes, and then check again for leaks, and thereafter (10) apply the cure cycle. The whole procedure should be strictly followed, or the quality of the final composite laminates may not satisfy the general requirements for this study.

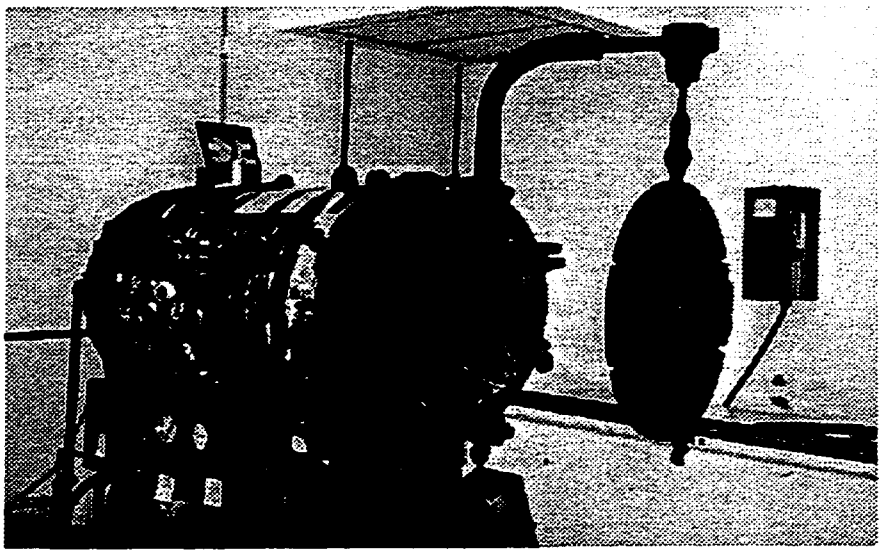

Figure 2-2 An autoclave used at the Concordia Center for Composites

The fabrication of Hercules 3501-6 epoxy resin is, on the other hand, slightly different. Before handling this epoxy resin, one must make sure that the material is in a fume hood in case an exotherm occurs, because nasty smoke comes out once there is an exotherm. The procedure can be summarized as follow [111]: (1) place about 90 g chunked epoxy resin into a 300 ml glass beaker; (2) pre-heat the oven connected with the vacuum system to between 95°C to 105°C, dwell for 20 minutes, and then move the beaker into the chamber (to avoid the risk of an exotherm); (3) apply the vacuum, when

the epoxy resin becomes a liquid, to suck out air, moisture and volatiles; (4) because the epoxy resin will foam over in the beaker, when the foam spills over to the top of the beaker, disconnect the vacuum and let the foam collapse; after that, apply the vacuum again until foam occurs again, and disconnect the vacuum; do this many times until there is no more foam, which means that all air, moisture and volatiles have already been sucked out; (5) pour the liquid epoxy resin into the Al mold, then proceed with the normal cure cycle.

The key point here is to strictly control the process time for the removal of entrapped air bubbles in the epoxy resin. This should be achieved normally within 2 hours. Beyond that period, the viscosity of the epoxy resin, because of being partially cured, may significantly increase.

2.1.3 Cure processing

The cure cycle refers to the combination of temperature and pressure cycles, which will be applied to the layup of the prepregs to produce a high-quality laminate. The viscosity of the composite resin varies enormously during the temperature cycle [7,17]. The composite resin will initially behave as a liquid and, with increasing temperature, its viscosity will fall and reach a minimum. As the temperature is further increased, the composite resin passes through a stage known as gelation period, which is associated with the change of phase towards the solid state. During this period, the viscosity of the composite resin dramatically increases. Thereafter, when the crosslinking of the composite resin proceeds, the viscosity gradually increases until full cure is reached.

The manufacturer's recommended cure process for AS4/3501-6 prepreg consists of two stages, as schematically shown in Figure 2-3 [110]. That is to say, the temperature is increased from the room temperature to the first dwell temperature of 116±2°C at a rate of approximately 2 to 3°C/min., and held there for 60±5 minutes; simultaneously the pressure of 85±5 psi is applied to squeeze out excess resin; thereafter the temperature is increased again to the second dwell temperature of 176±2°C and held there for another 120±5 minutes; pressure of 85±5 or 100±5 psi is applied; the vacuum should be

maintained throughout the whole cure cycle to achieve a uniform pressure on the laminate and to draw out volatiles created during the cure; after the completion of the cure reaction, the pressure should be maintained until the inside temperature has dropped to room temperature, in order to reduce thermal residual stresses inside the composite laminate.

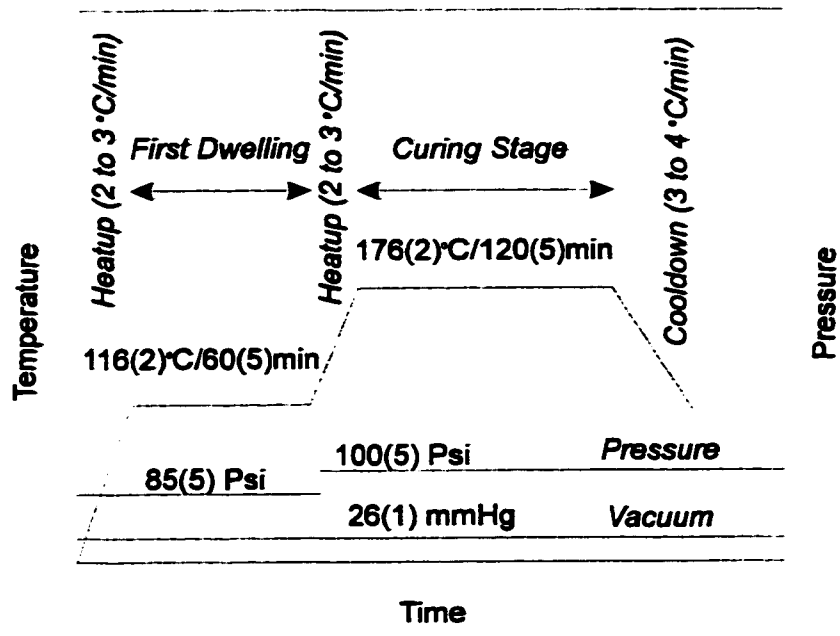

Figure 2-3 The recommended cure cycle for AS4/3501-6 Graphite/Epoxy composites

Obviously, in the production of the composite laminate, the pertinent processing parameters are time, temperature and pressure. A judicious choice of these three parameters produces a composite which is fully cured, compacted, and of high quality [112]. The first dwell temperature must be chosen to allow the viscosity of the composite resin to be low while keeping curing to a minimum. Isothermal viscosity of the composite resin *vs.* time profiles are helpful in determining the pot life of the composite resin, the maximum length of time at a specific temperature for the composite resin to remain fluid-like. The first dwell time must be within the pot life of the composite resin at the dwell temperature. Moreover, the most critical period in the process cycle is the second dwell stage, because it allows crosslinking of the composite resin to take place and the mechanical properties of the composite to be fully developed. DSC scans are useful for

providing information about the exothermic crosslinking reaction which takes place, and determining the second dwell temperature and time. A certain minimum temperature must be reached before the crosslinking reaction can commence. Moreover, at low temperatures the cure reaction will take longer and may not proceed to completion. This will not only adversely affect the mechanical performance of the materials, but may not be economically feasible. On the other hand, higher cure temperatures enhance the viscoelastic stress relaxation of chemically induced stresses. However, these higher temperatures will increase thermally induced residual stresses. A compromise must be reached between these two concerns [112].

For simplicity, during the course of this study, the first dwell stage is not of concern, and more emphasis is placed on the second dwell stage. In the following part of the thesis, the second dwelling temperature and time will be referred to as cure temperature and cure time, respectively. We investigate the behavior of AS4/3501-6 Gr/Ep composites processed at various cure temperatures (in intervals of 10°C from 146°C to 186°C) or cure time (in intervals of 20 minutes from 60 to 120 minutes) at 176°C. The cure cycle of Hercules 3501-6 epoxy is selected to be the same as that of the prepregs for a reference. However, we should be cautious, before making any comparison; because the thermal history for the pure epoxies may not exactly be the same as that of the prepregs, even though they are processed by using the "same" cure cycle, the epoxy resin in the fiber composite and neat epoxy resin may exhibit different final properties.

2.2 Quality assurance of processed composites

In order to assure the quality of the final composite laminates, all samples must be carefully examined microscopically and ultrasonically. The samples with poor quality should be rejected definitely.

2.2.1 Fraction of porosity

An optical microscope can be used to examine the void content and distribution of graphite fibers inside the samples. The samples used for optical observation can be prepared as follows [16]: (1) cut the sample to expose the desired cross-section; (2) place the sample inside a mounting cup and pour mounting material (using EPOFIX small kit HQ from Struers, Denmark) into the cup; after the mounting material is cured at room temperature for more than 24 hours, the sample is ready for polishing. (3) polish the sample by working through three sandpaper grades (240, 400 and 800), and then proceed to 1μ, and if necessary, to 0.3 μ particles. (4) when the sample is polished, it is ready to be examined in an optical microscope.

The optical microscopic observation for these samples indicates that (a) the porosity is below 1 vol.%, and (b) the graphite fibers are uniformly distributed. As an example, the optical microstructure of cross-section of laminates with the layup of $[(0_4/90_4)]_S$ is shown in Figure 2-4.

2.2.2 Delamination

Ultrasonic C-scan technique is used to examine any possible process-induced delamination inside the samples. The examination is carried out in an immersion tank by using a 10 MHz point focus ultrasonic transducer. The whole measurement is controlled by a computer running the LabVIEW® (National Instrument Co., Austin, TX) application program. The obtained images were processed, and under this spatial resolution of the transducer, no delamination was found.

2.2.3 Density of composites and fraction of graphite fibers

The density of the composite and neat epoxy resin can be determined using a liquid of known density. To do this, the sample is first weighed in air, and then immersed in a liquid. From these two weights, the density of the sample is calculated by:

$$\rho = \frac{A}{A-B} \cdot \rho_0 \tag{2-1}$$

where A and B are the weights of the sample in air and when immersed in a test liquid respectively, and ρ_0 is the density of the test liquid at a given temperature. In order to eliminate air bubbles which adhere to the submerged sample, a wetting agent such as Echowet®(Sonotech, Inc., Bellingham, WA) is added to the test liquid. The whole test can be performed by using METTLER® electronic balance with the density determination kit.

(x 400)

Figure 2-4 Microstructure of cross-ply laminate processed by the recommended cure cycle

Once the densities of the composites and their constituents are determined, the weight fraction m_f and volume fraction V_f of graphite fibers can be obtained using the following relations:

$$m_f = \frac{\rho_f(\rho_c - \rho_m)}{\rho_c(\rho_f - \rho_m)} \tag{2-2}$$

and

$$V_f = \frac{\rho_c - \rho_m}{\rho_f - \rho_m} \tag{2-3}$$

$$V_m = 1 - V_f \tag{2-4}$$

where subscripts 'c', 'm' and 'f' represent the composite, resin matrix and graphite fibers, respectively. The density of AS4 graphite fibers is ρ_f= 1.790 g/cm^3 [16].

The experimental results in Table 2-3 indicate that the density of the composites and the fraction of graphite fibers from the same batch are very close. However, they indeed have minor fluctuations from one batch to another, due to human and environmental factors.

Table 2-3 Density and fiber fraction of AS4/3501-6 Gr/Ep composites

Batch I			Batch II		
Process conditions (Cure temperature / time)	Density (g/cm^3)	Fraction of fiber (wt.)	Process conditions (Cure temperature / time)	Density (g/cm^3)	Fraction of fiber (wt.)
146°C/120min.	1.597	0.71	176°C/60min.	1.573	0.66
156°C/120min.	1.596	0.70	176°C/80min.	1.571	0.66
166°C/120min.	1.605	0.72	176°C/100min.	1.570	0.66
176°C/120min.	1.603	0.72	176°C/120min.	1.576	0.67
186°C/120min.	1.598	0.71	176°C/140min.	1.571	0.66

- The average density of cured Hercules 3501-6 epoxy is 1.269±1 g/cm^3;

2.3 Chemical kinetic analysis of cure processing

Study of cure kinetics using the DSC technique, has been used to assess chemical or thermal stability of epoxy and Gr/Ep prepregs [25-26]. The term DSC refers to the instrumental technique which maintains the measured sample and a reference material isothermal to each other by proper application of electrical energy, as they are heated or cooled at a linear rate. The curve obtained is a recording of heat flow dQ/dt as a function of temperature or time.

In this study, DSC experiments are undertaken using a TA Differential Scanning Calorimeter, as indicated in Figure 2-5. A sample ranging in weight from 5 to 15 mg is

encapsulated in a standard aluminum (Al) sample pan. The encapsulated sample is placed in a DSC sample holder, while an empty Al sample pan and cover are used as a reference, and then the rate of heat generation dQ/dt from the sample is measured as a function of temperature or time, depending on the selected DSC measurement mode.

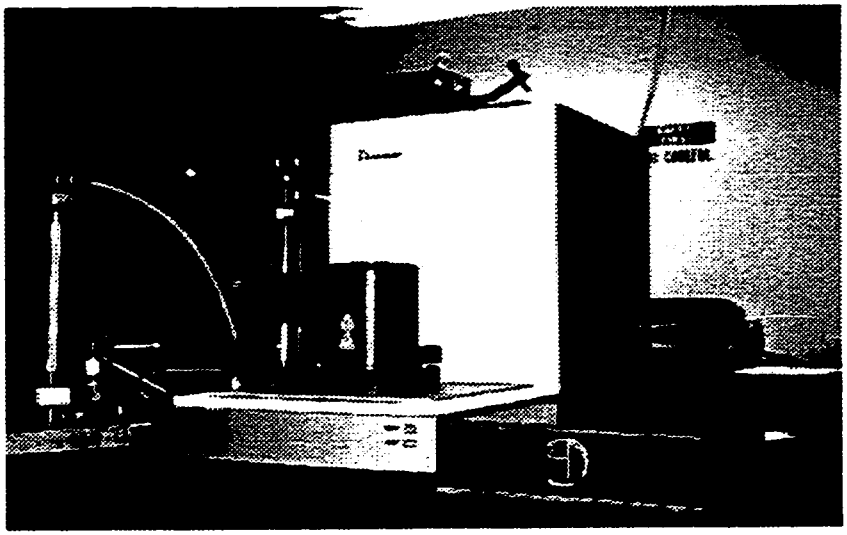

Figure 2-5 TA Differential Scanning Calorimeter (DSC)

2.3.1 Dynamic DSC analysis

2.3.1.1 Experimental method

In dynamic DSC experiments, a baseline scan is first acquired from room temperature to 260°C at a heating rate of 5°C/min. using an empty sample pan. The sample is then placed in the instrument and ramped up using identical conditions to the baseline. The rate of heat generation dQ/dt measured as a function of increasing temperature is recorded, as indicated in Figure 2-6.

This mode can be used to characterize the degree of cure by measuring the residual heat of post-manufactured samples. The residual heat ($\Delta H_{residual}$) evolved during the completion of the crosslinking can be calculated by the expression:

$$\Delta H_{resdual} = \int_0^{t'} (dQ/dt)dt \qquad (2\text{-}5)$$

where t_f is the time required to complete the cure reaction.

If ΔH_{total} represents the ultimate heat of reaction liberated per gram of uncured sample (*e.g.* $\alpha_{DOC} = 0$) when scanned under the same conditions, the degree of cure α_{DOC} can then be expressed as

$$\alpha_{DOC} = \frac{\Delta H_{total} - \Delta H_{residul}}{\Delta H_{total}} \tag{2-6}$$

2.3.1.2 Degree of cure for processed composites

The thermal behavior obtained by dynamic DSC measurements for uncured Hercules 3501-6 epoxy, as shown in Figure 2-7, reveals two "humps" in the dQ/dt *vs.* scanning temperature. This indicates that at least two dominant reactions occur during cure. This was also observed by Springer *et al.* [17]. For AS4/3501-6 Gr/Ep prepregs, the same features have been captured. The ultimate heats of reaction ΔH_{total} of Hercules 3501-6 epoxy and AS4/3501-6 Gr/Ep prepreg are 434.6 ± 19.6 J/g and 162.8 ± 0.2 J/g, respectively.

The final degrees of cure for the epoxies and composite laminates cured by different processing conditions are tabulated in Table 2-4. As expected, the degrees of cure of the epoxies and composites monotonically increase with increasing cure temperature and time. It is also noted that, after being cured for one hour at 176°C, the degree of cure of the sample has achieved a level higher than 95%. This indicates that the cure reaction has essentially fully completed. A further increase in cure process time does not significantly promote the cure reaction. On the other hand, when cure process temperature is varied from 146°C to 186°C, the final degrees of cure for the epoxies and composites also have a significant increase, as indicated in Table 2-4.

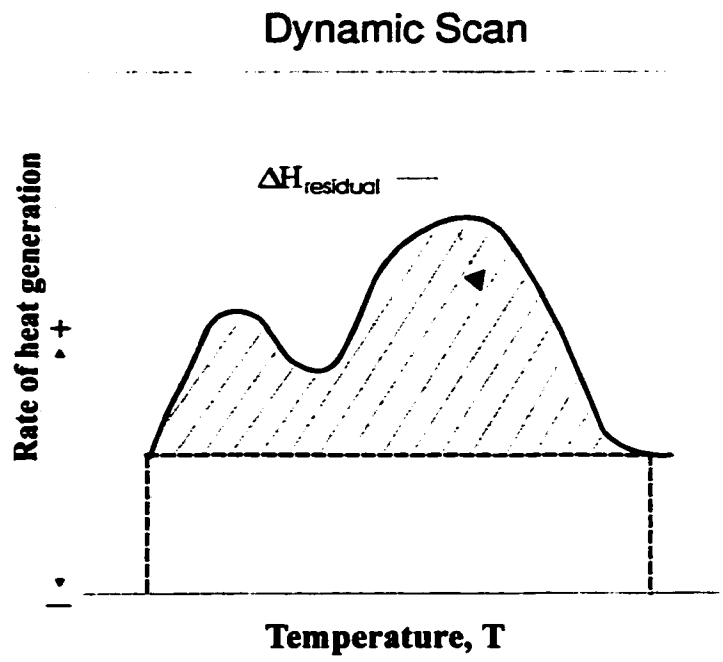

Figure 2-6 Experimental characteristics of dynamic DSC scan

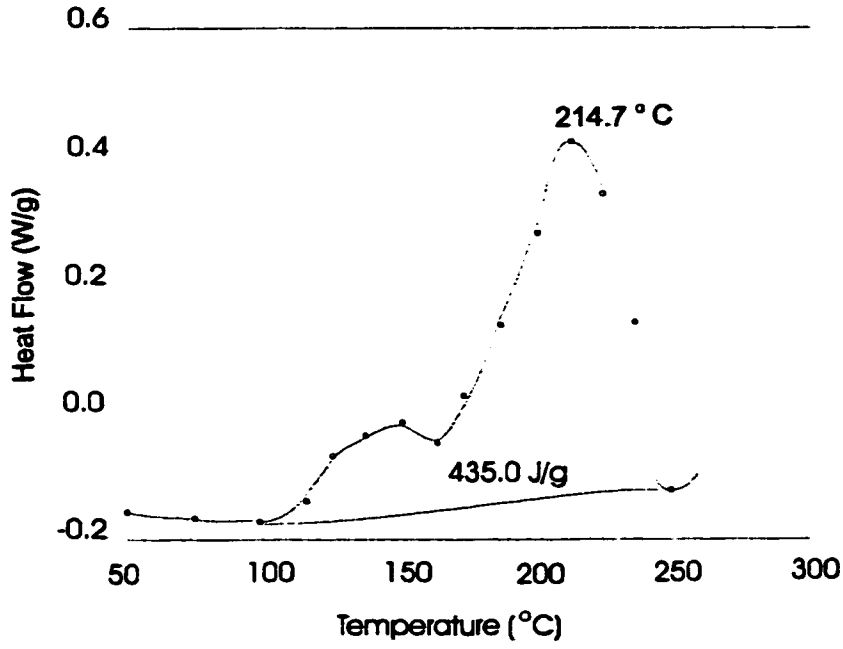

Figure 2-7 Dynamic DSC characteristics of Hercules 3501-6 epoxy

Table 2-4 Final degree of cure *vs.* cure conditions for Hercules 3501-6 epoxies and AS4/3501-6 Gr/Ep composites

Hercules 3501-6 epoxies		AS4/3501-6 composites	
Process conditions (Cure temperature/time)	Degree of cure α_{DOC} (%)	Process conditions (Cure temperature/time)	Degree of cure α_{DOC} (%)
146°C/120min.	79.6±1.3	146°C/120min.	87.9±2.1
156°C/120min.	88.4±0.6	156°C/120min.	88.8±2.0
166°C/120min.	94.7±0.6	166°C/120min.	97.0±0.5
176°C/120min.	98.3±0.1	176°C/120min.	98.5±0.4
186°C/120min.	≈100	186°C/120min.	≈100
176°C/60min.	95.4±0.3	176°C/60min.	96.4±1.2
176°C/80min.	96.9±0.2	176°C/80min.	97.5±0.6
176°C/100min.	98.0±0.1	176°C/100min.	97.8±0.5
176°C/120min.	98.3±0.1	176°C/120min.	97.9±0.5
176°C/140min.	98.5±0.1	176°C/140min.	98.7±0.3

2.3.2 Isothermal DSC analysis

2.3.2.1 Experimental method

The isothermal DSC test has been widely used to model the cure kinetics of polymers, auto-catalyzed and/or n-th order [113]. When temperature dependence of kinetic parameters is known, the degree of cure can be predicted for any temperature history by integration of kinetic equations.

In an isothermal DSC test, the heat flow dQ/dt from the sample is monitored over time. Generally as crosslinking reaction commences, the DSC monitors the release of energy and the dQ/dt is mapped in the exothermic region. After a short period of time the dQ/dt reaches its maximum, and begins to decrease gradually until reaching the baseline (zero heat flow) upon the completion of the reaction. As schematically shown in Figure 2-8, the degree of cure at time t* is found from

$$\alpha_{DOC} = \frac{\Delta H(t^*)}{\Delta H_{total}} \tag{2-7}$$

where $\Delta H(t^*) = \int_0^{t^*} \frac{dQ}{dt} dt$ is the area of the partial exotherm up to t*, and ΔH_{total} the ultimate heat of reaction generated during dynamic scan. The baseline used for the numerical integration of isothermal data is obtained by horizontal extrapolation of the final heat flow data points to intersect with the initial onset of the reaction exotherm.

To obtain the rate of degree of cure $d\alpha_{DOC}/dt$ at any time, the height of the exotherm from the baseline, dQ/dt, is divided by the ultimate heat of reaction ΔH_{total}:

$$\frac{d\alpha_{DOC}}{dt} = \frac{dQ/dt}{\Delta H_{total}} \tag{2-8}$$

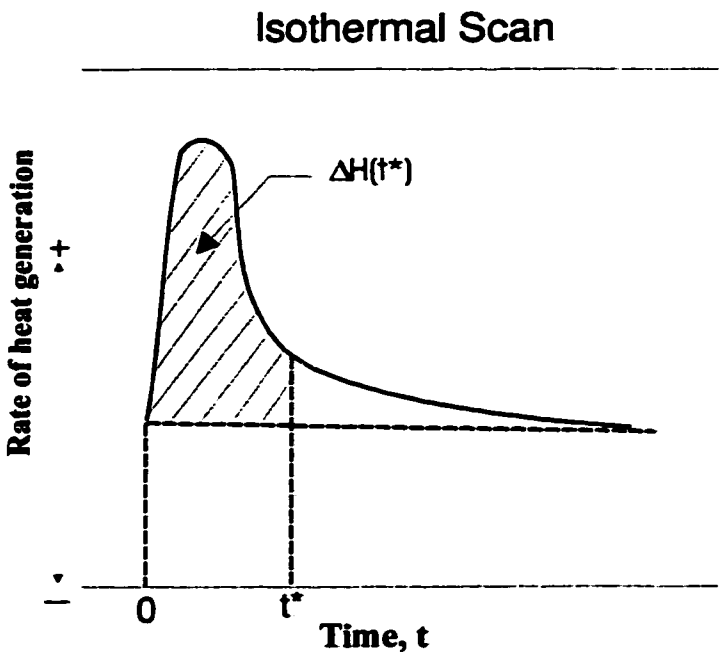

Figure 2-8 Experimental characteristics of isothermal DSC scan

Due to the complexity of cure reactions, a phenomenological model is selected for this study because it can capture the major features of the reaction kinetics while ignoring the details of how individual species react with each other.

Phenomenological models for reaction rate have the general formula [20]:

$$\frac{d\alpha_{DOC}}{dt} = Kf(\alpha_{DOC}) \tag{2-9}$$

where $f(\alpha_{DOC})$ represents some function of α_{DOC}, t is the reaction time, K is a specific rate constant at absolute temperature T, having an Arrhenius temperature dependence:

$$K = Z\exp(-\frac{\Delta E}{RT}) \tag{2-10}$$

where Z is a pre-exponential or frequency factor, R is the universal gas constant, and ΔE is the activation energy.

Many attempts have been made to describe the $d\alpha_{DOC}/dt$ *vs.* α_{DOC} relation with a modified Arrhenius type equation; Springer *et al.* [17] showed that Hercules 3501-6 epoxy resin could be modeled by

$$\frac{d\alpha_{DOC}}{dt} = (K_1 + K_2\alpha_{DOC})(1-\alpha_{DOC})(B-\alpha_{DOC}) \quad \text{for } \alpha \leq 0.3 \tag{2-11}$$

and

$$\frac{d\alpha}{dt} = K_3(1-\alpha_{DOC}) \quad \text{for } \alpha > 0.3 \tag{2-12}$$

in which

$$K_i = Z_i\exp(-\frac{\Delta E_i}{RT}) \qquad (i = 1,2,3) \tag{2-13}$$

where B was 0.47, a constant independent of temperature [17]. The constants K_1, K_2 and B were determined by a non-linear least square curve fit, and the constant K_3 by linear regression.

For the present isothermal DSC tests, a fresh, pre-weighed sample is loaded into the preheated DSC cell. The cell should be heated to the desired isothermal temperature by using an "initial temperature" segment. After the sample is dropped into the cell, the lid, cover, and dome should be replaced as soon as possible [113]. When the displayed temperature is within 4°C of the set temperature, the run should be allowed to proceed, and data acquisition is begun. Data acquisition continues until the reaction rate is negligible (*i.e.* final baseline returns to linear behavior). Isothermal DSC scans are

performed in intervals of 10°C from 146°C to 186°C. It should be noted that since some of the reaction takes place before the cell and the sample achieve equilibrium, a certain amount of heat remains unrecorded because the onset temperatures of the first exotherm, indicated as the first "hump" in Figure 2-7, is between 100°C to 160°C, which is lower than the isothermal testing temperature. Moreover, data in the range greater than 85% of the area of the exotherm should not be used for the analysis, because the reaction is approaching the diffusion control region.

2.3.2.2 Analysis of cure kinetics

Several experimental observations on the cure kinetics of Hercules 3501-6 epoxy and AS4/3501-6 Gr/Ep prepregs can be made. Figure 2-9 shows the variation of the degree of cure *vs.* cure time during the isothermal DSC scan. It is noted that as cure process temperature increases, the development of the degree of cure is greatly accelerated, and the time for the completion of the cure reaction is significantly shortened. For Hercules 3501-6 epoxy cured at 176 °C and 186°C, the degrees of cure reach higher than 0.95 after curing for one hour. This means that the cure reaction is fully completed, while when cured at 146°C, the degree of cure only reaches around 0.75 after curing for 2 hours. Other cure temperatures fall between these extremes. Figure 2-10 shows the variation of the rate of degree of cure *vs.* the cure time during the isothermal DSC scan, indicating that the initial cure reaction proceeds rapidly; afterwards, as the chemical reaction progresses, the reaction rate gradually decreases; eventually, the reaction rate approaches zero as the vitrification of the composite epoxy achieves.

In the present case, the kinetic equations for both auto-catalyzed and/or n-th order reactions are employed to describe the rate of cure reactions. Because there are at least two dominant reactions occurring during the cure, these reactions (represented by the two "humps" in Figure 2-6) cannot be correlated by a single equation [17]. Thus two forms of reaction rate are chosen to provide a proper balance between computational complexity and material versatility. Equation (2-11) is used to describe the auto-catalyzed model, and Equation (2-14) the n-th order model:

$$\frac{d\alpha_{DOC}}{dt} = K_3(1-\alpha_{DOC})^n \tag{2-14}$$

in which

$$K_3 = Z_3 \exp(-\frac{\Delta E_3}{RT}) \tag{2-15}$$

where n is reaction order (dimensionless) [113].

For the auto-catalyzed reaction, K_1, K_2 and B at T can be obtained using non-linear regression [17] while for the n-order reaction, K_3 and n at T are determined using linear regression [113]. Moreover, the activation energy ΔE_i (i=1,2,3) requires plotting the natural log of K *vs.* the inverse of cure temperature. According to Equations (2-13) and (2-15), the result should be a straight line with slope of - $\Delta E/R$ and intercept of ln(K). Figure 2-11 shows the Arrhenius constants for Hercules 3501-6 epoxy, and their dependence on temperature.

Meanwhile, the order of the cure reaction, n, may be a function of temperature. Figure 2-12 shows the plot of n *vs.* isothermal temperature T in K. A curve is fit to the data to determine n = f(T).

Figure 2-13 indicates the variation of the rate of degree of cure *vs.* the degree of cure, in which the symbols denote experimental data, whereas the solid lines are numerically generated by the present kinetic model. Obviously, both approaches agree reasonably well with each other, except the transition range between auto-catalyzed and n-order reactions. Another fact is that the residual error of a non-linear regression for auto-catalyzed reaction analysis is somewhat large, while that of a linear regression for n-order reaction analysis is much lower. Even so, the present kinetic model has captured the major features of these cure reactions. The values of these constants are listed in Table 2-5. In comparison with Springer's results [17], the difference may be ascribed to the fact that the epoxy used for Springer's experiments may not have had exactly the same composition as the one used in the present experiments.

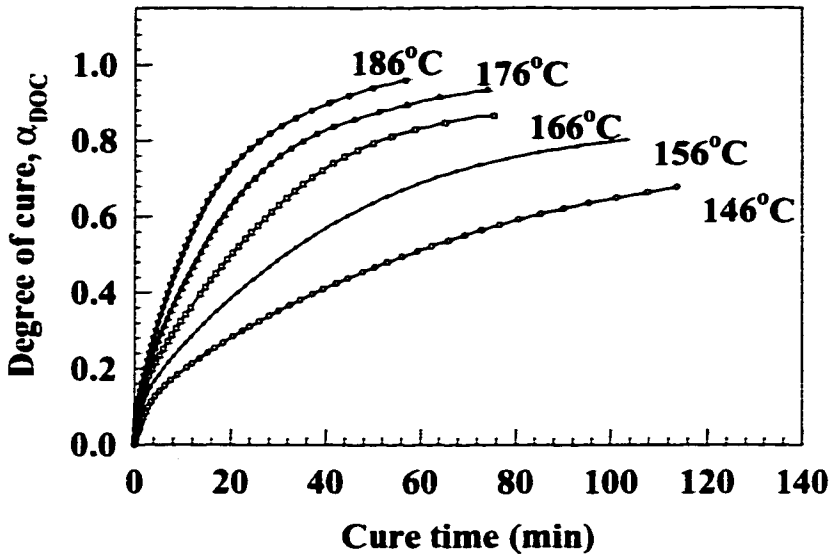

(a)

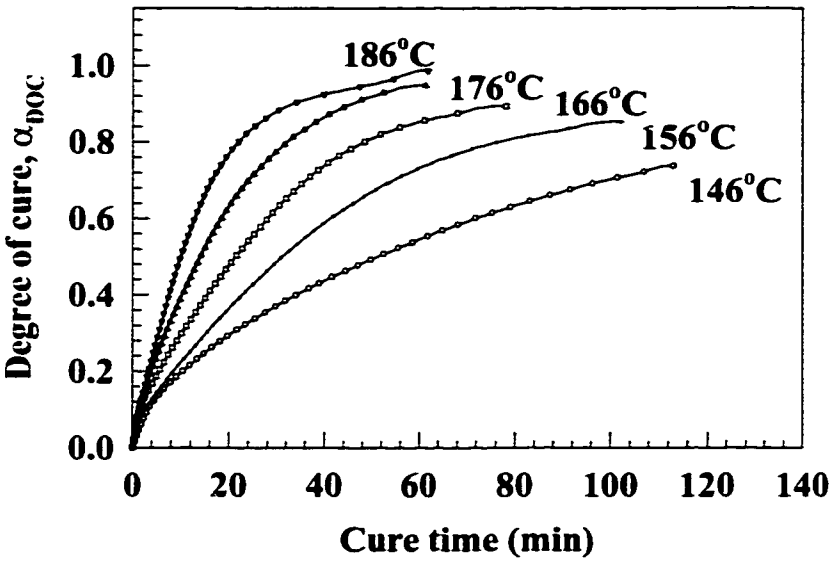

(b)

Figure 2-9 Degree of cure *vs.* cure process time
for (a) Hercules 3501-6 epoxies and (b) AS4/3501-6 Gr/Ep prepregs

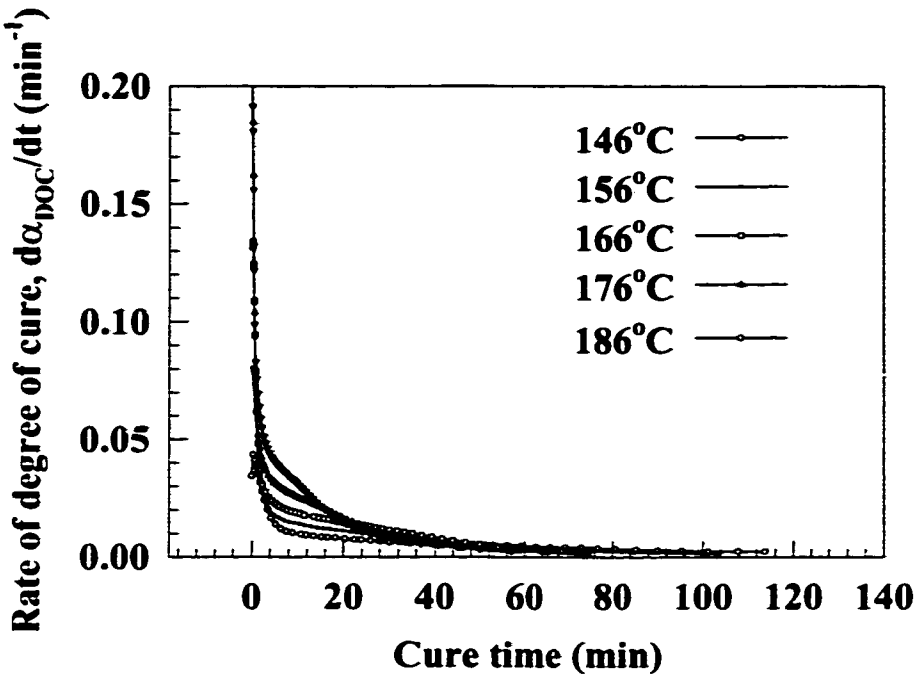

Figure 2-10 Rate of degree of cure *vs.* cure process time for Hercules 3501-6 epoxy

Once the expression of the rate of reaction is determined, the degree of cure at any time given a prescribed temperature history may be obtained by integrating Equations (2-11) and (2-14) [20]:

$$\alpha_{DOC}(t^*) = \int_0^{t^*} \frac{d\,\alpha_{DOC}(\tau)}{d\,\tau} d\,\tau \tag{2-16}$$

In the case of Hercules 3501-6 epoxy,

$$t = \frac{a}{K_2} Ln(1 + \frac{K_2}{K_1}\alpha_{DOC}) - bLn(1-\alpha_{DOC}) - cLn(1-\frac{\alpha_{DOC}}{B}) \quad (t<t_c) \tag{2-17}$$

and

$$t = t_c + \frac{1}{K_3(1-n)}[(1-\alpha_{DOC})^{1-n} - (1-\alpha_{DOC.C})^{1-n}] \quad (t>t_c) \tag{2-18}$$

in which [17]

$$\begin{aligned} a &= K_2^2(B-1)/d \\ b &= (K_1 + K_2 B)/d \\ c &= -(K_1 + K_2)/d \\ d &= (K_1 + K_2)\{K_1 B^2 + (K_1 - K_2)B - K_1\} \end{aligned} \tag{2-19}$$

and $\alpha_{DOC,C}$ and t_c are the specific degree of cure and cure time when the n-order reaction starts.

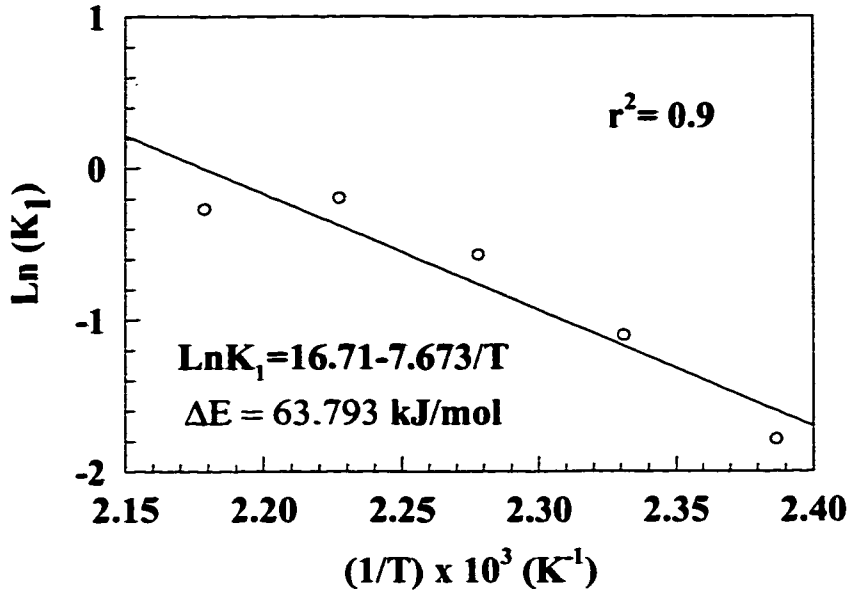

(a)

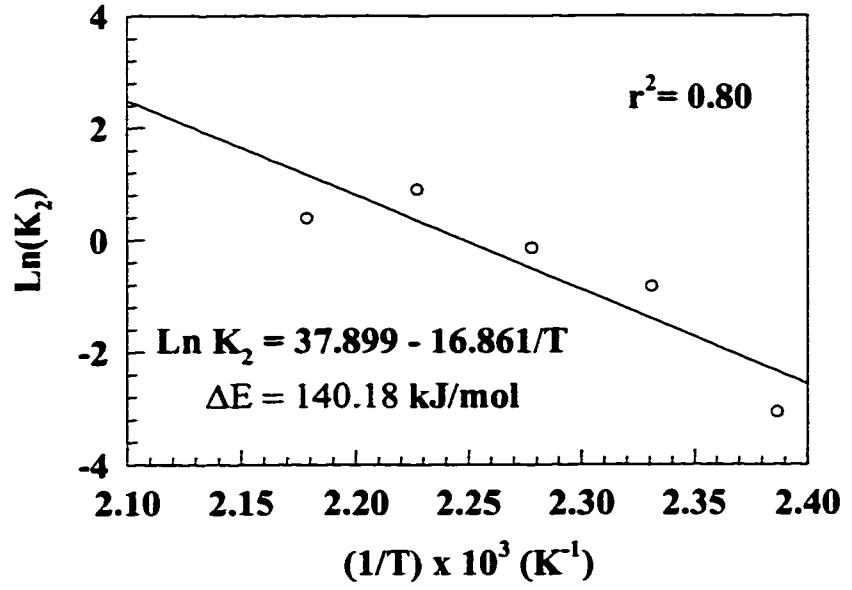

(b)

Figure 2-11 Arrhenius plot for Hercules 3501-6 epoxy (natural log(K) *vs.* inverse temperature)

(continued)

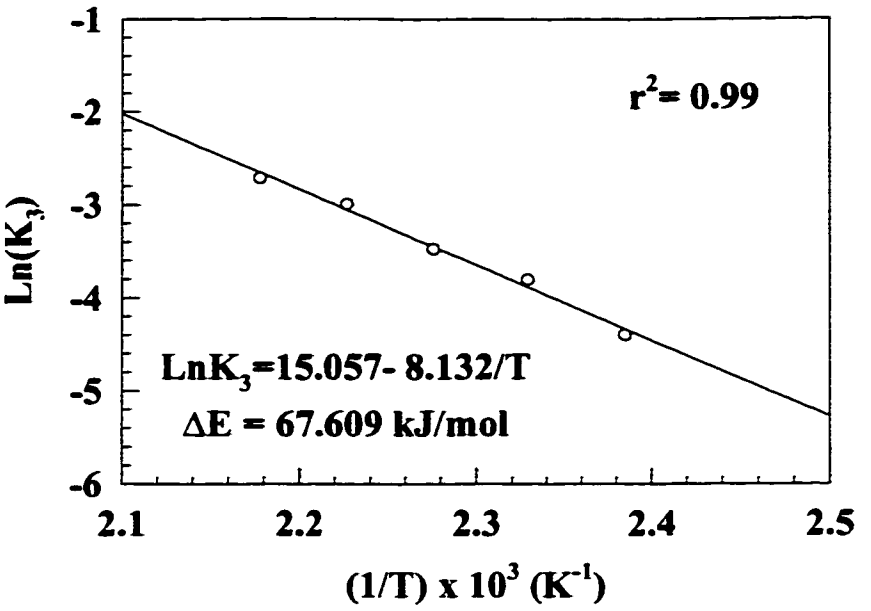

(c)

Figure 2-11 Arrhenius plot for Hercules 3501-6 epoxy (natural log(K) *vs.* inverse temperature) (completed)

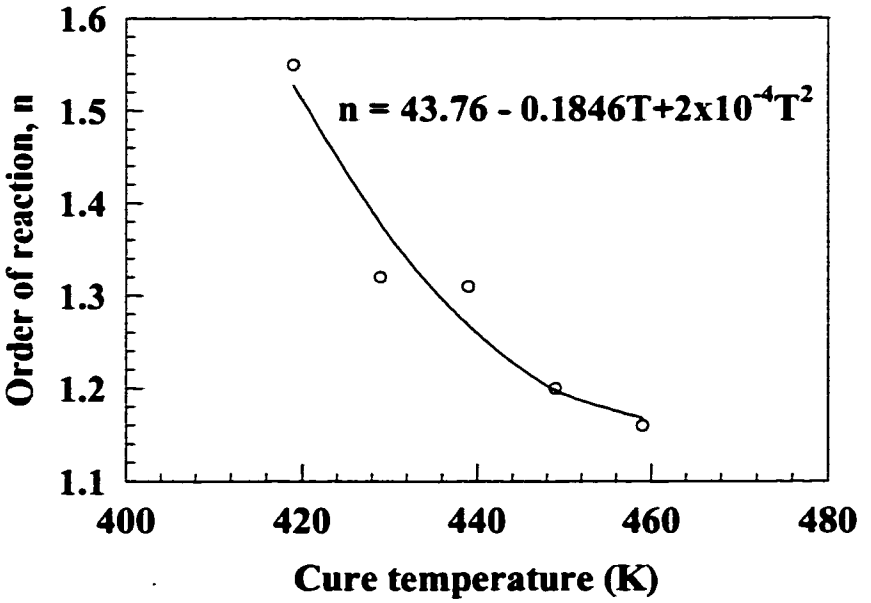

Figure 2-12 Order of reaction n *vs.* isothermal temperature T in K for Hercules 3501-6 epoxy

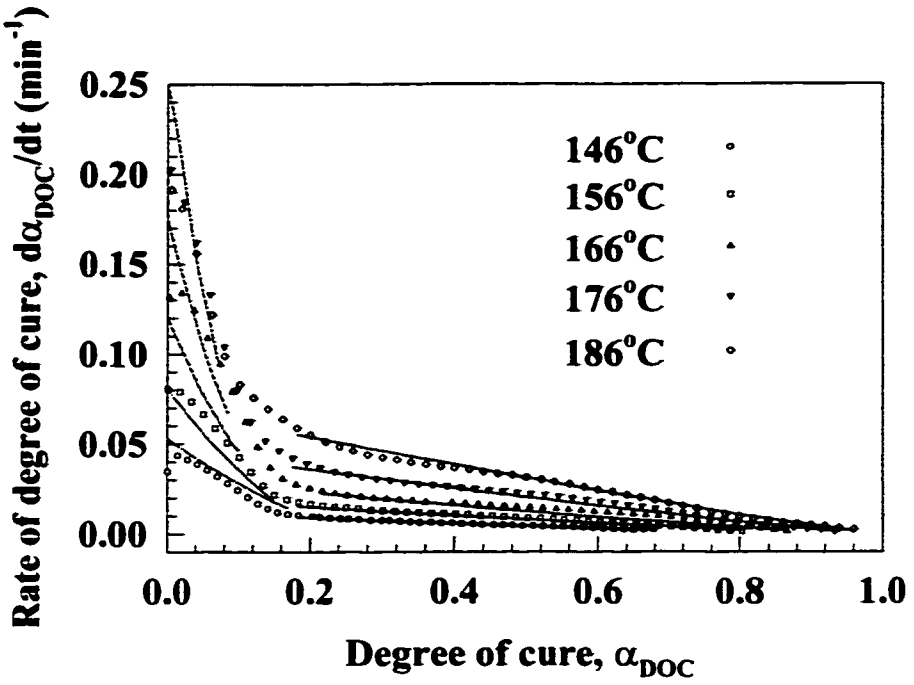

Figure 2-13 Rate of degree of cure *vs.* degree of cure for Hercules 3501-6 epoxy (the symbols denote experimental data, whereas the solid lines represent the model)

Table 2-5 The values of the constants in Equations (2-10), (2-12), (2-13) and (2-14)

Sample	Type of Cure reaction	Constants in Equations	Present results	Springer's results [17]
Hercules 3501-6 epoxy	Auto-catalyzed	Z_1 (min^{-1})	1.807×10^7	2.101×10^9
		Z_2 (min^{-1})	2.880×10^{16}	-2.014×10^9
		ΔE_1 (kJ/mol)	63.79	80.7
		ΔE_2 (kJ/mol)	140.18	77.8
		B	0.263	0.47
	n-order	Z_3 (min^{-1})	3.461×10^6	1.960×10^5
		ΔE_3 (kJ/mol)	67.61	56.6
		n	$43.76 - 0.1846T + 2 \times 10^{-4}T^2$	1

2.4 Dynamic mechanical properties

The properties of polymer composites depend strongly on both temperature and time. This exactly reflects their viscoelastic nature, which refers to the behavior similar to

both viscous liquid, in which the rate of deformation is proportional to the applied force, and purely elastic solid, in which the deformation is proportional to the applied force [27,28]. A knowledge of viscoelastic behavior of the polymer composites is essential to an understanding of both processing and end-use properties [114]. A dynamic mechanical analyzer is used for precisely such purposes.

In general, dynamic mechanical properties may be characterized by storage modulus E', loss modulus E", and loss tan δ, *etc*. Dynamic mechanical properties are very sensitive to the features of the molecular structure of polymer chains and the morphology of bulk materials, for example, glass transitions, local motion of molecular groups in, or attached to, the polymer chain, *etc*. [28].

In this part of the Chapter, the investigation of dynamic modulus E* and loss tan δ over a wide range of temperatures has proven to be very useful in studying their relations to end-use performance. These dynamic parameters have been also used to determine the glass transition region of the end materials.

2.4.1 Background

Dynamic mechanical testing is based on the fundamentally different responses of viscous and elastic elements to a sinusoidally varying stress or strain [28]. The applied force and the resulting deformation both vary sinusoidally with time, the rate usually being specified by the frequency f or angular frequency $\omega=2\pi f$. For linear viscoelastic behavior, the strain will alternate sinusoidally but will be out of phase with the stress, as shown in Figure 2-14 [28]. This phase lag results from the time necessary for molecular rearrangements, and is associated with relaxation phenomena.

The stress σ and strain ε can be expressed as follows:

$$\sigma = \sigma_0 \sin(\omega t + \delta) \tag{2-20}$$

and

$$\varepsilon = \varepsilon_0 \sin(\omega t) \tag{2-21}$$

where δ is the phase angle. Expanding Equation (2-20) yields:

$$\sigma = \sigma_0 \sin \omega t \cos \delta + \sigma_0 \cos \omega t \sin \delta \tag{2-22}$$

The stress can be considered to consist of two components, one 0° in phase with strain ($\sigma_0 \cos\delta$) and the other 90° out of phase ($\sigma_0 \sin\delta$). When these are divided by the strain, we can separate the modulus into an in-phase (real) and out-of-phase (imaginary) component [28]. These relationships are

$$\sigma = \varepsilon_0 E' \sin \omega t + \varepsilon_0 E'' \cos \omega t \tag{2-23}$$

where

$$E' = \frac{\sigma_0}{\varepsilon_0} \cos \delta \quad \text{and} \quad E'' = \frac{\sigma_0}{\varepsilon_0} \sin \delta \tag{2-24}$$

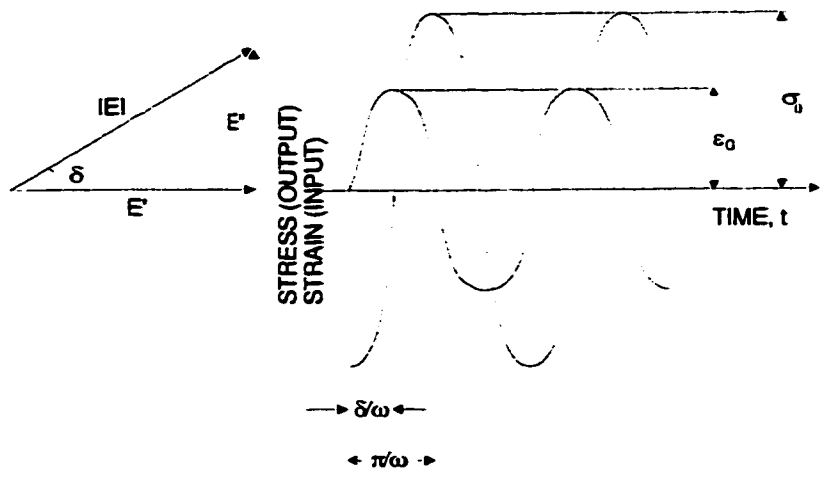

Figure 2-14 Relations between various parameters used to express the results of a dynamic mechanical measurement [28]

The real part of modulus E' is called the storage modulus, because it is related to the storage of energy as potential energy, and its release in periodic deformation. The imaginary part of the modulus E" is called the loss modulus, and is associated with the dissipation of energy as heat when the materials are deformed. The complex representation E* for the moduli E' and E" can be defined as

$$E^* = E' + jE'' \tag{2-25}$$

in which E* is called a complex or dynamic modulus, and the phase angle δ can be expressed as

$$\tan \delta = \frac{E''}{E'} \tag{2-26}$$

where tan δ is called the loss tangent.

Moreover, the glass transition temperature T_g of the composite epoxy is also one of the important properties. Perhaps the simplest of many definitions of T_g is the temperature below which the polymer is glassy and above which it is rubbery. This description applies strictly only to amorphous polymers. The molecular interpretation of T_g is the temperature of the onset of large-scale motion of molecular chain segments. At very low temperatures, near absolute zero, chains of atoms undergo only low-amplitude vibratory motion around fixed positions. As the temperature is raised, both the amplitude and the cooperative nature of these vibrations among neighboring atoms increase, until at a well-defined transition at temperature T_g, segmental motion becomes possible, and the material becomes leathery or rubbery. Around T_g, the chain segments can undergo cooperative rotational, translational, and diffusional motions [27,28,114,115].

2.4.2 Experimental method

Dynamic mechanical (rheological) tests are performed by using the TA 983 Dynamic Mechanical Analyzer (DMA), as the one shown in Figure 2-15, in fixed frequency mode at 1 Hz and with 0.20 mm oscillation amplitude. In order to carry out this measurement, a rectangular specimen, heated from 60°C to 260°C at a rate of 5°/min., is clamped at each end. A flexural bending motion is induced on one end while the specimen's response is measured at the other end. The dependence of E', E", loss tan δ and T_g of Hercules 3501-6 epoxy and AS4/3501-6 Gr/Ep composite on temperature are evaluated. However, it should be noted that when the T_gs are used to characterize glass transition temperatures of the composites, the presence of graphite fibers and the angle of

the layups indeed complicate the characterization, because they induce extra energy dissipation during DMA testing. In order to consistently use the above T_g definition, in the case of composites, the T_gs will be implied by a prefix "apparent". The T_gs of the epoxies and composites are hereby experimentally determined by the temperature under which the loss modulus E" is maximized.

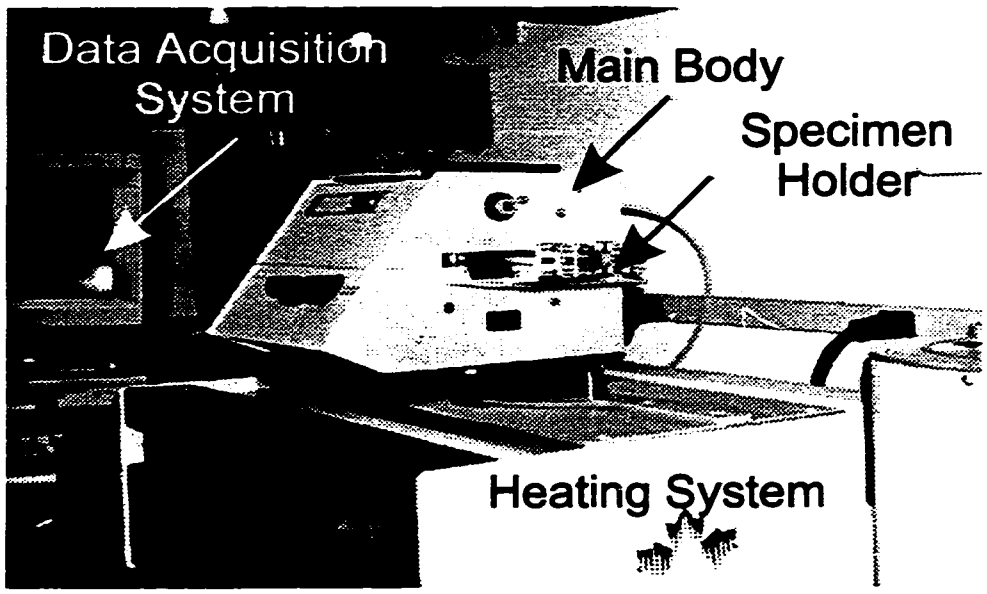

Figure 2-15 TA 983 Dynamic Mechanical Analyzer (DMA)

2.4.3 Results and discussion

2.4.3.1 Effect of cure temperature

The dependence of E' and loss tan δ of Hercules 3501-6 epoxy and AS4/3501-6 Gr/Ep composite, processed at different cure temperatures at intervals of 10°C from 146°C to 186°C, on DMA scanning temperature is presented in Figure 2-16. It is seen that all tested samples experience: (1) with increasing temperature, the E' decreases while loss tan δ increases; (2) in the range of glass transition, E' drops sharply whereas loss tan δ achieves a maximum value; the corresponding T_gs of the tested samples can be deduced from the temperatures achieving maximum E"; (3) after the transition, the tested samples

have rubber-like behavior, which, however, is not of concern in the present study. It is also noted that for the epoxy cured at 146°C, its tan δ curve exhibits a double "humps", as indicated in Figure 2-16(a). The reason may be ascribed to that the cure temperature for the sample cured at 146°C is so lower that the sample is quite undercure, and thus the sample will continue curing when the DMA scanning temperature becomes higher than the cure temperature (146°C).

All results are tabulated in Table 2-6. It can be observed that when the cure process temperature increases in intervals of 10°C from 146°C to 186°C, the T_gs of Hercules 3501-6 epoxy and AS4/3501-6 composite with the layup of $[90_{16}]$ are dramatically increased by around 55°C and 74°C, respectively, indicating that increasing cure process temperature significantly influences the T_gs of the samples. Meanwhile, the values of maximum loss tan δ reduce and their location noticeably shifts to higher temperature with increasing cure temperature, as exhibited in Figure 2-16. It is understood [27,28,114] that glass transition is related to the motion of molecular chains; increasing cure process temperature accelerates the crosslink reaction, thus reducing the damping property and increasing the T_gs of the materials, by introducing restrictions on molecular motion of chains.

Furthermore, the T_gs and maximum loss tan δ are disturbed by the presence of graphite fibers. For instance, the T_gs obtained by testing the beams with the layup of $[0_{16}]$ are generally higher than that of the beams with the layup of $[90_{16}]$, while the maximum loss tan δ obtained by testing the beams with the layup of $[0_{16}]$ are generally lower than that of the beams with the layup of $[90_{16}]$, as indicated in Figure 2-17.

Moreover, as seen in Table 2-6, the difference in T_g between the epoxies and composites processed by the "same" cure cycle may be ascribed to their different thermal history and effect of the graphite fibers.

2.4.3.2 Effect of cure time

The length of cure time, while held at 176°C, also affects the dynamic mechanical properties of the materials, as shown in Figure 2-18. The experimental results are tabulated in Table 2-6.

Although after curing for one hour at 176°C, the degree of cure of the epoxies and composites reaches to around 0.95, their T_gs, for another one hour curing, still exhibit a noticeable increase by about 21°C and 6°C, respectively. This suggests that the development of the T_g may lag behind the degree of cure during processing.

Table 2-6 The T_gs of Hercules 3501-6 epoxy and AS4/3501-6 Gr/Ep composite beams with the layups of $[90_{16}]$ or $[0_{16}]$

Process conditions (Cure temperature / cure time)	T_g of 3501-6 epoxy beam (°C)	T_g of AS4/3501-6 beam with layup of $[90_{16}]$ (°C)	T_g of AS4/3501-6 beam with layup of $[0_{16}]$ (°C)
146°C/120 min.	160±0	160±3	166±2
156°C/120 min.	190±1	178±3	193±2
166°C/120 min.	211±0	198±3	208±1
176°C/120 min.	225±2	206±1	218±3
186°C/120 min.	234±1	213±1	229±1
176°C/60 min.	204±1	205±2	N/A
176°C/80 min.	211±0	209±1	N/A
176°C/100 min.	212±1	212±1	N/A
176°C/120 min.	225±2	211±2	N/A

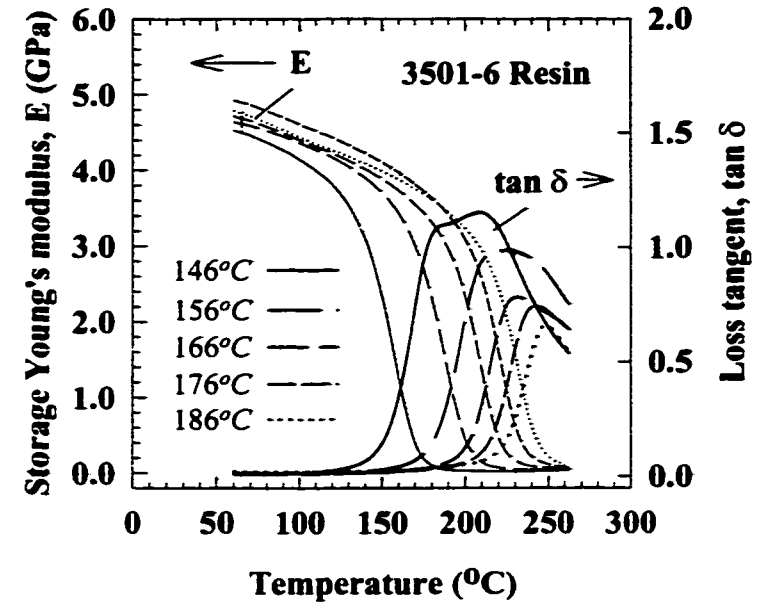

(a)

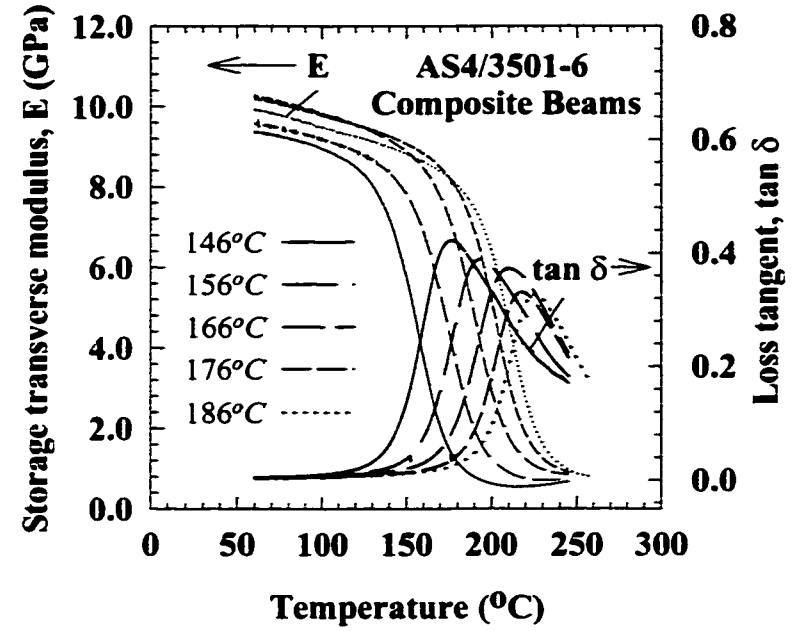

(b)

Figure 2-16 DMA characteristics of (a) Hercules 3501-6 epoxy and (b) AS4/3501-6 Gr/Ep laminate with the layup of $[90_{16}]$ processed by different cure temperatures

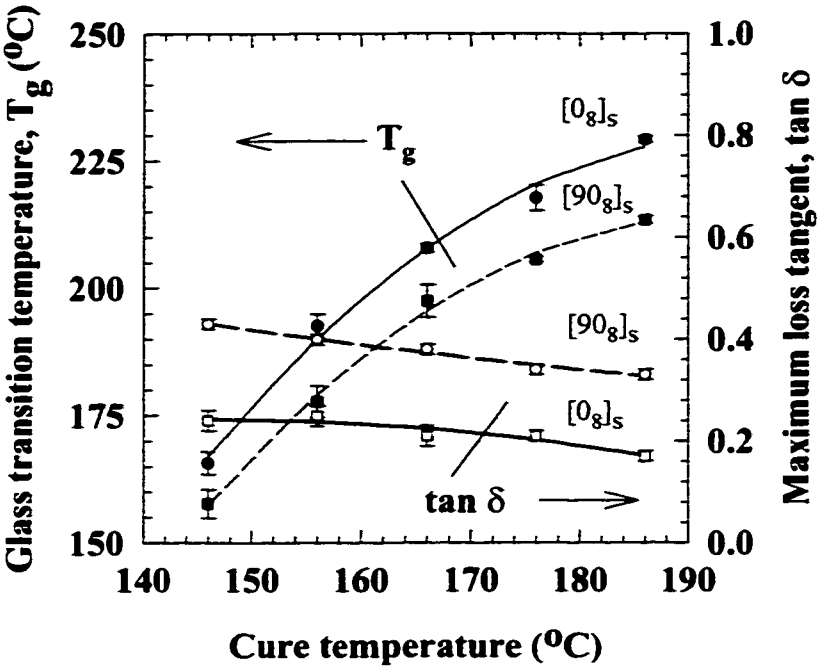

Figure 2-17 The T_g and maximum loss tan δ of AS4/3501-6 Gr/Ep composite beams with different layups, as a function of cure process temperature

2.5 Summary

The DSC and DMA characterization shows that:

(1) Cure temperature profoundly affects the degree of cure during the curing process. As cure temperature increases, the degree of cure increases, while the time for the completion of the cure reaction decreases. At cure temperatures of 176°C and 186°C, the cure reaction is almost fully completed after one hour, while after curing for 2 hours at 146°C, the degree of cure only reaches around 70%. The degree of cure measured at 156°C and 166°C falls between these extremes.

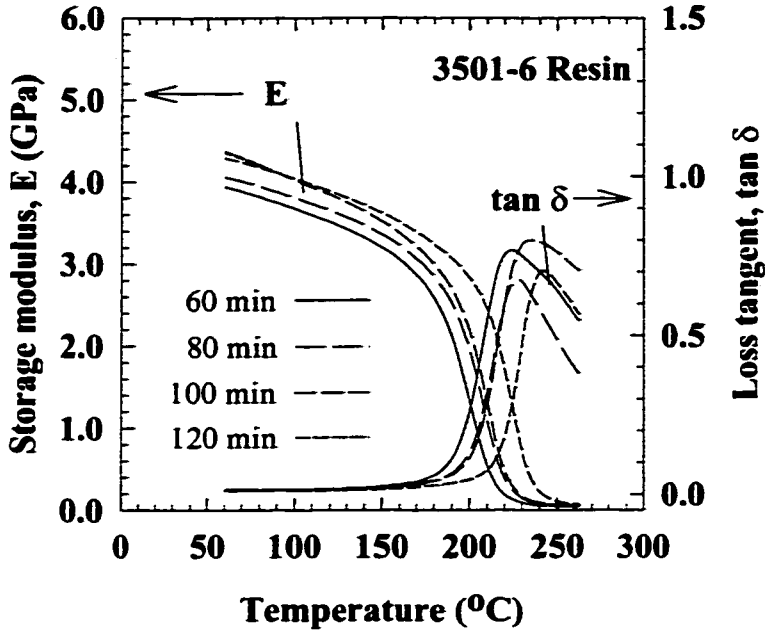

(a)

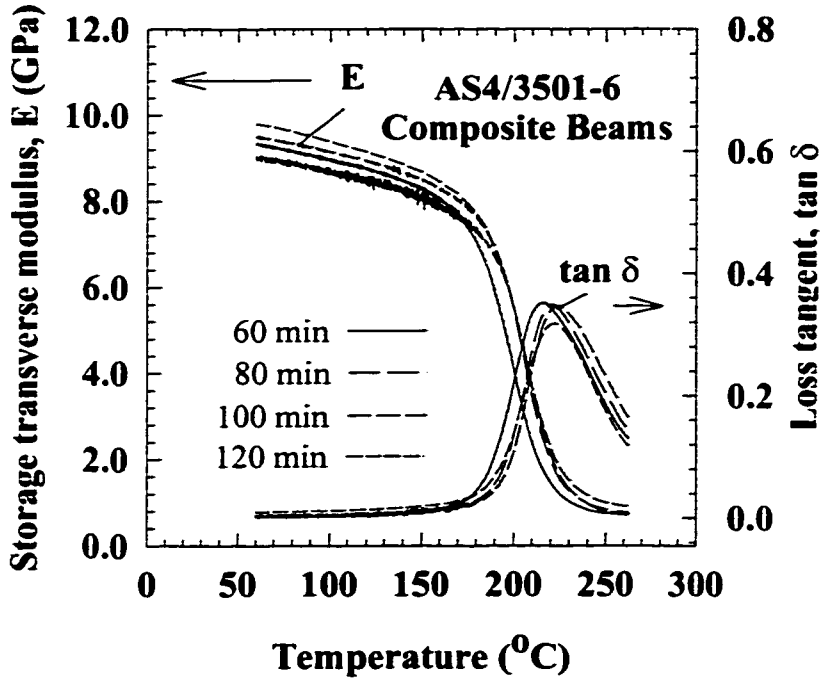

(b)

Figure 2-18 DMA characteristics of (a) Hercules 3501-6 epoxies and (b) AS4/3501-6 Gr/Ep laminates with layups of $[90_{16}]$ processed by different cure times

(1) From isothermal DSC measurement in intervals of 10°C from 146°C to 186°C, the kinetics of the cure reaction of Hercules 3501-6 epoxy and AS4/3501-6 Gr/Ep prepreg is investigated. The analytical results demonstrate that modified Springer's equations can be used to describe the observed cure kinetics of Hercules 3501-6 epoxy. The initial stage of the curing is dominated by an auto-catalyzed reaction:

$$\frac{d\alpha_{DOC}}{dt} = (K_1 + K_2\alpha_{DOC})(1-\alpha_{DOC})(B-\alpha_{DOC})$$

and the later stage by an n-order reaction:

$$\frac{d\alpha_{DOC}}{dt} = K_3(1-\alpha_{DOC})^{n(T)}$$

The obtained kinetic equations can be used to predict the rate of cure reaction and the degree of cure at any cure time.

(3) Increasing cure temperature causes a noticeable decrease in the values of loss tan δ of the processed epoxies and composites, and a profound increase in T_g by around 55°C and 74°C, respectively. At the cure temperature of 176°C, after being cured for one hour, although the development of the degree of cure of the materials has been fully completed, during another one hour of curing, the T_gs of the epoxies and composites are still increased by around 21°C and 6°C, respectively.

Both DSC and DMA results are consistent. These results exhibit an interesting phenomenon that after curing for one hour at 176°C, the degree of cure of the epoxies and composites is almost fully developed, whereas their T_gs still keep increasing during further cure processing. The reason could be ascribed to that during the cure processing, after the curing composite resin vitrifies (that is, the glass transition temperature of the resin is higher than cure temperature), the cure reaction becomes diffusion-controlled, and slow-down. That is why usually post-curing procedure is performed to ensure that the ultimate glass transition temperature be achieved.

Moreover, the recommended cure time at 176°C was 2 hours, but the DSC results indicate that at that cure temperature, one hour of curing is enough in terms of the development of degree of cure. Since the degree of cure is the indication of the extent of

chemical reactivity, is it a good indicator to determine the "end-of-cure' during the cure processing? This will be further addressed in Chapter 5.

Chapter 3

ULTRASONIC EVALUATION OF PROCESSED GRAPHITE/EPOXY COMPOSITES

3.1 Introduction

The ultrasonic technique is known to have the capability to characterize elastic properties of a composite, by using densities of composite and phase velocities of elastic waves which propagate in various directions in the composite. Although ultrasonic methods for determining elastic properties have a relatively short history compared to mechanical testing methods, these techniques are being rapidly developed because of their high accuracy, especially for measuring shear properties [79-87]. Moreover, all elastic constants of a single sample may be obtained by ultrasonic measurement. Since we seek changes of epoxy-matrix dominated mechanical properties resulting from different cure processes, the high sensitivity of ultrasonically measured shear properties becomes critical. Also, the velocity dispersion and attenuation of ultrasonic waves may be used to characterize viscoelastic properties of a composite [102, 103].

The investigation in this Chapter is an attempt to determine the mechanical properties which can monitor variations in cure processing. Such measures may thereafter be taken as process monitoring parameters during the course of composite fabrication.

3.2 Ultrasonic anisotropic evaluation

3.2.1 Christoffel's equation

Wave propagation in a composite material is mathematically more complex than in an isotropic material. It has been studied by many investigators [79-98, 116]. The algorithm used for obtaining elastic constants from bulk acoustic wave phase velocities in an arbitrary direction of a measured sample is Christoffel's equation [85, 116]. Since linear elastic behavior is assumed, an arbitrary wave can be decomposed into its harmonic components, and all frequency components travel with the same velocity (non-dispersion). It is thus sufficient to consider these components separately. We can just consider a plane harmonic wave propagating inside a bulk material. The displacement of a plane harmonic wave is

$$u_m = U_m \exp[kj(n_i x_i - Vt)] \tag{3-1}$$

where k is the wave number, j the unit imaginary number, n_i the direction cosines of the normal to the wave front, U_m the displacement amplitude, and V the phase speed. If a small displacement is assumed, the constitutive equation of stress (σ_{ij}) and strain (ε_{ij}) tensors for a generally anisotropic material may be expressed in the form

$$\sigma_{ij} = C_{ijkl}\,\varepsilon_{kl} \tag{3-2}$$

where C_{ijkl} is the stiffness tensor of the material, and $\varepsilon_{kl} = u_{k,l} + u_{l,k}$. Substituting Equations (3-1) and (3-2) into the equation of motion for displacement in a perfectly elastic homogeneous anisotropic medium with no body force,

$$\frac{\partial \sigma_{ij}}{\partial x_j} = \rho \frac{\partial^2 u_i}{\partial t^2} \tag{3-3}$$

yields the following Christoffel's eigenvalue equation:

$$(C_{ijkl} n_i n_j - \rho V^2 \delta_{ik}) U_k = 0 \tag{3-4}$$

where δ_{ik} is the Kronecker delta and ρ the density of the material. If the contracted Voigt notation [11] is used to express the stress-strain relation in the form of the matrix equation, the stress-strain relationship for orthotropic materials, in which the 21 constants may be reduced to 9, is expressed in the form of

$$\begin{Bmatrix}\sigma_1\\ \sigma_2\\ \sigma_3\\ \sigma_4\\ \sigma_5\\ \sigma_6\end{Bmatrix}=\begin{bmatrix}C_{11} & C_{12} & C_{13} & 0 & 0 & 0\\ C_{12} & C_{22} & C_{23} & 0 & 0 & 0\\ C_{13} & C_{23} & C_{33} & 0 & 0 & 0\\ 0 & 0 & 0 & C_{44} & 0 & 0\\ 0 & 0 & 0 & 0 & C_{55} & 0\\ 0 & 0 & 0 & 0 & 0 & C_{66}\end{bmatrix}\begin{Bmatrix}\varepsilon_1\\ \varepsilon_2\\ \varepsilon_3\\ \varepsilon_4\\ \varepsilon_5\\ \varepsilon_6\end{Bmatrix} \tag{3-5}$$

where $[C_{ij}]$ is the stiffness matrix, and the subscripts 1,2,3 denote the principal material axes. Then, Equation (3-4) takes the form of

$$\begin{pmatrix}\Gamma_{11}-\rho V^2 & \Gamma_{12} & \Gamma_{13}\\ \Gamma_{12} & \Gamma_{22}-\rho V^2 & \Gamma_{23}\\ \Gamma_{13} & \Gamma_{23} & \Gamma_{33}-\rho V^2\end{pmatrix}\begin{Bmatrix}U_1\\ U_2\\ U_3\end{Bmatrix}=\begin{Bmatrix}0\\ 0\\ 0\end{Bmatrix} \tag{3-6}$$

where the Γ_{ij}s are so-called Christoffel's stiffnesses, given by

$$\begin{aligned}\Gamma_{11} &= n_1^2C_{11}+n_2^2C_{66}+n_3^2C_{55}\\ \Gamma_{22} &= n_1^2C_{66}+n_2^2C_{22}+n_3^2C_{44}\\ \Gamma_{33} &= n_1^2C_{55}+n_2^2C_{44}+n_3^2C_{33}\end{aligned}$$

and (3-7)

$$\begin{aligned}\Gamma_{12} &= n_1n_2(C_{12}+C_{66})\\ \Gamma_{23} &= n_2n_3(C_{23}+C_{44})\\ \Gamma_{13} &= n_1n_3(C_{13}+C_{55})\end{aligned}$$

A nontrivial solution of the homogeneous system of Equation (3-6) exists when the determinant of the square matrix vanishes, and it takes the form of the following determinantal equation:

$$\det\begin{vmatrix}\Gamma_{11}-\rho V^2 & \Gamma_{12} & \Gamma_{13}\\ \Gamma_{12} & \Gamma_{22}-\rho V^2 & \Gamma_{23}\\ \Gamma_{13} & \Gamma_{23} & \Gamma_{33}-\rho V^2\end{vmatrix}=0 \tag{3-8}$$

which is cubic in V^2 [85, 94].

In general, the components of the stiffness tensor for orthotropic symmetry are composed of 9 independent elastic constants, but this number may be further reduced

where there is more symmetry in the material. For example, since a unidirectional graphite/epoxy composite laminate could be considered as transversely isotropic, its stiffness matrix (3-9) holds true [11]:

$$\begin{bmatrix} C_{11} & C_{12} & C_{12} & 0 & 0 & 0 \\ C_{12} & C_{22} & C_{23} & 0 & 0 & 0 \\ C_{12} & C_{23} & C_{22} & 0 & 0 & 0 \\ 0 & 0 & 0 & (C_{22}-C_{23})/2 & 0 & 0 \\ 0 & 0 & 0 & 0 & C_{66} & 0 \\ 0 & 0 & 0 & 0 & 0 & C_{66} \end{bmatrix} \tag{3-9}$$

in which, only 5 elastic constants C_{11}, C_{22}, C_{12}, C_{23} and C_{66} are independent. Once the 5 stiffness components are known, the engineering elastic constants can be obtained in terms of compliance matrix $[S_{ij}] = [C_{ij}]^{-1}$:

(1) the axial and transverse Young's Moduli:

$$\begin{aligned} E_1 &= \frac{1}{S_{11}} = \frac{C}{C_{22}^2 - C_{23}^2}, \\ E_2 &= \frac{1}{S_{22}} = \frac{C}{C_{11}C_{22} - C_{12}^2} = E_3 \end{aligned} \tag{3-10}$$

(2) the shear moduli:

$$\begin{aligned} G_{12} &= \frac{1}{S_{66}} = C_{66} = G_{31}, \\ G_{23} &= \frac{1}{S_{44}} = C_{44} \end{aligned} \tag{3-11}$$

and (3) Poisson's ratios:

$$\begin{aligned} \nu_{12} &= \frac{C_{12}}{C_{22} + C_{23}}, \\ \nu_{23} &= \frac{C_{11}C_{23} - C_{12}^2}{C_{11}C_{22} - C_{12}^2}, \end{aligned} \tag{3-12}$$

where $C = (C_{22} - C_{23})[C_{11}(C_{22} + C_{23}) - 2C_{12}^2]$.

As seen in Equation (3-6), there are three different waves traveling with different velocities in an anisotropic material. These three waves are usually not pure modes since each wave generally has particle displacement components both parallel and perpendicular to the wave normal. However, one of these components is usually much larger than the other, and thus the wave with a large parallel component is called quasi-longitudinal (QL mode), whereas the other two waves with large perpendicular components are called quasi-shear (QS mode) [116].

Therefore, by making a sufficient number of measurements for different propagation directions, it is possible to determine all stiffness components of a composite. Of course, a detailed computation of stiffness components is tedious and requires a nonlinear least-square fit of the data to the predictions of a model for wave propagation.

3.2.2. Experimental technique

The determination of the elastic constants of a unidirectional laminate, which is the basic building block of composite laminates and structures, is especially important because this characterization allows the prediction of the properties of any multidirectional laminates [12]. A rectangular Cartesian coordinate system (x_1, x_2, x_3) attached to this unidirectional laminate is schematically shown in Figure 3-1. For the plane 2-3, which is the plane of transverse isotropy, thus, $n_1 = 0$, $n_2^2 + n_3^2 = 1$, Christoffel's characteristic equation (3-8) reduces to

$$(C_{22} - \rho V^2)(C_{44} - \rho V^2)(C_{66} - \rho V^2) = 0 \qquad (3\text{-}13)$$

The waves with the velocities of $(C_{22} / \rho)^{1/2}$ and $(C_{44} / \rho)^{1/2}$ are pure longitudinal and shear, respectively, and are polarized in the plane 2-3. The third wave with velocity of $(C_{66} / \rho)^{1/2}$ is also pure shear, but is polarized normal to the plane 2-3.

In the case of the plane 1-3, $n_1^2 + n_3^2 = 1$, $n_2 = 0$, the characteristic equation (3-8) can be then reduced to

$$(n_1^2 C_{66} + n_3^2 C_{44} - \rho V^2)[(n_1^2 C_{66} + n_3^2 C_{22} - \rho V^2)(n_1^2 C_{11} + n_3^2 C_{66} - \rho V^2) - n_1^2 n_3^2 (C_{12} + C_{66})^2] = 0 \quad (3\text{-}14)$$

The factor which is linear in V^2 leads to pure shear polarized normal to the plane 1-3. The solution of the factor which is quadratic in V^2 gives the velocities of two other waves which are, in general, quasi-longitudinal (QL) and quasi-shear (QS) and are polarized in the plane 1-3. Therefore, provided the measurement is made in both planes 1-3 and 2-3, a complete characterization will be possible since all the 5 constants are involved for these modes.

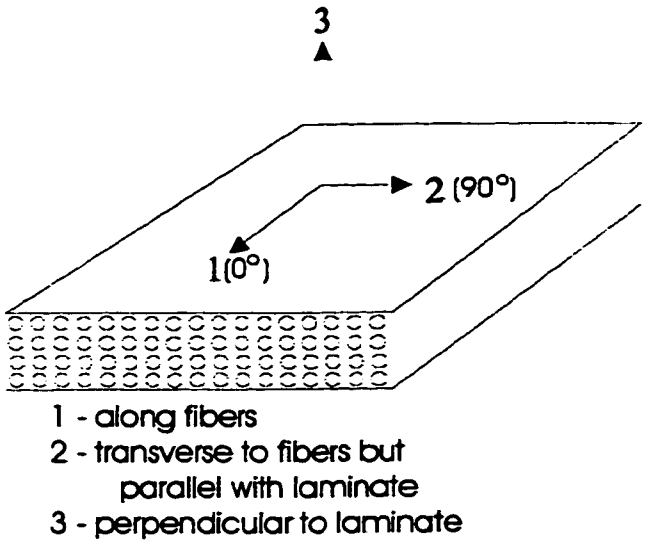

Figure 3-1 Coordinate system attached to a unidirectional laminate

Anisotropy of a composite may be characterized by ultrasonic immersion testing using the mode conversion phenomenon, as indicated in Figure 3-2. The phase velocities of the sample, which are directly related to the elastic properties of the sample, can be deduced from the measured time delay and the direction of energy flux by the line scanning with a receiving transducer. The temperature is monitored throughout the whole experiment.

Currently, the measured sample is a unidirectional laminate with transverse isotropy. Its slowness curve (inverse velocity curves) can be depicted by Figure 3-3 [87]. The plane 2-3 is a plane with transverse isotropy; it is analogous to that for an isotropic medium with three (not two) concentric circular sheets corresponding to pure-mode longitudinal and pure-mode shear propagation, in which the mode with pure shear, but polarized normal to the plane 2-3 cannot be generated by mode conversion. Meanwhile, in the plane 1-3, the mode with pure shear polarized normal to the plane 1-3 is not excited.

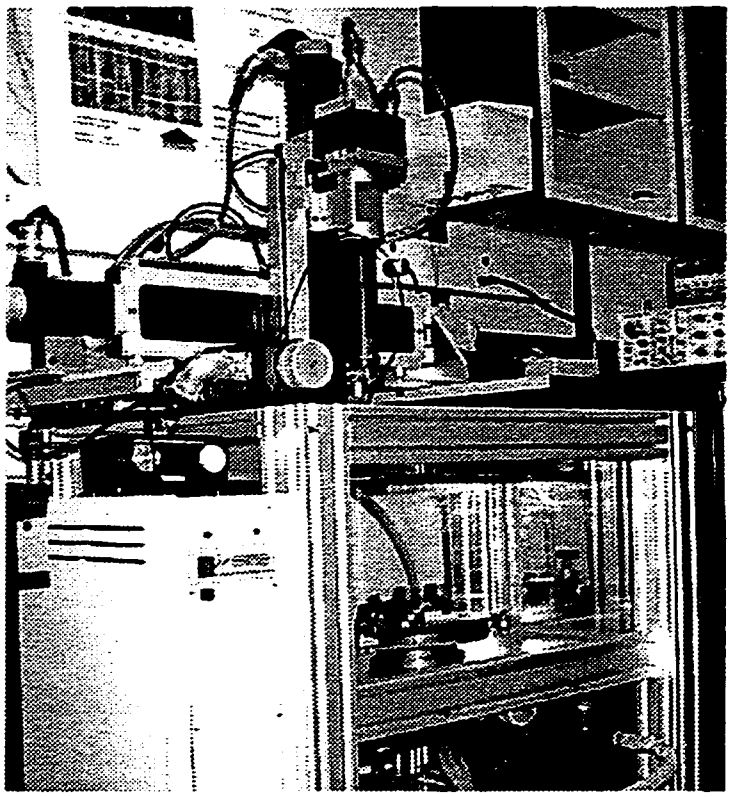

Figure 3-2 Immersion tank used for anisotropic measurement

Unidirectional laminates with the layup of 16-ply are selected for this study. The cure cycles are applied according to Section 2.1.3 in Chapter 2. The post-manufactured samples are mechanically cut into rectangular plates with approximate dimensions of 100 mm (L) x 100 mm (W) x 16 ply (T). The thickness of each sample is precisely measured with a micrometer. Their density and fraction of graphite fibers are tabulated in Table 2-3,

indicating that the fluctuation of the density of the samples and fraction of graphite fibers can be neglected.

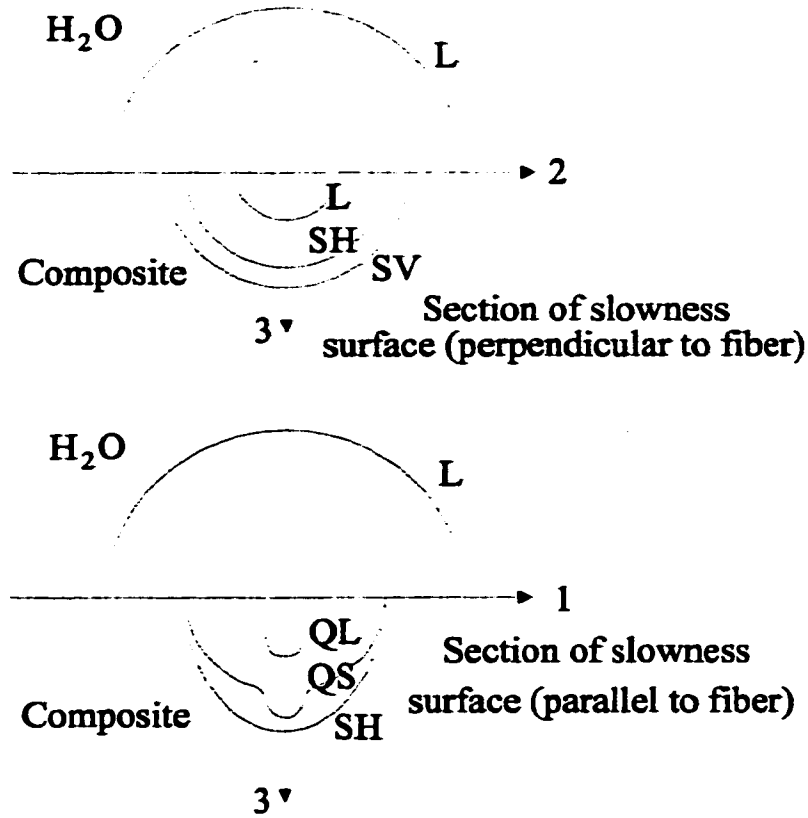

Figure 3-3 Slowness curves for a unidirectional Gr/Ep composite [87]

The measurement technique is described in Figure 3-4. A measured sample is held on a turntable, which can be adjusted to change the angles of incidence. A 5 MHz ultrasonic transducer is used to launch a wave beam toward the sample, and another identical ultrasonic transducer is used to collect the ultrasonic waves which are transmitted through the sample. The receiving transducer is mounted in a fixture attached to a computer-driven micropositioner which has three translational and two rotational degrees of freedom. The precision of ultrasonic measurement of anisotropic elastic constants is very sensitive to the alignments of the ultrasonic transducers, the measured sample and the positioners. The details are described in Appendix I. Afterward, the ultrasonic signals received are digitized at a sampling rate of 250 MHz, and averaged 10 times to increase the signal-to-noise (S/N) ratio.

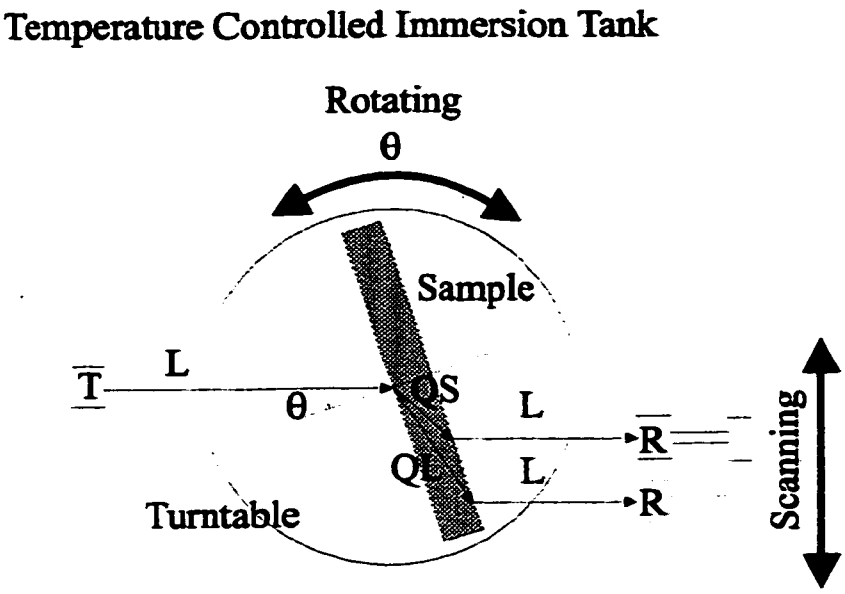

Figure 3-4 Schematic diagram of ultrasonic anisotropic measurement. T is the transmitting transducer, and R is the receiving transducer

The measurements are carried out in both planes 1-3 and 2-3 of the sample. When the plane 1-3 is the plane of incidence, the critical angle[1] of QL wave is near 10°, whereas when the plane 2-3 is the plane of incidence, the critical angle of QL wave is around 30°. The ultrasonic waveform *vs.* the angle of incidence is shown in Figure 3-5. For the plane 2-3, the circular pattern on the slowness of phase velocity will be experimentally observed, indicating that the phase velocities for QL and QS modes are constants; therefore, they are transversely isotropic. This validates the assumption that unidirectional laminates currently used can be regarded as transversely isotropic material.

[1] The critical angle condition for anisotropic material is that the propagation of the energy flux of the elastic wave in the solid be parallel to the surface (90° refraction angle for energy flux), which does not necessarily mean 90° refraction for the phase velocity. (Henneke II, E. G. and G. L. Jones, J. Acoust. Soc. Am., **59**, 1976:204-205)

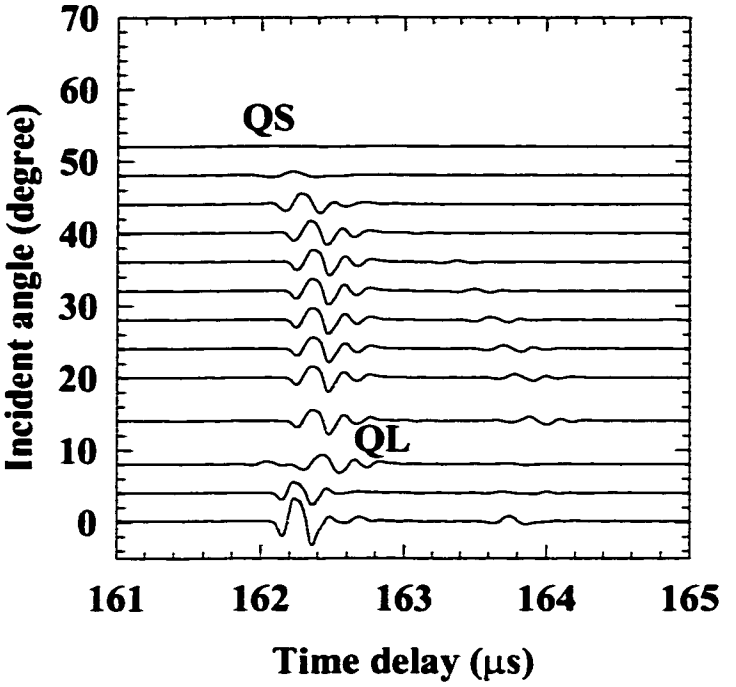

(a)

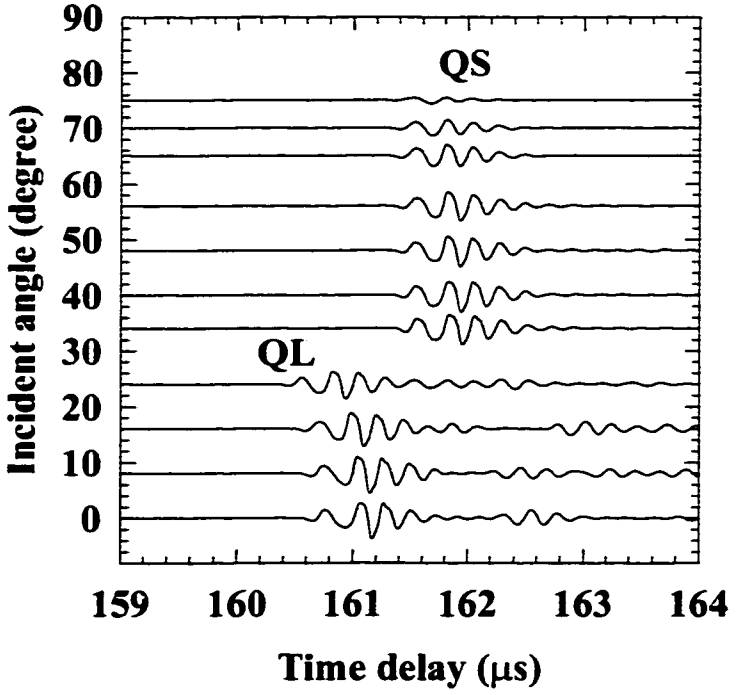

(b)

Figure 3-5 Ultrasonic waveforms obtained from a unidirectional AS4/3501-6 Gr/Ep laminate cured at 176°C for 2 hrs. in (a) incidence plane 1-3 (b) plane 2-3

During the measurements, the phase velocity $V_p(\theta_r)$ in the sample for wave propagation at refraction angle θ_r can be deduced as a function of incident direction in terms of the time-of-flight measurement [80]:

$$V_p(\vartheta_r) = \left(\frac{1}{V_0^2} - \frac{\Delta t \cos \vartheta_i}{h V_0} + \frac{(\Delta t)^2}{4h^2} \right)^{-\frac{1}{2}} \tag{3-15}$$

with refraction angle

$$\theta_r = \sin^{-1}\left(\frac{V_p(\theta_r) \sin \theta_i}{V_0} \right) \tag{3-16}$$

where $\Delta t = t_0 - t(\theta_i)$ is the time-of-flight difference between the reference t_0 (through fluid) and through the sample $t(\theta_i)$ (at angle θ_i), and θ_i is the incidence angle, as illustrated in Figure 3-6, and where h is the thickness of the sample and V_0 is the velocity of the ultrasonic wave in fluid. Accurate estimation of phase velocities for each mode along its own direction can thus be made.

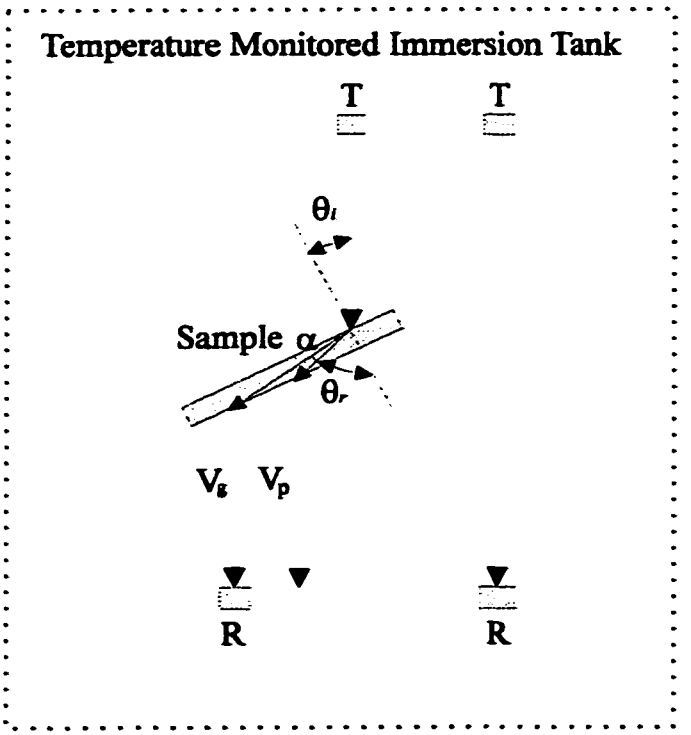

Figure 3-6 Schematic diagram of fluid-reference ultrasonic testing where V_g and V_p denote the group and phase velocities, respectively [80]

Varying the incidence angle according to Snell's refraction law provides numerous directions from QL and QS modes in the sample. The elastic properties of the composite can then be reconstructed by minimizing the sum of the squares of the deviations between the experimental and the calculated velocities, considering the elastic constants as variables, *e.g.*

$$\min \sum_{i=1}^{m} \left(\frac{1}{\left(V_i^e\right)^2} - \frac{1}{\left(V_i^c\right)^2} \right)^2 \tag{3-17}$$

where m is the number of measurements of velocities in different directions, V^e and V^c are the experimental and the calculated phase velocities, respectively. The full set of elastic constants can be, therefore, restructured from the phase velocities [94].

The accuracy of the measured elastic constants is a major concern. In the current experimental setup, during the ultrasonic scan of the plane 1-3, the incidence angle cannot be larger than the critical angle over which the incidence wave energy is totally reflected from the sample surface. Since C_{11} does not play a major role in the range of the angles scanned, due to the fact that its contribution is mostly concentrated around the 1-direction, its value cannot be accurately evaluated. In addition, G_{23} is dependent on C_{44}, which is only related with the shear wave in the plane 2-3. Therefore, its standard deviation is generally less than 1%. Furthermore, E_2 is determined by

$$E_2 = \frac{(C_{22} - C_{23})\left[(C_{22} + C_{23}) - 2C_{12}\left(\frac{C_{12}}{C_{11}}\right)\right]}{C_{22} - C_{12}\left(\frac{C_{12}}{C_{11}}\right)} \tag{3-18}$$

where C_{22} is only related to the longitudinal wave in the plane 2-3. The error associated with this value is less than 0.5%. Because of the high anisotropy of uniaxially aligned, high-modulus graphite fibers, $C_{12}/C_{11} \ll 1$, the inaccuracy in C_{11} has thus little influence on the accuracy of E_2 evaluation. Thus, E_2 may be evaluated with a reasonable accuracy.

On the other hand, owing to the insensitivity of relative wave velocity to the magnitude of G_{12}, the uncertainty of this component is large.

Moreover, during the measurements of acoustic velocities for anisotropic materials, it is important to note the difference between phase velocity V_p and group velocity V_g, referred to as the propagation velocity of energy flux. For an anisotropic material, wave propagation direction does not generally coincide with the direction of energy flux due to the normal-shear coupling [116]. The confusion between group velocity V_g and phase velocity V_p may raise serious questions about the correctness of the technique. Kim [88-90] has developed an algorithm to restructure all elastic constants from V_gs. This provides another approach to evaluate the anisotropy of a composite.

The next concern when dealing with fibrous composites is a frequency-dependent propagation velocity because of inhomogeneity. Ultrasonic attenuation of fibrous composite materials is generally high. Thus, effects of both velocity dispersion and frequency-dependent attenuation probably cause changes in a pulse shape as it propagates through a composite, making time delay measurement slightly difficult.

The last, but not least, concern is that one must distinguish between the macroscopic elastic constants and those of the micro-structural components, and in order to measure the macroscopic constants, the probing wavelength must exceed by a sufficient margin of the macroscopic constants. Hence, a working frequency, for example, 5.0 MHz ultrasonic transducer, which corresponds to a wavelength of about 0.5 mm, may be suitable for the current measurement.

3.2.3 Results and discussion

The dependence of engineering elastic moduli of Hercules 3501-6 epoxy and AS4/3501-6 Gr/Ep composite on cure temperature is shown in Figure 3-7. These figures clearly indicate that while increasing the cure temperature up to 176°C, the moduli of the composite gradually increase, but when exceeding 176°C, the moduli exhibit a small

drop. The reason for this drop is not so clear. Lee *et al.* [117] showed that over-cure due to temperature over-shoot may deteriorate the final moduli of the composite. However, it is not sure whether their conclusion is suited for our case. Obviously more experimental study is needed. On the other hand, as indicated in Figure 3-7(a), the variation of moduli of the epoxy with cure temperature monotonically increases throughout the whole cure temperature range, from 146°C to 186°C. Furthermore, when cured at the temperature of 176°C, the dependence of the engineering elastic moduli of the epoxy and composite on cure time is shown in Figure 3-8. After curing for one hour at 176°C, the moduli of the composite still maintain a detectable increase of 5% during another 1 hour and 20 minutes curing, even though the degree of cure, at that period, varies only little. The mechanism for such an increase in moduli of the composite after nearly full development of degree of cure is not so clear. One possible reason may be ascribed to the contribution of the development of interface between graphite fibers and epoxy matrix. On contrary, the moduli of the epoxy, after curing for one hour and 20 minutes, show no change from further curing, as shown in Figure 3-8(a).

Obviously, cure temperature is a more critical process parameter than cure time. The experimental results also indicate that the manufacturer's recommended cure cycle applied for AS4/3501-6 Gr/Ep prepregs is acceptable for the present processing.

3.2.4 Line-Focus-Beam (LFB) acoustic microscope

In order to obtain in-plane properties of a composite laminate, for example C_{11}, another ultrasonic measurement method, the Line-Focus-Beam acoustic microscope (LFB) [100] illustrated in Figure 3-9(a), has been introduced. This technique measures the velocities of the leaky surface-skimming compressional wave (LSSCW), which is assimilated to a longitudinal wave propagating along the surface of the sample. LSSCW can be excited and received by defocusing, *i.e.* reducing the distance between the focused (lens) transducer and the sample surface to values shorter than the focal length. In that case, the focused transducer radiates an angular spectrum of plane waves, one of which is

incident on the interface at the longitudinal wave critical angle. Part of the incident energy is thus efficiently converted into a surface skimming compressional wave which propagates along the surface of the sample. This wave is shortly converted back into a wave propagating in the surrounding water and then picked up by the transducer.

If D denotes the reflected wave and θ_{LSSCW} denotes the critical angle of a LSSCW, from each wave's propagation in Figure 3-9(a), the arrival times of pulses D and LSSCW are

$$t_D = \frac{2(F-z)}{V_W} \tag{3-19}$$

and

$$t_{LSSCW} = \frac{2(F - \frac{z}{\cos\theta_{LSSCW}})}{V_W} + \frac{2z\tan\theta_{LSSCW}}{V_{LSSCW}} \tag{3-20}$$

respectively [100], where

$$\theta_{LSSCW} = \sin^{-1}\left(\frac{V_W}{V_{LSSCW}}\right) \tag{3-21}$$

is the critical angle, F is the focal length of the transducer, z is the defocus distance from the focal plane, V_W is the longitudinal wave velocity of the coupling water, and V_{LSSCW} is the LSSCW velocity of the sample. For a given sample, θ_{LSSCW} and V_W are constants. It is noted that Equations (3-19) and (3-20) exhibit linear relationships between the distance z and the arrival time t_D and t_{LSSCW}. From the two slope relationships of z *vs.* t_{LSSCW}, the V_W and V_{LSSCW} of the sample can be determined by

$$V_W = -2\frac{\Delta z}{\Delta t_D} \tag{3-22}$$

and

$$V_{LSSCW} = \left[\frac{1}{V_W^2} - \frac{1}{4}\frac{1}{\left(\frac{\Delta z}{\Delta t_{LSSCW}}\right)^2}\right]^{1/2} \tag{3-23}$$

Thus, the V_{LSSCW} can be deduced from the relations between the arrival time of the wave and the defocusing distance. For example, the V_{LSSCW} (=2757 m/s at 10 MHz) of Hercules 3501-6 epoxy cured for 2 hours at 176°C can be obtained, as shown in Figure 3-9(b).

In order to precisely retrieve all elastic constants of a thin composite laminate, the experimental combination of both methods illustrated in Figures 3-4 and 3-9(a) is suggested. Since C_{11} is the modulus related to the graphite fiber dominant direction, thus not sensitive to variation in cure conditions, the experimental determination of the variation of the leaky wave velocities in the composite cured at different conditions will not be demonstrated here.

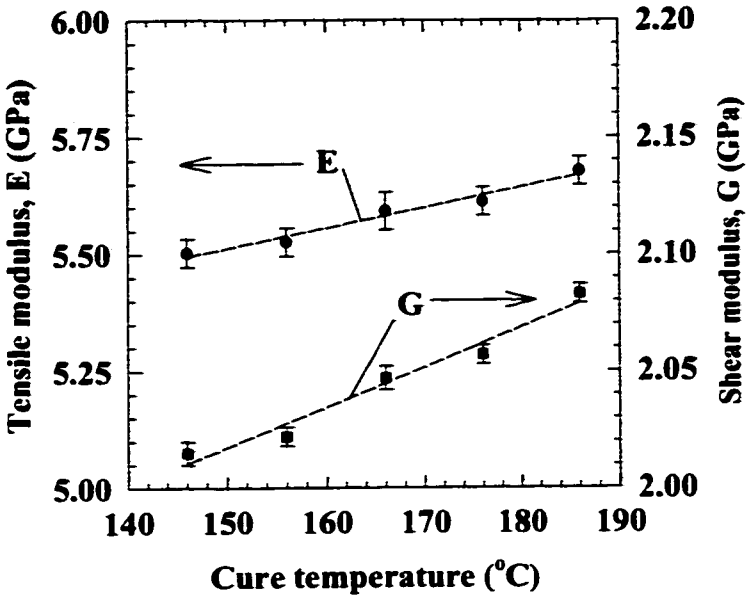

(a)

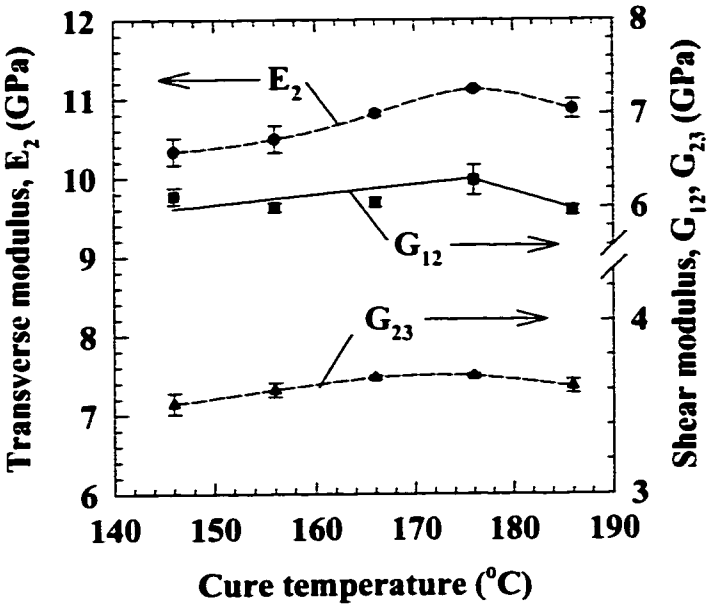

(b)

Figure 3-7 Elastic moduli *vs.* cure temperature for (a) Hercules 3501-6 epoxy, and (b) AS4/3501-6 Gr/Ep composite

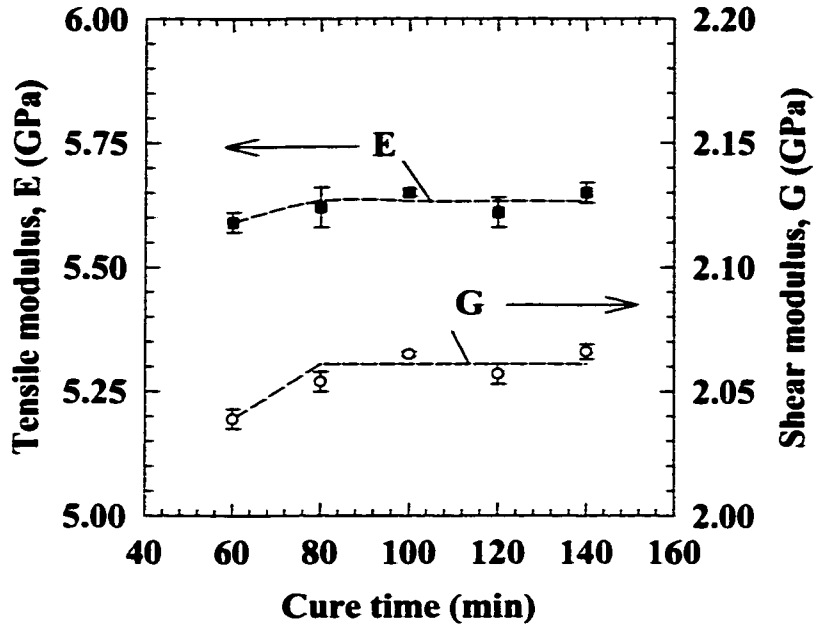

(a)

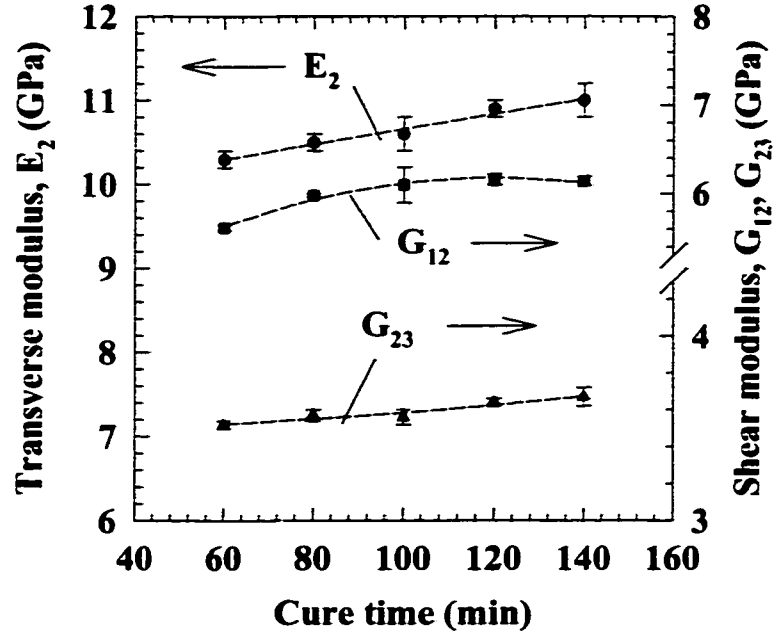

(b)

Figure 3-8 Elastic moduli *vs.* cure time for (a) Hercules 3501-6 epoxy, and (b) AS4/3501-6 Gr/Ep composite

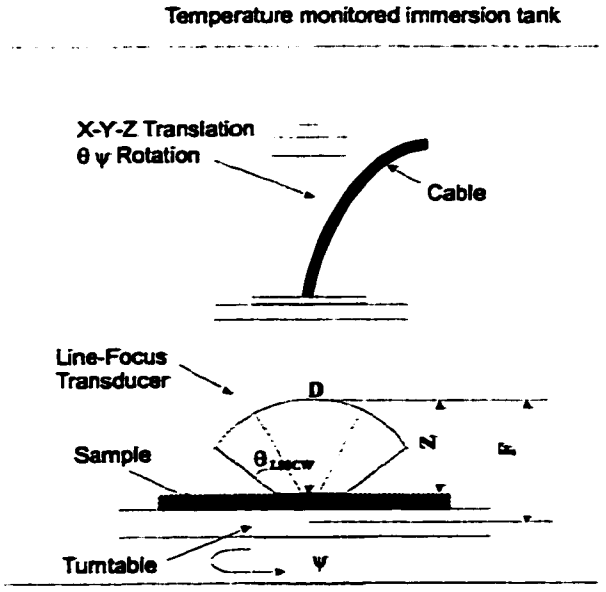

(a)

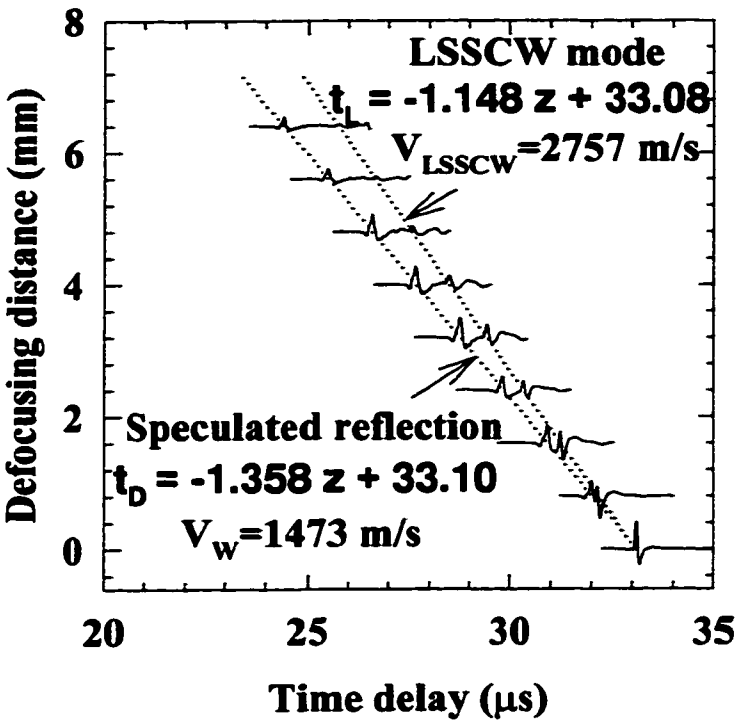

(b)

Figure 3-9 Schematic diagram of (a) LFB lens [100] and (b) waveforms and defocusing distance as a function of arrival time for Hercules 3501-6 epoxy cured at 176°C for 2 hrs.

3.3 Ultrasonic dispersion and attenuation characterization

3.3.1 Experimental technique

Ultrasonic through-thickness dispersion and attenuation measurements are based on a spectroscopic analysis of broadband acoustic pulses [107]. A numerical Fourier analysis technique is used to evaluate the spectrum of the response over a wide range of frequencies. Both the phase velocity and attenuation measurements are made with the same experimental setup. The whole measurement system, as illustrated in Figure 3-10, is kept in a temperature monitored chamber where the temperature variation is less than ± 0.5°C. The measured samples are carefully polished in order to avoid bias due to surface roughness or non-parallelism. The thickness of the samples is precisely measured with a micrometer.

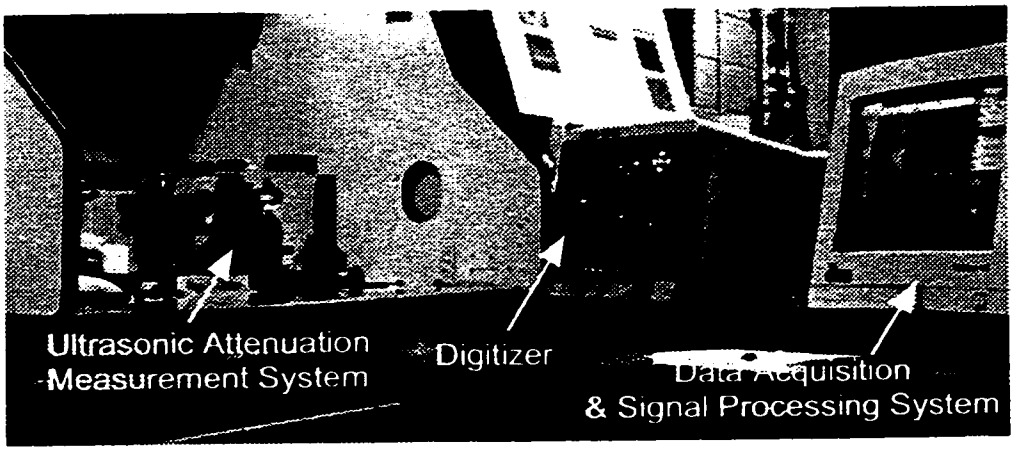

Figure 3-10 Actual ultrasonic dispersion and attenuation measurement system

Currently, two setups are used for different frequency ranges, in order to satisfy the far-field condition. In the setup of Figure 3-11, a pair of MR 203 Pulser/101 Receiver from MetroTek Inc. (Kennewick, WA) is used to generate and receive ultrasonic pulses, whereas in the setup of Figure 3-12, Panametrics 5601 Pulser/Receiver (Waltham, MA) used to generate and receive ultrasonic pulses. The repetition rate for both setups is set to 1 kHz. The received signals are displayed on a Tektronix 7854 digital oscilloscope (Beaverton, OR), and then acquired by digital sampling in a LeCroy 8013A modular data-

acquisition system (LeCroy Co., Chestnut Ridge, NY), and averaged 100 times to increase the S/N ratio. The data are then transferred, over a GPIB interface, to a PC computer, where further signal processing is performed. The whole data-acquisition and subsequent signal processing are handled by a computer running LabVIEW®-based self-developed application programs.

The measurement procedure usually includes: (1) cleaning the measured sample; (2) carefully aligning the amplitude of the reference echo from the front surface of the measured sample to the maximum, by using an RF detector branch and scope plug-in with DC offset, in order to have the best possible sensitivity; (3) digitizing each echo individually in order to limit the quantification error; and (4) processing the signals in order to obtain ultrasonic dispersion and attenuation of the measured sample.

3.3.2 Spectroscopic analysis of ultrasonic dispersion and attenuation

The pulse/echo technique in Figure 3-11 is to use a single broadband transducer with the central frequency of 5 MHz, at normal incidence, to excite a sample immersed in water. Usually the time history of the signal reflected from a sample with thickness h consists of the echo A reflected from the front face of the sample, followed by a family of consecutive reflections B, C from the back face of the sample with one and two round-trips. The time delay between two consecutive reflections results from twice the thickness of the sample, as the wave must traverse the sample twice to be received back by the probe. Furthermore, an echo R coming from the water/reference sample interface is measured for diffraction and reflection correction. In order to enhance the strength of echoes B and C, the sample is air-backed. Echo A is out of phase with echoes B and C, as indicated in Figure 3-13(a), because the impedance of the sample is higher than that of air. A cross-correlation algorithm is used to determine the time delay between two consecutive reflection echoes. Ultrasonic through-thickness dispersion and attenuation, over a frequency range of 3 to 7 MHz, can be obtained by evaluating the phase and amplitude spectra of echoes B and C.

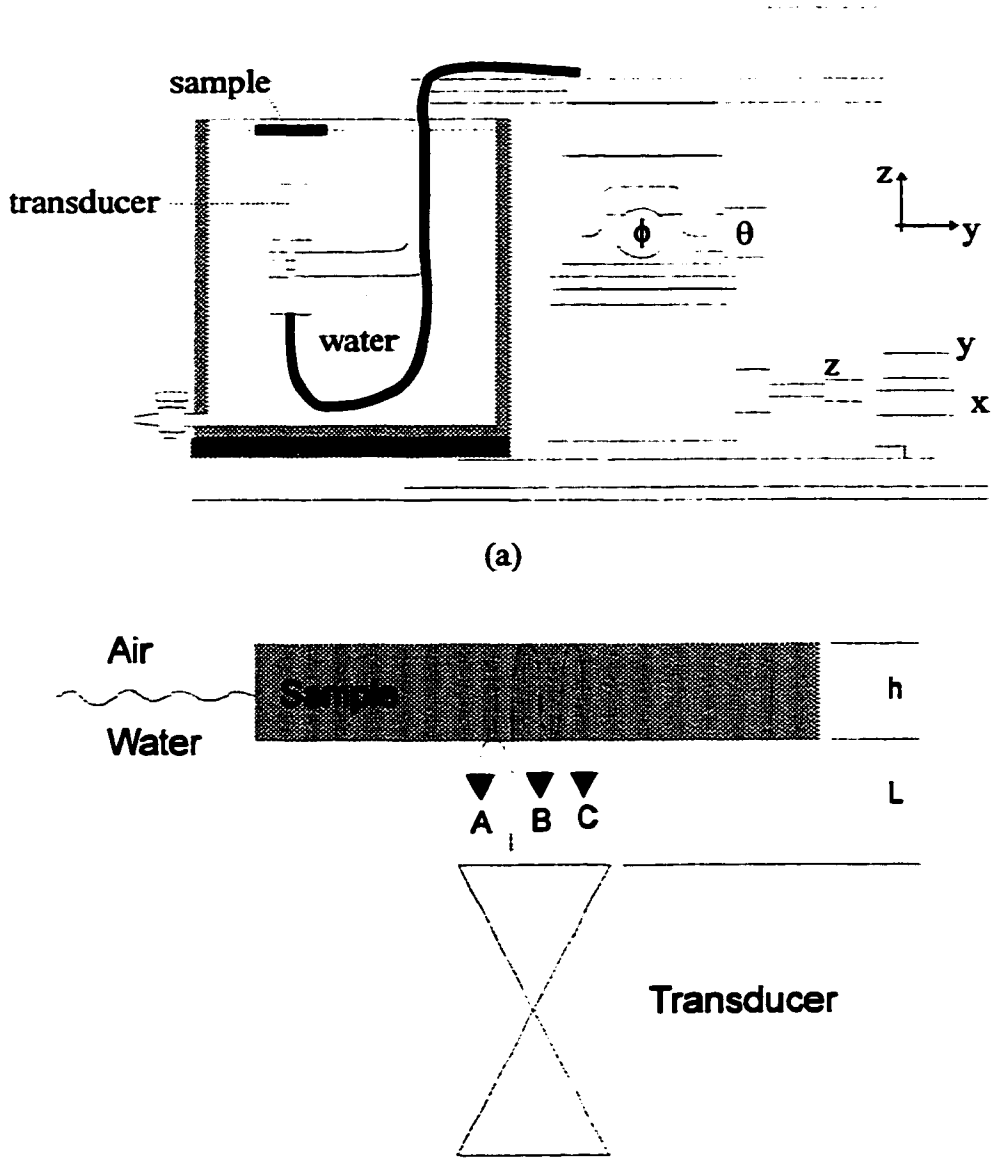

Figure 3-11 Schematic diagram of ultrasonic phase velocity and attenuation measurement (5 MHz ultrasonic transducer)

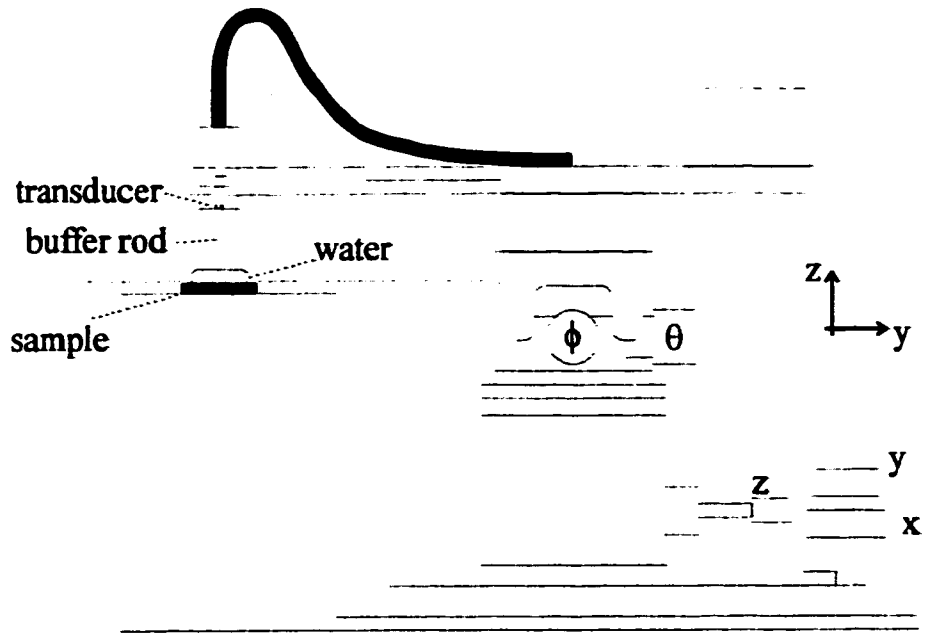

(a)

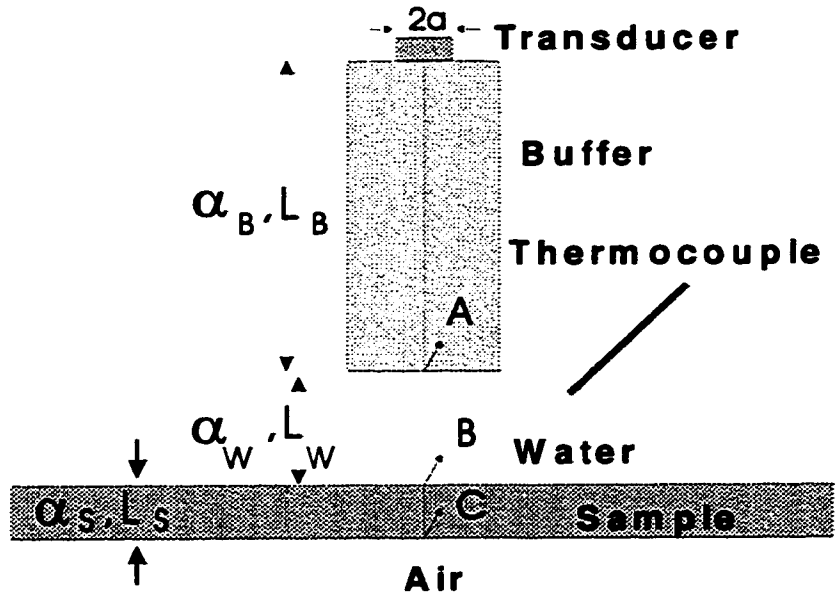

(b)

Figure 3-12 Schematic diagram of ultrasonic attenuation measurement (50 MHz ultrasonic transducer)

The pulse/echo technique in Figure 3-12 is used to measure ultrasonic attenuation in the frequency range of 20 to 80 MHz by using a broadband transducer with a central

frequency of 50 MHz. Usually four echoes are acquired and digitized, as indicated in Figure 3-13(b): (a) echo A coming from the buffer rod/water interface, (b) echo B coming from the water/measured sample front interface, (c) echo C coming from the measured sample/air backing interface, and (d) echo R coming from the water/reference sample interface for diffraction and reflection correction.

(a) Experimental setup in Figure 3-11

When an ultrasonic pulse, being a superposition of many different frequencies, propagates in a composite, the viscoelastic nature of the sample will cause ultrasonic velocity dispersion and attenuation.

A linear system can support a one-dimensional plane wave in the form of $e^{j(k(\omega)x-\omega t)}$, where k(ω) is the effective wave-number, and ω is the circular frequency of the incident wave. To describe the above behavior one can define a complex wave-number k(ω), where the real part is dispersive, related to the frequency-dependent phase velocity V(ω), while the imaginary part is attenuative, related to the frequency-dependent attenuation, α(ω) [118,119]. This relation can be written as

$$k(\omega) = \frac{\omega}{V(\omega)} + j\,\alpha(\omega) \tag{3-24}$$

Then, a broadband longitudinal pulse u(x,t), propagating in a positive direction, can be expressed as a linear combination of all plane harmonic waves,

$$u(x,t) = \frac{1}{2\pi}\int_{-\infty}^{+\infty} F_0(\omega) e^{j(k(\omega)x-\omega t)}\, d\omega \tag{3-25}$$

where $F_0(\omega)$ is the Fourier transform of u(0,t).

The time domain technique, however, is unable to cope with a dispersive medium, where the pulse changes its shape as it propagates. This problem should usually be studied in the frequency domain. Therefore, a Fast Fourier Transform (FFT) is applied to Equation (3-25), yielding:

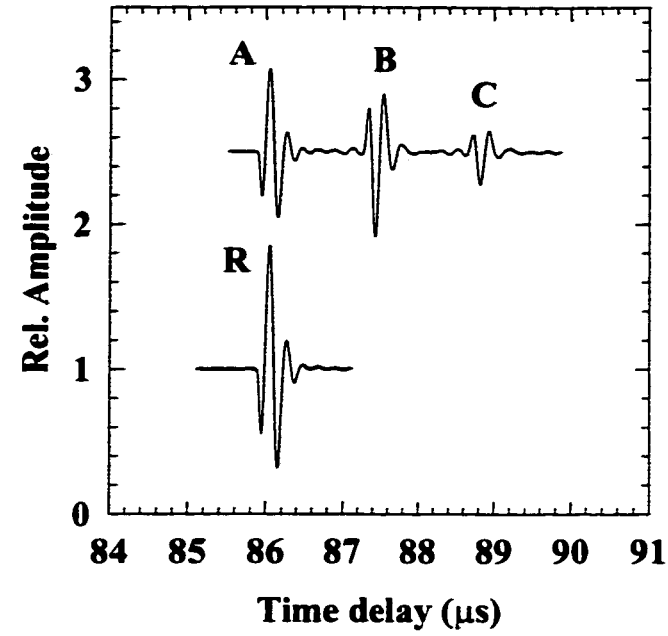

(a)

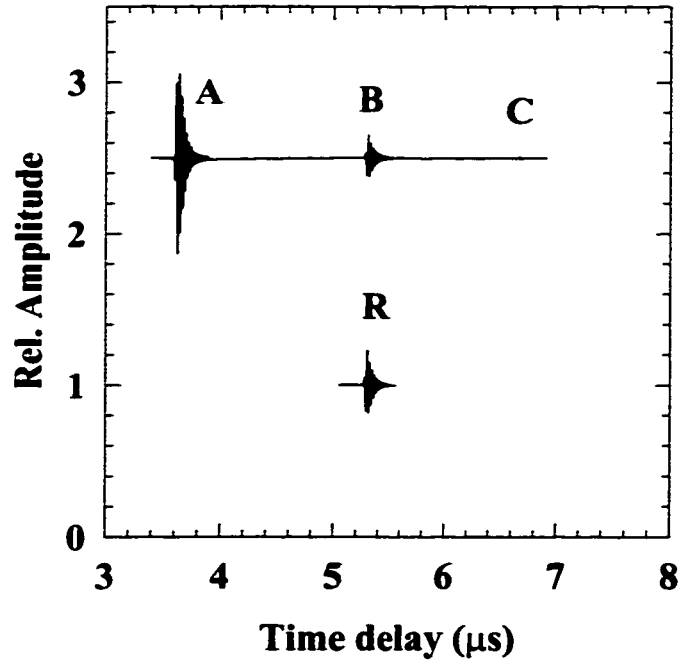

(b)

Figure 3-13 Ultrasonic waveforms obtained from the setups in (a) Figure 3-11, and (b) Figure 3-12

$$F(u(x,t)) = F_0(\omega)\exp[-\frac{\omega x}{V(\omega)}]\exp[-\alpha(\omega)x] \tag{3-26}$$

The measured attenuation contains loss such as diffraction and reflection, in which the loss associated with acoustic-impedance mismatch at the boundaries of a sample may be corrected by using the expressions in the Appendix of Krautkramer and Krautkramer's textbook [120], while the loss caused by diffraction (beam-spread) of a ultrasonic beam from the finite aperture of the ultrasonic transducer can be corrected by Rogers and Van Buren's theory [121]:

$$D_L(s) = 1 - e^{-j\left(\frac{2\pi}{s}\right)}\left[J_0\left(\frac{2\pi}{s}\right) + jJ_1\left(\frac{2\pi}{s}\right)\right] \tag{3-27}$$

where D_L is diffraction correction, J_0 and J_1 refer to the Bessel function of the first kind, and $s = \frac{2\pi z}{ka^2}$, where z is the distance from the transducer, while $k = \frac{\omega}{V(\omega)}$ is the wave vector of the ultrasonic wave and a is the transducer radius. Currently, the reflection correction can be made by measuring ultrasonic low-loss synthetic silica glasses of C-7940 (Corning Co.), which has acoustic properties of V_L = 5933 m/s and ρ = 2201.9 kg/m^3, as a reference sample.

Hence, "A", "B", "C" and "R" denote the corresponding amplitudes of echoes A, B, C and R, respectively, R_S, R_R the reflection coefficients for the water/tested sample interface and the water/reference sample interface, respectively, and Z_R, Z_W acoustic impedance of the reference sample and water, respectively. Moreover, the water behaves in a non-attenuative, non-dispersive manner, *i.e.* its wave number k(w) is real and phase velocity $V_w = \frac{\omega}{k(\omega)}$ is a constant, then for echoes A, B, C and R, one can get

$$F(u_A) = A(\omega) = F_0(\omega)R_S D_1(\omega)e^{-j\omega\frac{2L}{V_W}} \tag{3-28}$$

$$F(u_B) = B(\omega) = F_0(\omega)(1-R_S^2)D_2(\omega)e^{-2\alpha(\omega)h}e^{-j\omega\left[\frac{2L}{V_W}+\frac{2h}{V_S}\right]} \tag{3-29}$$

$$F(u_C) = C(\omega) = F_0(\omega)(1-R_s^2)R_s D_3(\omega)e^{-4\alpha(\omega)h}e^{-j\omega[\frac{2L}{V_W}+\frac{4h}{V_S}]} \tag{3-30}$$

and

$$F(u_R) = R(\omega) = F_0(\omega)R_R D_1(\omega)e^{-j\omega\frac{2L}{V_W}} \tag{3-31}$$

where $\alpha(\omega)$ is the ultrasonic attenuation coefficient in the sample, and h the thickness of the sample. $D_1(\omega)$, $D_2(\omega)$ and $D_3(\omega)$ are diffraction corrections for echoes A, B and C, given by

$$D_1(\omega) = D_0\left[\frac{4\pi V_W L}{\omega a^2}\right] \tag{3-32}$$

$$D_2(\omega) = D_0\left[\frac{4\pi}{\omega a^2}(V_W L + V_S h)\right] \tag{3-33}$$

and

$$D_3(\omega) = D_0\left[\frac{4\pi}{\omega a^2}(V_W L + 2V_S h)\right] \tag{3-34}$$

where $D_0(s)$ is given by Equation (3-27) [121].

In Equations (3-28) and (3-31), the reflection correction can be evaluated by

$$R_S = R_R\frac{A(\omega)}{R(\omega)} \tag{3-35}$$

in which

$$R_R = \frac{Z_R - Z_W(T^oC)}{Z_R + Z_W(T^oC)} \tag{3-36}$$

Furthermore, from Equations (3-29) and (3-30), it can be obtained that

$$\frac{C(\omega)}{B(\omega)} = \frac{R_S D_3(\omega)}{D_2(\omega)}e^{-2\alpha(\omega)h}e^{-j\omega\frac{2h}{V_S}} \tag{3-37}$$

hence, the corresponding phase spectrum is

$$-\phi_c + \phi_B = -\Delta\phi(\omega) = -\omega\frac{2h}{V_s} \tag{3-38}$$

and thereafter the phase velocity can be calculated from the expression

$$V_s = \frac{2h\omega}{\Delta\phi(\omega)} \tag{3-39}$$

where $\Delta\phi(\omega)$ is the phase shift between echoes B and C. Equation (3-39) does not consider the phase bias which may be induced by diffraction, reflection or other unknown factors. Moreover, in the phase shift measurement, there is always $\alpha \pm 2\pi m$ uncertainty in $\Delta\phi(\omega)$, from lack of knowledge about the exact number of wavelengths in the wave path. However, it is understood that the group velocity V_g (velocity of the wave energy), which is directly measurable in the measurements, can be derived from the phase velocity through the relation $V_g(\omega) = V^2(\omega)/[V(\omega) - \omega dV(\omega)/d\omega]$ [116]. Here, the m value is then chosen to specify that the group velocity derived from the phase velocity $V(\omega)$ is the measured group velocity through the relation $h/\Delta t$, where Δt is the time-of-flight of the ultrasonic pulses traveling through the thickness h of the sample.

Once the phase velocity of the sample is determined, its through-thickness attenuation can be evaluated by

$$\alpha(\omega) = -\frac{10}{h}\log\left[\frac{C(\omega)}{D_3(\omega)}\Big/\frac{B(\omega)}{D_2(\omega)}R_S\right] \tag{3-40}$$

where α is expressed in dB per h unit.

(b) Experimental setup in Figure 3-12

Using a similar analytical approach, the through-thickness ultrasonic attenuation of the sample in Figure 3-12 can be evaluated by

$$\alpha(\omega) = -\frac{10}{h}\log\left[\frac{C(\omega)}{D_3(\omega)}\Big/\frac{B(\omega)}{D_2(\omega)}\cdot\frac{R_s}{1-R_s^2}\right] \tag{3-41}$$

in which

$$R_S = R_R \cdot \frac{B(\omega)}{R(\omega)} \tag{3-42}$$

and

$$R_s = \frac{Z_R - Z_W(T^oC)}{Z_R + Z_W(T^oC)} \tag{3-43}$$

where R_S and R_R are the reflection coefficients of the water/sample interface and the water/ reference sample interface, respectively. Diffraction correction may be made by

$$D_2(\omega) = D_0\left[\frac{4\pi}{\omega a^2}(V_B L_B + V_W L_W)\right] \tag{3-44}$$

and

$$D_3(\omega) = D_0\left[\frac{4\pi}{\omega a^2}(V_B L_B + V_W L_W + V_S h)\right] \tag{3-45}$$

where V_B, V_W and V_S correspond to acoustic velocities in the buffer rod, water and the measured sample, respectively, while L_B, L_W and h are the lengths of the buffer rod and the water buffer, and the thickness of the measured sample, respectively.

3.3.3 Results and discussion

The current results demonstrate that the correlation between the through-thickness ultrasonic dispersion and curing conditions of Hercules 3501-6 epoxy and AS4/3501-6 Gr/Ep composite is not so obvious. All the samples evaluated show a behavior similar to the one plotted in Figure 3-14, which exhibits the existence of a very low dispersion in the given frequency range.

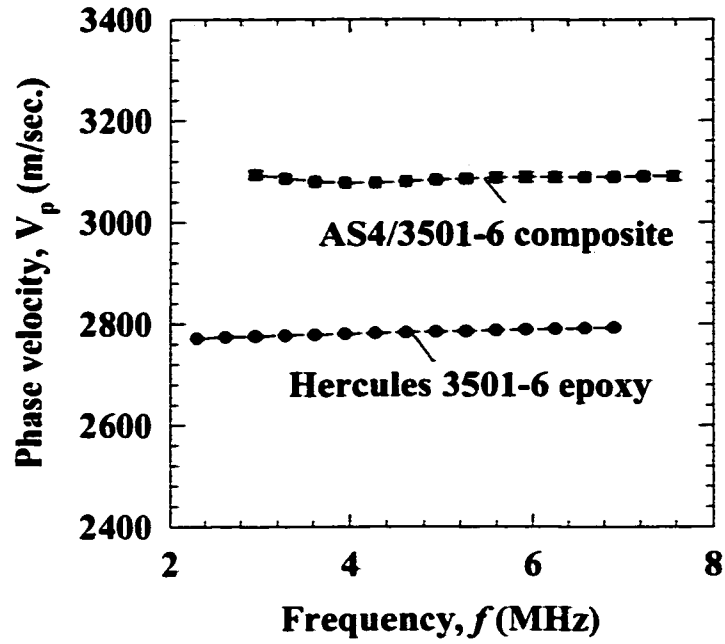

Figure 3-14 Dependence of ultrasonic dispersion of Hercules 3501-6 epoxy and AS4/3501-6 Gr/Ep composite cured at 176°C for 2 hrs.

Similarly, the ultrasonic attenuation and curing conditions are not strongly correlated, as indicated in Figure 3-15. Figure 3-16 shows the through-thickness attenuation spectra obtained from Hercules 3501-6 epoxy and AS4/3501-6 Gr/Ep composite cured for 2 hours at 176°C. In this Figure, the attenuation is plotted in a log-log graph. This technique is convenient for identifying any power-law dependence of the attenuation on frequency, since the slope of the plotted curve is proportional to the exponent of the dependence. It can be observed that over the frequency range of 3 to 8 MHz, the epoxy and composite have almost the same frequency dependence, proportional to f^n (n = 1.3 to 1.4). This indicates that the mechanism responsible for the ultrasonic attenuation is most likely dominated by the viscoelastic contribution, which is essentially the same in both types of sample. At higher frequency range (20 to 40 MHz), the n is much higher in the composite than in the epoxy. This suggests that when the frequency increases, the wavelength decreases and becomes shorter than the ply thickness in the composite. The inhomogeneities of the composite laminate then become a major source of the ultrasonic loss caused by scattering.

3.4 Summary

The ultrasonic evaluation of Hercules 3501-6 epoxy and AS4/3501-6 Gr/Ep composite indicates that:

(1) The moduli of Hercules 3501-6 epoxy monotonically increase with increasing cure temperature, whereas the moduli of AS4/3501-6 Gr/Ep composite show maximum value around the recommended cure temperature (176°C). Also, the moduli of the composite monotonically increase with increasing cure time at 176°C, whereas the moduli of the epoxy, after being cured for one hour and 20 minutes at 176°C, reaches a plateau.

(2) The ultrasonic through-thickness velocity dispersion and attenuation of the epoxy and composite are less sensitive to variation in cure conditions than elastic constants in the present study. Furthermore, over 2 to 8 MHz frequency range, the measured ultrasonic through-thickness phase velocities of the epoxy and composite exhibit little dispersion. The study of the ultrasonic attenuation mechanism reveals that over a lower frequency range of 3 to 8 MHz, the viscoelastic attenuation is dominant in the composites, while over a higher frequency range of 20 to 40 MHz, fiber scattering plays a predominant role.

In short, ultrasonic testing is an effective technique to evaluate the elastic properties of composites processed by different cure conditions. The sensitivity of the measurement is much higher than the conventional mechanical technique. However, ultrasonic velocity dispersion and attenuation may not be suitable to characterize the variation of mechanical properties of the composite caused by different cure conditions, because of their low sensitivity in this case.

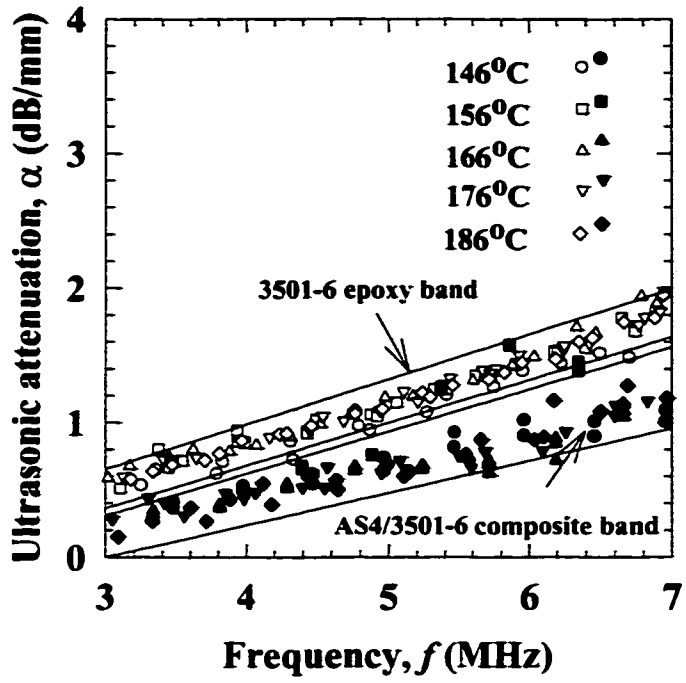

(a)

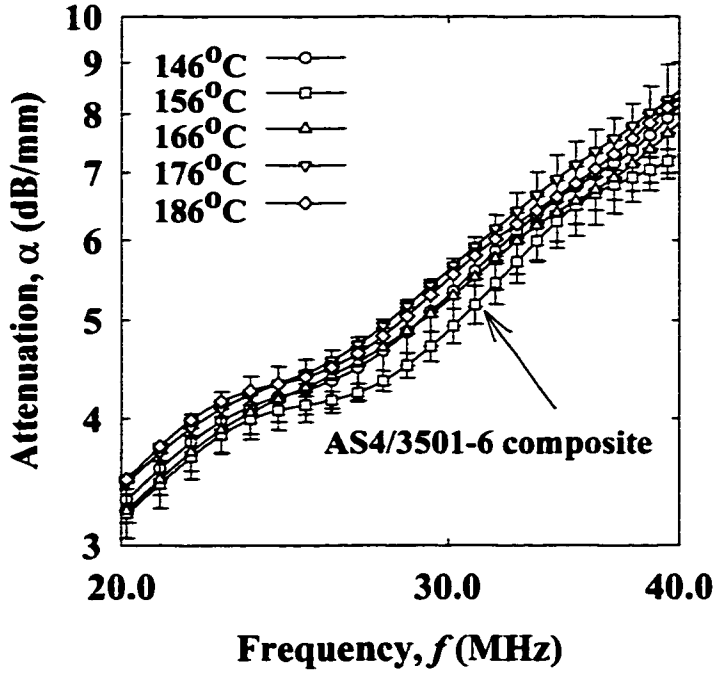

(b)

Figure 3-15 Ultrasonic attenuation obtained by using (a) 5 MHz, and (b) 50 MHz broadband ultrasonic transducers

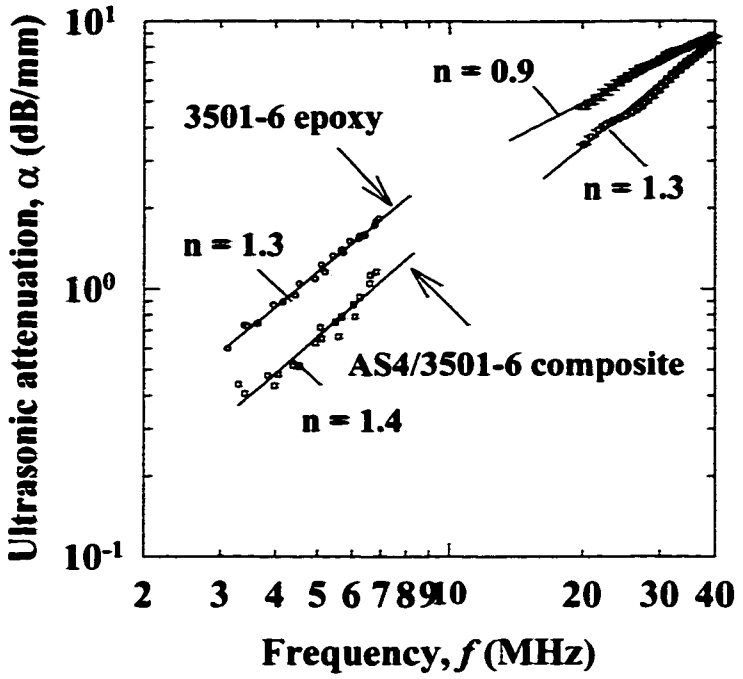

Figure 3-16 Dependence of ultrasonic attenuation of Hercules 3501-6 epoxy and AS4/3501-6 Gr/Ep composites cured at 176°C for 2 hrs. (n is the slope of the plotted curves)

Chapter 4

IN-SITU CURE MONITORING OF GRAPHITE/EPOXY COMPOSITES USING FIBER OPTICS

4.1 Introduction

As mentioned in Chapter 1, the curing process of composites is the most critical and costly stage in the manufacturing of composite structures. Considerable research and development effort have been expended to improve the quality and reliability of these types of materials. For a given structure, it is highly desirable to end the curing process when the properties of the composite are fully developed, rather than according to a fixed cure cycle. An adaptive control will reduce manufacturing time and lead to savings in production costs. This requires the use of sensing devices to provide real-time *in-situ* information about the condition of the material being processed. In the following two Chapters, some novel and refined existing techniques are developed to provide a basis for the eventual intelligent processing of the composites.

A prerequisite for any *in-situ* sensing is that it must not be detrimental to the operational requirements of the structure. The optical fiber sensor technique may suitable for *in-situ* cure monitoring of laminated composites, because the fibers can be incorporated into the component while laying up the prepregs. The dimension and orientation of optical fibers within the prepregs can be selected to have a minimal impact, for example, minimizing the resin-rich zone around the embedded sensors, on the mechanical properties of the composite [49]. Moreover, the technique possesses a clear potential for further monitoring the structural integrity of the composite, during part qualification and throughout its service life. However, the current cost of using fiber-optic

sensors is quite high. Due to the fragility of fiber optic sensors, improper autoclave feedthrough or any mishandling of the sensors may result in damage to the sensors [48], which further increases the cost.

The sensing mechanisms behind fiber-optic sensors for cure monitoring are various. In the present experimental study a strain sensor based on the change in optical path length in an optical fiber is used. This type of sensor was first proposed by Butter and Hoker [122] in 1978 and has been developed to measure strain, vibration, acceleration, pressure and temperature [37,40]. The current fiber-optic strain gages feature small size and high resolution. This makes them well suited for *in-situ* cure monitoring, because an embedded gage can directly detect the evolution of process-induced strain in a curing composite. Also, due to their tiny dimension and axial response to the detected strain, the fiber-optic strain gages can be embedded at different locations, between selected layers and along preferred directions in a laminate, so that monitoring distributed state-of-cure in the composite structure can be achieved.

In this Chapter, an Extrinsic Fabry-Perot Interferometric (EFPI) fiber-optic sensor [123] is investigated for its feasibility for *in-situ* cure monitoring of AS4/3501-6 Gr/Ep composites in an autoclave. The EFPI sensors are embedded in the composite to detect local strain development due to chemical shrinkage, process-induced stresses and temperature variation [20,21,124-127]. Thermocouples are also embedded to measure temperature profiles during the cure cycle. The experimental results will compared with the predicted results calculated by using Classical Lamination Theory (CLT) [11,12], and the limitations of this technique are also discussed.

4.2 Experimental setup

The fiber-optic cure monitoring system is comprised of optical fiber sensors, a K-type thermocouple, and the associated signal processing instruments, as shown in Figure 4-1. A special autoclave feedthrough is designed for the optical fibers and thermocouple wires to penetrate the autoclave, which can maintain a seal at 100 psi. It also keeps the sensors and their lead-in fibers intact after autoclaving, so the sensors can be directly used

for in-service monitoring of the composite structure after the processing. Two aluminum (Al) plates with 1 cm thick are used as the mold.

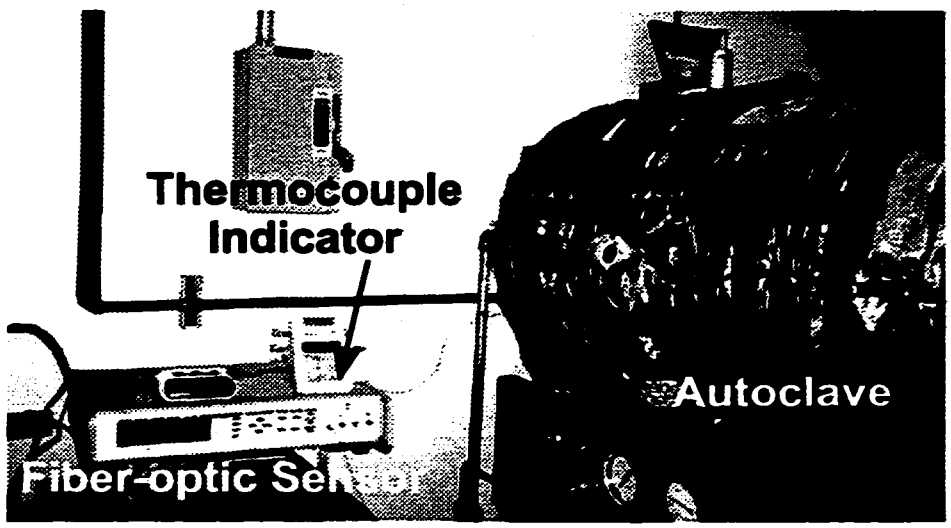

Figure 4-1 Actual *in-situ* fiber-optic cure monitoring system

4.2.1 Fiber-optic sensor

A four-channel WFS-100 EFPI fiber-optic strain sensor system, developed by FISO Technologies, Inc. (Quebec City, Quebec), is used for the *in-situ* cure monitoring. The sensing mechanism of a typical EFPI strain gage is shown in Figure 4-2 and detailed in references [40,123]. Light from a white light source is coupled into a lead-in fiber. The end of the lead-in fiber is attached to a small portion of a hollow fiber, and a reflecting fiber is attached at the opposite end of the hollow fiber. An air-gap is left between the end faces of the two fibers. The sensor detects the strain (*i.e.* the gap increment of the Fabry-Perot cavity over the gage length) by measuring the difference in optical path length between the light beams reflected from both ends of the cavity, *i.e.* R_1 from the lead-in fiber end and R_2 from the reflector fiber end. A fiber coupler can be used to separate the source light from the returning signal, which can be demodulated and translated into the strain value.

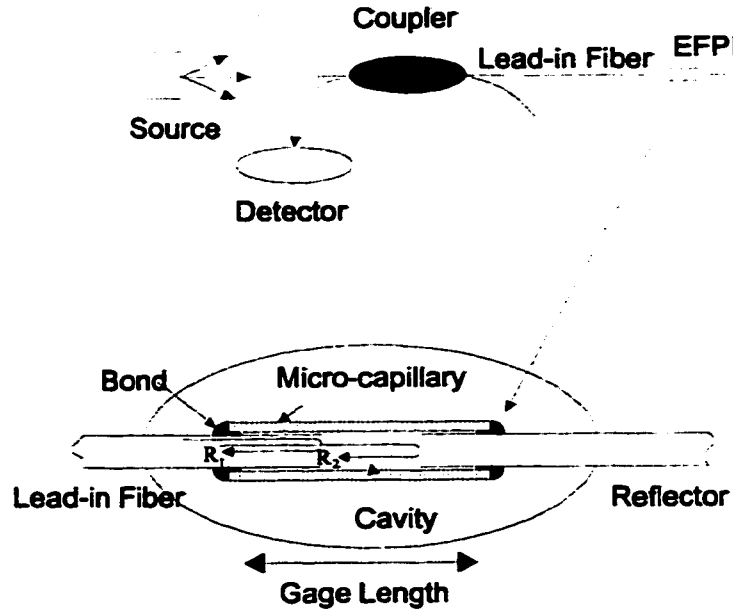

Figure 4-2 Basic configuration of an EFPI strain gage (SG) [40,123]

The gages used in this study feature a resolution of 0.5 με over ±2,000 με, and dimensions of about 10 mm gage length and 250 μm outer diameter. The gages are relatively insensitive to strain transverse to the longitudinal axis of the optical fiber. Their disadvantage is that the hollow-core fiber is usually larger than the lead-in fiber, which can create some difficulties for embedding.

It should be noted that the sensors are configured so that they exhibit apparent readings when a bare fiber-optic strain gage is subjected to temperature loading. This effect, resulting from the thermal expansion of glass fiber, becomes negligible after the gage is embedded and fully bonded to the host material. In other words, the fully integrated sensor responds only to the deformation of the host material, while its own thermal expansion can be neglected [128]. Similar to the recommended test in [37], the apparent thermal expansion of the bare fiber-optic strain gages is calibrated using a thermal chamber. Figure 4-3 shows typical results obtained by the calibration test. It is seen that the gage shows a linear response to temperatures from 23 °C to 180 °C. The average apparent thermal expansion coefficient (TEC) is 4.4 με/°C.

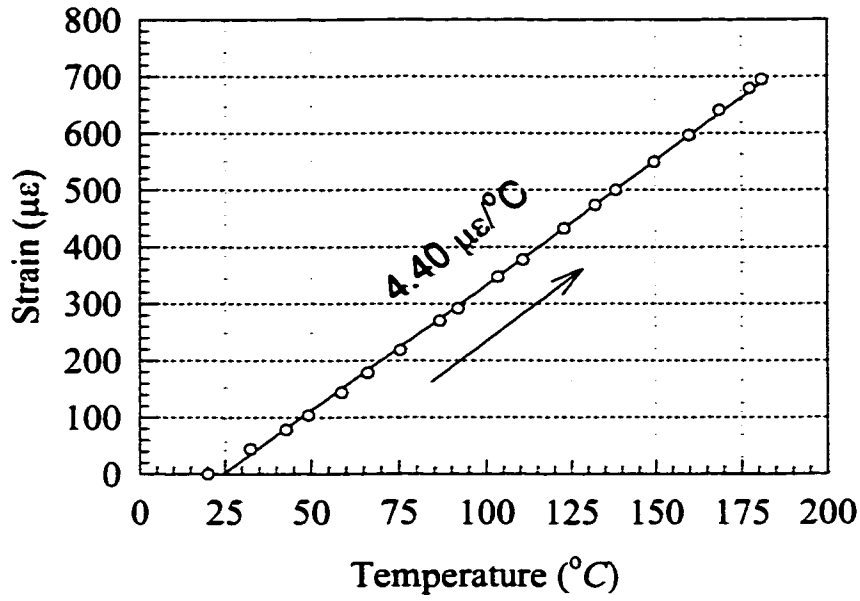

Figure 4-3 Thermal expansion of bare fiber-optic gage with temperature

4.2.2 Layout of sensors and panel processing

In this study, the fiber-optic strain gages are embedded in the 16-ply AS4/3501-6 Gr/Ep panels with either unidirectional or cross-ply layups, *i.e.* $[0_8/SG/0_8]$, $[90_6/0_2/SG/0_2/90_6]$ or $[90_3/SG1/90_3/0_2/SG2/0_2/90_6]$, where SG represents the embedded fiber-optic strain gage(s). In all cases, the strain gage is aligned with the direction of graphite fibers, so as to minimize the gage disturbance to the host composite, and to achieve best load transfer between them. It is noted that, given the composite ply thickness of 130 μm, the total thickness of the grouped plies containing the strain gage is more than twice the gage diameter. This prevents the gage from causing local bending to the adjacent composite layers [49]. To avoid any edge effect, the strain gages are placed at least 50 mm away from the edges of the panel. Figure 4-4 illustrates the location of the embedded gages.

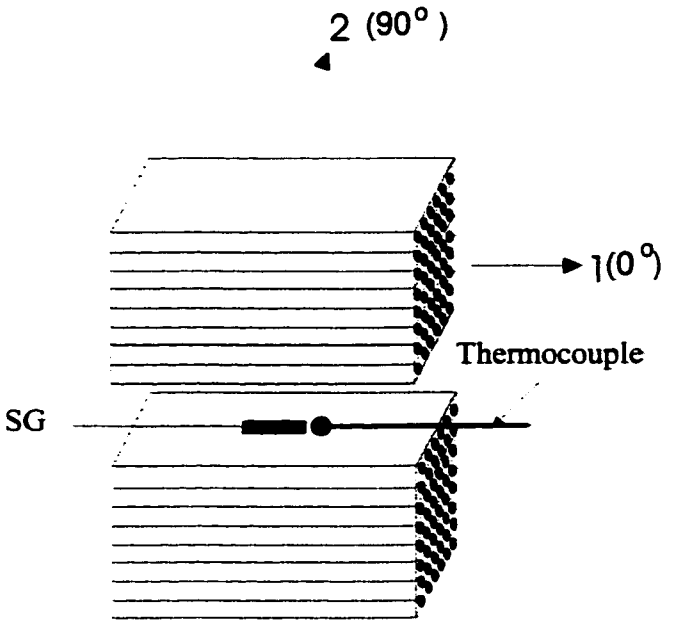

(a)

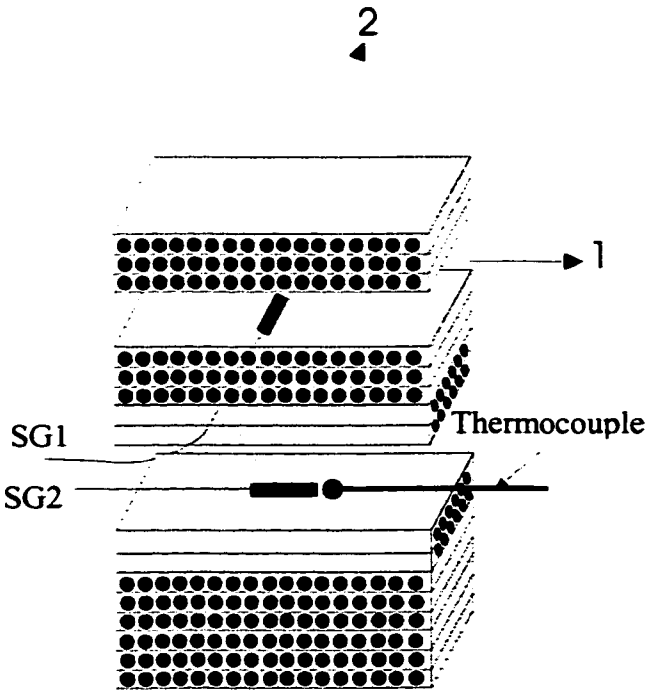

(b)

Figure 4-4 Location of fiber-optic strain gages in (a) unidirectional and (b) cross-ply composite panels

The commercially recommended cure cycle is used to process AS4/3501-6 Gr/Ep composites [112], *i.e.* (1) phase I: the prepreg is debulked under vacuum while the temperature is raised to 116°C and held there for one hour; (2) phase II: the temperature is then raised to the cure temperature of 176°C and held there for 2 hours. (the length of this dwelling time is called cure time); and (3) cool-down phase: the cured panel is then slowly cooled to room temperature. The autoclave air pressure is kept at 85 psi during the entire cure process, to secure prepreg compaction and good thermal conduction. The temperature of the panel is monitored by a K-type thermocouple embedded into the panel close to the location of the embedded fiber-optic gages. The cure process time is defined as run time. Figure 4-5 shows an example of the post-manufactured composite panel embedded with the fiber-optic strain gage.

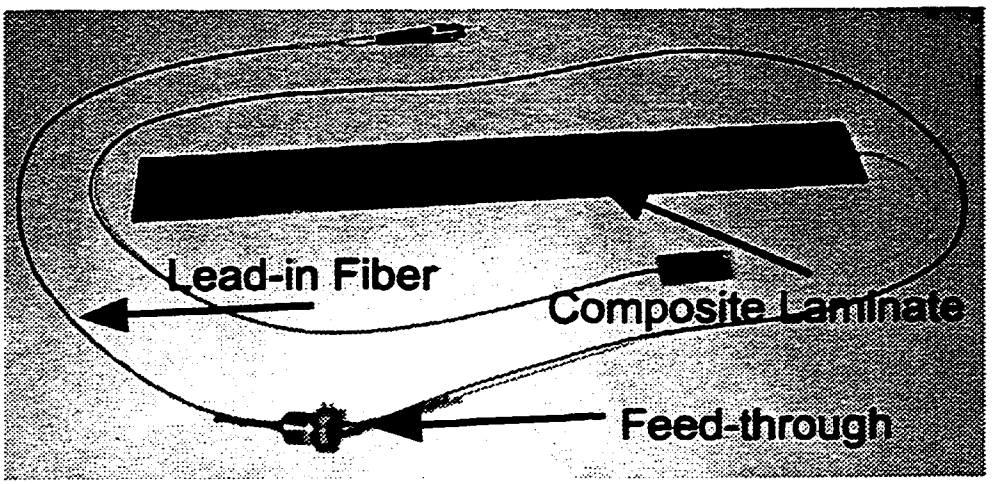

Figure 4-5 A composite panel embedded with a fiber-optic strain gage

4.3 Cure monitoring results using fiber-optic sensors

It is assumed, during the following discussion, that the temperature is uniform throughout the composite panel during the processing. Actually, the panel thickness is less than 2.5 mm, and thus the heat transfer is so rapid that the temperature gradient is negligible.

4.3.1 Unidirectional panel

Figure 4-6 presents typical *in-situ* strain sensing results of a $[0_8/SG/0_8]$ panel cured at 176°C, and the reference one cured at 146°C for 2 hours. The thermocouple measurements during the two different cure cycles are also presented in the same Figure. In either case, three phases of the cure process can be identified from the recorded temperature profiles. The corresponding plots of strain *vs.* panel temperature are presented in Figures 4-7. Moreover, in order to observe the detailed variation of the strain reading of the gage during the cure reaction, Figure 4-6 is reproduced in Figure 4-8 with local enlarged scale.

Referring to Figures 4-6 and 4-7(a), in the case of 176°C cure, it is seen that during the ramp-up period from room temperature, through the first dwell stage, to just below 170°C, the strain reading increases linearly with temperature. The rate of increase, 4.55 με/°C, is close to the calibrated TEC of 4.40 με/°C of the bare fiber-optic strain gages. This implies that, during the ramp-up period, the gage is almost free to expand with temperature, and the load transfer between the gage and the composite is negligible.

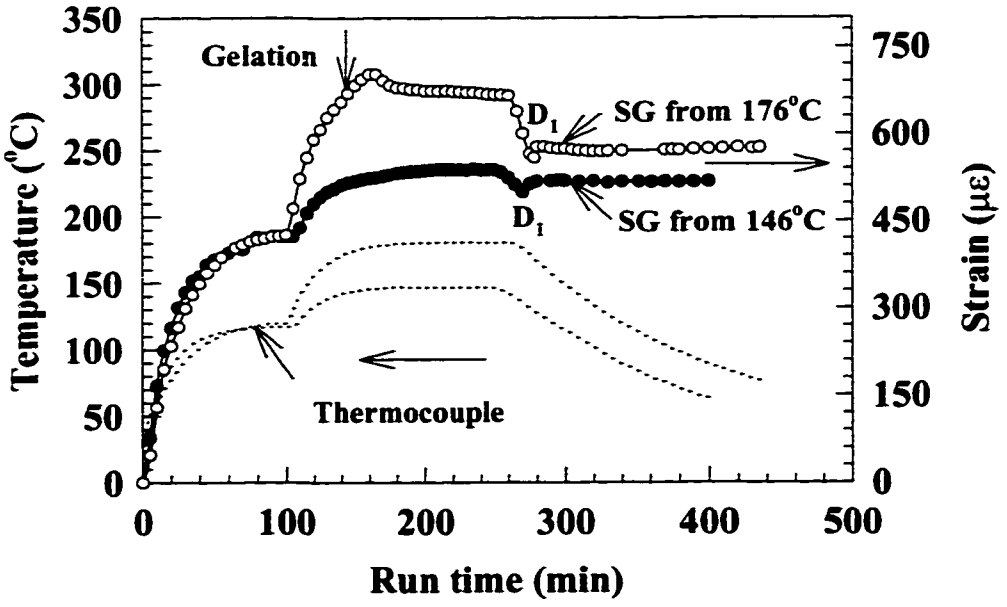

Figure 4-6 The fiber-optic cure monitoring of $[0_{16}]$ panels cured at 146°C or 176°C, where D_1 refers to the time when the detachment of the panel from the Al mold happens

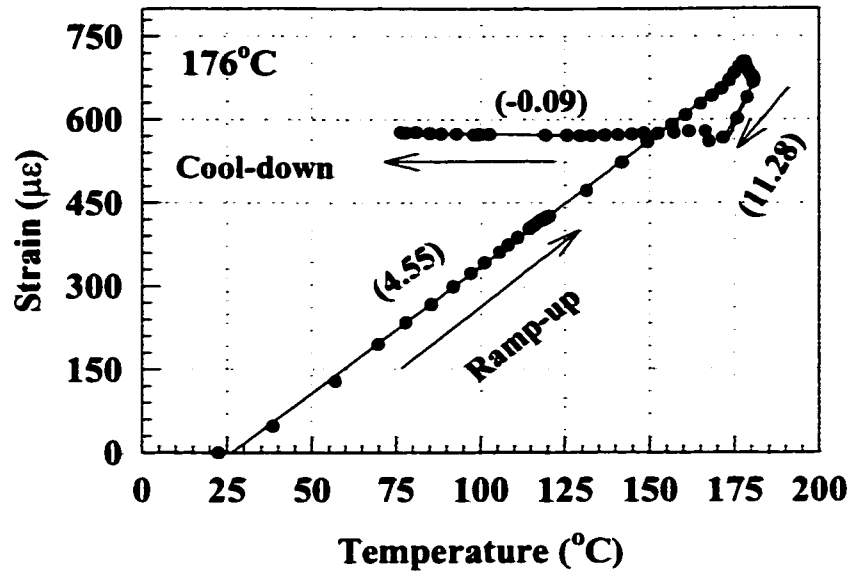

(a)

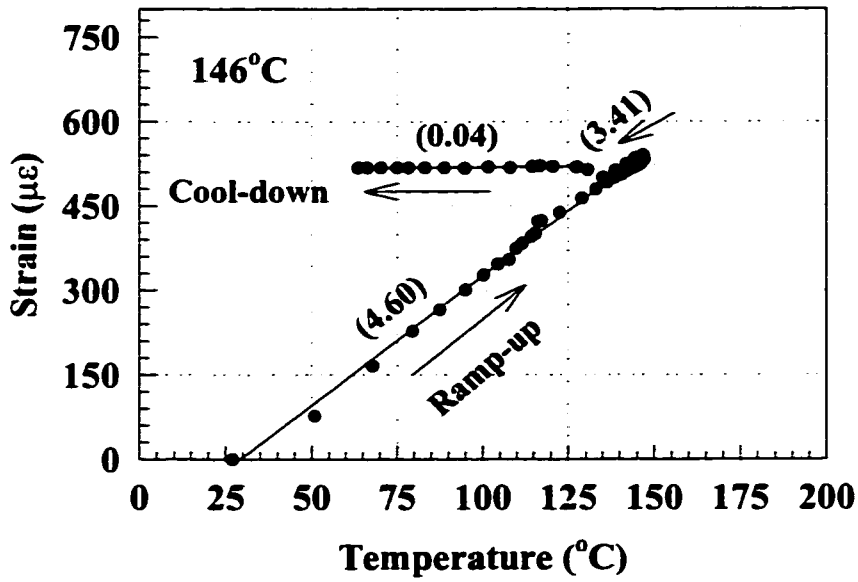

(b)

Figure 4-7 Temperature *vs.* strain readings for Gr/Ep panels cured at (a) 176°C, and (b) 146°C. The values in parentheses are thermal expansion coefficients (in με/°C) determined by linear regression.

At about 170°C, the strain reading starts to deviate from the original linear variation, presumably indicating the gelation period of the composite epoxy and the

combined effect of chemical shrinkage and the thermal expansion caused by temperature rise in the cure reaction of the composite epoxy.

At the start of cooling, the gage registers a prompt response to the thermal contraction of the panel, followed by a rapidly decreasing strain at the rate of 11.28 με/°C. At point D_1 as indicated in Figure 4-6, the strain reading shows a slight bouncing back, and then it follows a very small contraction at the rate of -0.09 με/°C. It is believed, as is further confirmed by later ultrasonic detection, that the initial rapid contraction results from the panel following the thermal contraction of the Al mold plates due to sticking. The TEC of Al is 28.7 με/°C (at 20°C to 600°C) [129], while that of unidirectional AS4/3501-6 Gr/Ep laminate is -0.07 με/°C in the graphite fiber direction [11,12]. The thermal mismatch eventually leads the panel to detach from the mold plates at point D_1. Then the less constrained panel basically follows its own contraction, exhibiting a reduced rate of contraction close to the longitudinal TEC of the composite.

Similar observations can be made in the case of 146°C cure in the ramp-up stage and then in the cooling stage, as shown in Figures 4-6 and 4-7(b). However, the strain development during the cure stage seems very different from that of 176°C cure, as indicated in Figures 4-8(a)(b). Actually, in Figure 4-7(b), after the close-to-free expansion of up to about 146°C, the strain reading shows no obvious deviation from the linear variation. Figure 4-8(b) shows that the strain continues to increase with temperature, and then gradually comes to a plateau after achieving constant temperature, while in the case of 176°C cure indicated in Figure 4-8(a), right after 170°C, the strain reading starts to deviate from the original linearity, and increases at an average rate of 7.74 με/°C for 20 minutes, and then the variation of the strain experiences a maximum. Thereafter, a rapid drop of the strain reading of the gage can be observed. During the subsequent curing process, the strain only drops slightly, whereas the temperature remains basically constant. The total decrease of the strain during the stage of the cure reaction is about -37.0 με.

It is noted that, before the composite is fully solidified, the sensor response should reflect the combined effect of its own thermal expansion and chemical shrinkage transferred from the curing composite. How much the contraction may be detected by the sensor depends highly on the condition of load transfer at the sensor/host composite interface. It has been shown that the load transfer is a function of the composite rigidity gained at a given instant [37]. Thus, if the process condition encourages a fast cure reaction with a rapid development of composite rigidity (for example, in the case of 176°C, the DSC and ultrasonic monitoring indicate a gel time of the composite epoxy around 6-12 minutes; during the gelation period, the rigidity of the composite increases rapidly, as shown later in Figure 5-1 and 5-8(b), respectively) so that the stress at the sensor/host composite interface can be effectively established and maintained, the chemical shrinkage will dominate the deformation and be detected by the sensor. It is noteworthy that although there is a temperature fluctuation during the cure dwell stage, the thermal expansion of the host composite may be negligible because the thermal expansion coefficient (TEC) of the composite along the graphite fiber direction is almost equal to zero. On the contrary, in a slow cure reaction, like the case of 146°C cure (Figure 5-1), if the time when α_{DOC} = 50% is defined as gel time [17], the gel time for 146°C curing is around 50 minutes. Meanwhile, the composite rigidity (Figure 5-8(b)) is low while the stress relaxation effect is significant, resulting in poor load transfer at the interface; so the sensor responds more to its own thermal expansion before full gelation.

4.3.2 Cross-ply panel

The typical result for a $[90_6/0_2/SG/0_2/90_6]$ panel is shown in Figure 4-9, where one strain gage embedded in the 0° plies is aligned with the direction of graphite fibers. From room temperature to about 170°C, the gage records the thermal expansion rate close to the calibrated free-expansion coefficient of the bare fiber-optic strain gages. Then, with the further progress of the gelation, the reading of the gage deviates from the original linearity and follows the local strain development of the composite. Over the entire cure reaction at 176°C, the gage records the variation of strain induced by chemical shrinkage, and thermal contraction/expansion of the composite caused by temperature fluctuation. In

this stage, the reading of the gage is more sensitive to the temperature fluctuation because 90° plies with large TEC are involved. When the cool-down phase comes, the gage shows an initial rapid thermal contraction at 18.78 με/°C, until the panel suddenly detaches from the mold plates at about 150°C, causing a small dip (D_1) on the strain curve. The subsequent strain variation of the gage follows a linear relation with the decreasing temperature, at the rate of 6.0 με/°C.

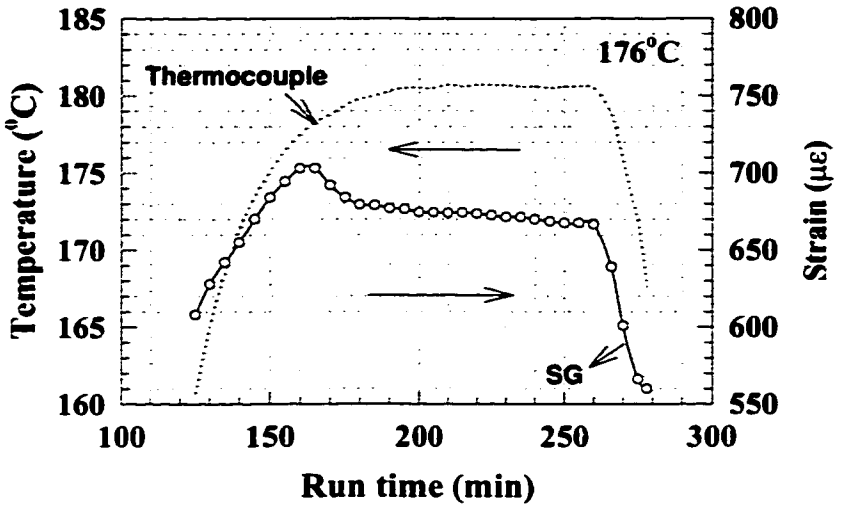

(a)

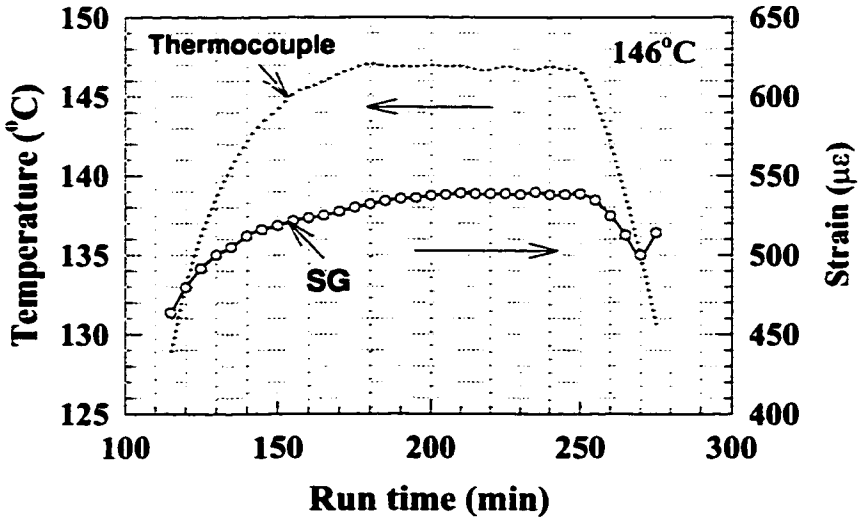

(b)

Figure 4-8 The local enlargement of Figure 4-6, in which the panels are cured at (a) 176°C and (b) 146°C

Similar observations are also made in the case of $[90_3/SG1/90_3/0_2/SG2/0_2/90_6]$ panels, as shown in Figure 4-10, where two strain gages embedded in the 0° and 90° plies, respectively, are aligned with the direction of the graphite fibers. As is seen, near 170°C, the readings of the two gages separate from each other and follow the local strain development of their respective sites. When the cool-down phase comes, gages SG1 and SG2 show an initial rapid thermal contraction at the rates of 3.23 and 22.93 με/°C, respectively, until the panel suddenly detaches from the Al mold plate at about 150°C, causing small dips (D_1s) on both strain curves. The subsequent strain variation of the two gages follows a linear relation, with the decreasing temperature, at the rate of 0.26 and 3.87 με/°C, respectively.

After cure processing, some panels were cut into beam-plates containing the gages, which were then calibrated by re-heating each beam in a thermal chamber with free-to-deform configuration. Furthermore, the TEC of the panel was predicted using the CLT [11,12], *i.e.*

$$\alpha_i^0 = a_{ij} \int Q_{jk}\, \alpha_k\, dz \qquad (i,j,k = 1,2) \tag{4-1}$$

where α_i^0 and a_{ij} are the in-plane TEC and compliance of the panel, respectively, and Q_{ij} and α_i are the stiffness and TEC of the composite lamina, respectively. All these quantities are presented in the global 1-2 coordinates of the panel. Figure 4-11 illustrates the relationship between the local x-y (on-axis) coordinate of the lamina and the global 1-2 coordinate of the panel, respectively, for any angle-ply laminates.

Considering the case of the cross-ply composite panels with thickness h, expression (4-1) can be expanded into

$$\alpha_1^0 = a_{11} \int_0^h (Q_{11}\alpha_1 + Q_{12}\alpha_2)dz + a_{12} \int_0^h (Q_{21}\alpha_1 + Q_{22}\alpha_2)dz \tag{4-2}$$

and

$$\alpha_2^0 = a_{21} \int_0^h (Q_{11}\alpha_1 + Q_{12}\alpha_2)dz + a_{22} \int_0^h (Q_{21}\alpha_1 + Q_{22}\alpha_2)dz \tag{4-3}$$

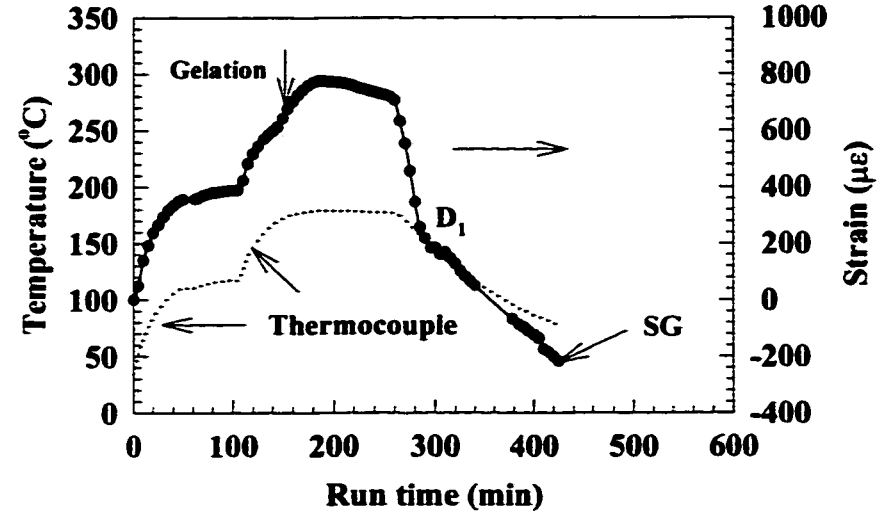

(a)

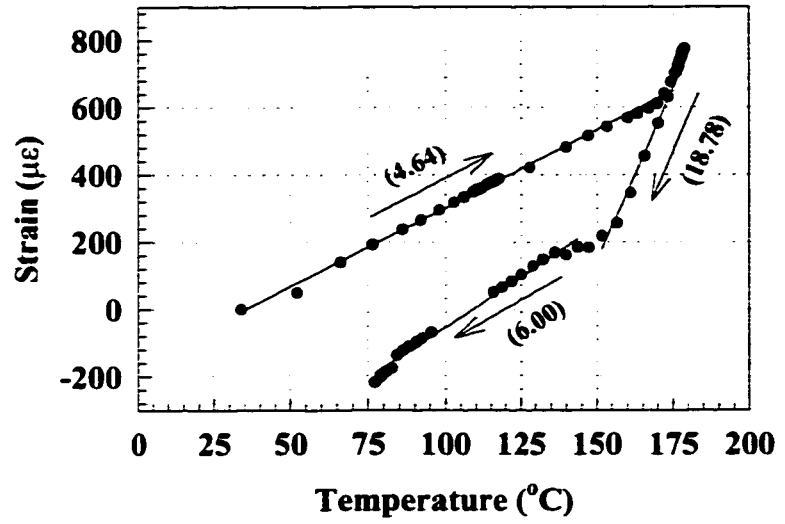

(b)

Figure 4-9 The fiber-optic cure monitoring of a $[90_6/0_2/SG/0_2/90_6]$ panel cured at 176°C. (a) Temperature profiles and strain readings; (b) Strain *vs.* temperature variation. The values in parentheses are thermal expansion coefficients (in με/°C) determined by linear regression.

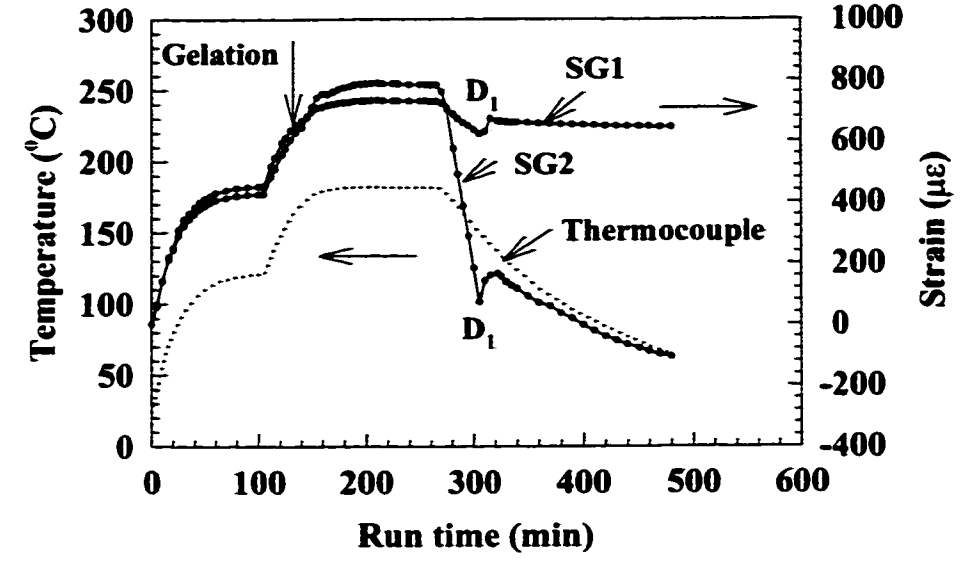

(a)

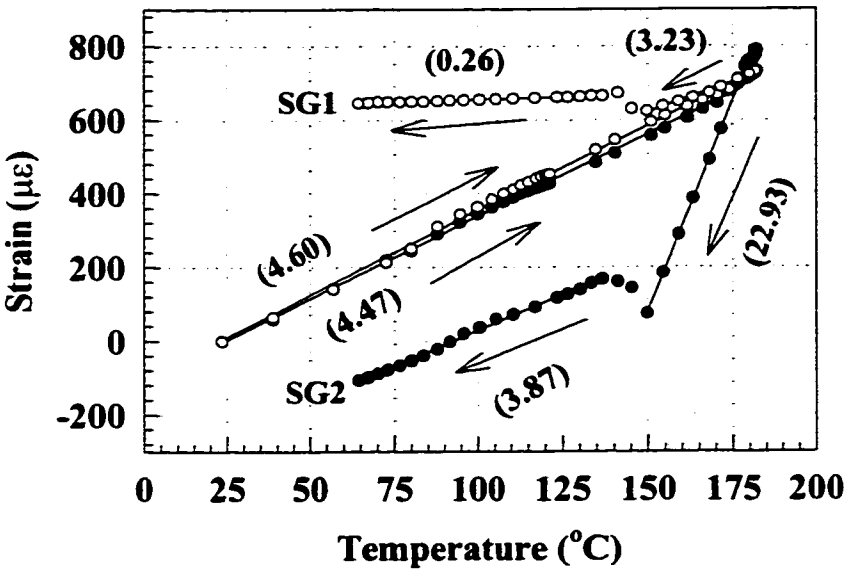

(b)

Figure 4-10 The fiber-optic cure monitoring of a [90_3/SG1/90_3/0_2/SG2/0_2/90_6] panel cured at 176°C. (a) Temperature profiles and strain readings; (b) Strain *vs.* temperature variation. The values in parentheses are thermal expansion coefficients (in με/°C) determined by linear regression.

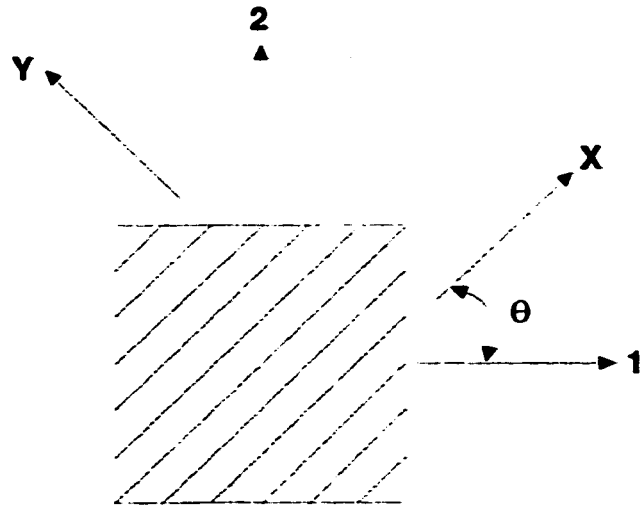

Figure 4-11 Local x-y coordinates of the lamina and global 1-2 coordinates of the panel, respectively, where θ = ply angle

where the integration can be evaluated by

$$\int_0^h (Q_{11}\alpha_1 + Q_{12}\alpha_2)dz = v_{90^0}h(Q_{yy}\alpha_y + Q_{xy}\alpha_x) + v_{0^0}h(Q_{xx}\alpha_x + Q_{xy}\alpha_y) \qquad (4\text{-}4)$$

$$\int_0^h (Q_{21}\alpha_1 + Q_{22}\alpha_2)dz = v_{90^0}h(Q_{xy}\alpha_y + Q_{xx}\alpha_x) + v_{0^0}h(Q_{xy}\alpha_x + Q_{yy}\alpha_y) \qquad (4\text{-}5)$$

where Q_{xx}, Q_{yy} and Q_{xy} are on-axis stiffnesses of the lamina in the local x-y coordinate, respectively, and v_{0^0} and v_{90^0} are the volume fraction of the plies with 0° and 90° orientation, respectively. Moreover, the in-plane compliance components of the panel can be expressed as

$$\begin{aligned} a_{11} &= Q_{22}/(Q_{11}Q_{22} - Q_{12}^2) \\ a_{22} &= Q_{11}/(Q_{11}Q_{22} - Q_{12}^2) \\ a_{12} &= -Q_{12}/(Q_{11}Q_{22} - Q_{12}^2) \\ a_{66} &= 1/Q_{66} \\ a_{16} &= a_{26} = 0 \end{aligned} \qquad (4\text{-}6)$$

in which the stiffness components of the panel can be expressed by the on-axis stiffness components of a lamina

$$Q_{11} = \frac{h}{2}\left[(Q_{xx} + Q_{yy}) + (v_{0^0} - v_{90^0})(Q_{xx} - Q_{yy})\right]$$

$$Q_{22} = \frac{h}{2}\left[(Q_{xx} + Q_{yy}) - (v_{0^0} - v_{90^0})(Q_{xx} - Q_{yy})\right]$$

$$Q_{12} = hQ_{xy} \tag{4-7}$$

$$Q_{66} = hQ_{ss}$$

$$Q_{16} = Q_{26} = 0$$

For the AS4/3501-6 Gr/Ep lamina, the engineering elastic constants are: the longitudinal Young's modulus, E_x =128.0 GPa; the transverse Young's modulus, E_y = 9.7 GPa; the shear modulus, G_s = 5.0 GPa; and the major Poisson ratio, v_{xy} = 0.3 [130], according to the conversion between stiffness and modulus [11,12], as given in Equations (4-8)(4-9)

$$Q = \begin{bmatrix} \dfrac{E_x}{1 - v_{xy}v_{yx}} & \dfrac{v_{xy}E_y}{1 - v_{xy}v_{yx}} & 0 \\ \dfrac{v_{yx}E_x}{1 - v_{xy}v_{yx}} & \dfrac{E_y}{1 - v_{xy}v_{yx}} & 0 \\ 0 & 0 & G_s \end{bmatrix} \tag{4-8}$$

and

$$v_{yx}E_x = v_{xy}E_y \tag{4-9}$$

The on-axis stiffness components thus can be obtained as Q_{xx} = 128.9 GPa, Q_{yy} = 9.8 GPa, Q_{xy} = 2.9 GPa and Q_{ss} = 5.0 GPa, respectively. Moreover, α_x and α_y are -0.07 με/°C and 21.6 με/°C respectively [130].

Table 4-1 summarizes the results of *in-situ* fiber-optic cure monitoring of AS4/3501-6 Gr/Ep laminates processed by the recommended cure cycle. Comparing with the free beam-plate calibration results and the predicted values, the strain gage-detected

TEC is close to the prediction in most cases. However, a certain disturbance of the gage embedded to the laminates is inevitable because of geometrical mismatch; the quality of embedding also varies from one gage to the other. These factors, among others, can cause the scatter and (in a few cases) the discrepancy between the detected and predicted values.

The present case study indicates that in the ramp-up period, all gages basically respond to their own thermal expansion. The gelation period of the composite epoxy may be detected from the strain-temperature record, while the gages record only a small strain variation during the curing stage. Though the prompt response of the gages to the start of cooling indicates the developed elastic properties of the composites, the recorded small strain variation makes it difficult to use the fiber-optic strain gage for the detection of the end-of-cure of the composite in terms of the development of chemical shrinkage.

The strain variation during cure reaction suggests that the strain due to chemical shrinkage of the composite epoxy is limited, particularly in the direction of graphite fibers. It is also possible that most of such strain has occurred at the beginning of the cure, where the material starts to gel but the viscosity is still low, which limits the load transfer to the gages because of the stress relaxation effect. In another respect, it is of interest to note that the early development of load transfer between the composite and the gage is similar to that of residual stresses in the laminate. Thus, at least along the fiber direction of the composite, the residual stress caused by cure reaction is very small, while most of it is by the significant thermal strain in the cooling stage, as can be seen in Figures 4-6, 4-9 and 4-10. Similar observations have also been made in a previous study [40].

Predicting residual stress in a composite is difficult because of the large number of factors which contribute to the stress, including thermal, chemical, and viscoelastic effects, as well as moisture absorption. Experimental determination of the development of the residual strains in the composite is also difficult, especially during the period of cure processing. However, the present experimental results indicate by using embedded EFPI

fiber-optic strain gages that most of information regarding the development of local residual strains during the processing has been captured.

4.4 Summary

The feasibility of using embedded EFPI fiber-optic strain gages in an autoclave has been demonstrated as a means of monitoring cure processing of Gr/Ep composites. This technique, particularly in combination with other types of sensors like the ultrasonic technique (to be discussed in the next Chapter), holds promise for alleviating some of the problems associated with the manufacture of advanced materials.

These sensors have demonstrated the ability to measure non-destructively and in real time the process-induced strains:

(1) The EFPI fiber-optic can sense the gelation period of AS4/3501-6 Gr/Ep composite, the start of cooling, and the build-up of post-cure residual strains during the cure; however, the EFPI fiber-optic monitoring can not determine the end-of-cure in terms of the development of chemical shrinkage.

(2) The timing of the detachment may provide information concerning the development of residual stresses during the cool-down phase; moreover, thermal mismatch between the Al mold and the composite panel, before the detachment, may result in micro-cracks during cool-down phase.

In short, this technique is particularly suited for non-destructive real-time monitoring of the development of residual stress in a curing composite. Moreover, this technique has been shown to possess clear potential for further monitoring the structural integrity of the composite during part qualification and throughout its service life. However, the EFPI fiber-optic gages can not sense the end-of-cure without the assistance of other sensors. This limits their usage as an individual sensor to monitor the entire cure process.

Table 4-1 Summary of *in-situ* fiber-optic cure monitoring results of AS4/3501-6 Gr/Ep composite cured at 176°C for 2 hrs., where the unit of thermal expansion coefficients (TECs) is in με/°C

No	Sample	*In-Situ* Monitoring				Post-Cure Calibration	
		Apparent TEC during ramp-up period	Cure Stage	Apparent TEC during cool-down before detachment	Apparent TEC during cool-down after detachment	Apparent TEC from free beam-plate	TEC predicted by CLT
1	Bare fiber-optic strain gage*	4.40					
2	$[0_8/SG/0_8]$	4.55	—	8.36	-0.09		-0.07
3	$[0_8/SG/0_8]$	4.98	—	7.72	-0.28		-0.07
4	$[90_6/0_2/SG/0_2/90_6]$	4.64	—	18.78	6.00	6.15	3.15
5	$[90_3/SG1/90_3/0_2/$ $SG2/0_2/90_6]$	4.25 (1) 4.09 (2)	— —	2.28 22.31	0.40 5.68	0.32 3.37	1.09 3.15
6	$[90_3/SG1/90_3/0_2/$ $SG2/0_2/90_6]$	4.60 (1) 4.47 (2)	— —	3.23 22.93	0.26 3.87	0.34 3.85	1.09 3.15
7	$[90_6/0_2/SG1,$ $SG2/0_2/90_6]$	5.42 (1) 5.38 (2)	— —	23.39 23.32	5.24 5.66	3.74 4.03	3.15 3.15

* by the calibration test prior to embedding

Chapter 5

IN-SITU CURE MONITORING OF GRAPHITE/EPOXY COMPOSITES USING ULTRASONICS

5.1 Introduction

During the cure of a composite, the composite epoxy experiences significant changes in its physical, chemical and mechanical properties, some of which may be used for *in-situ* monitoring of the state of cure of the composite. A typical case is the viscoelastic properties, such as the storage modulus E', loss modulus E" and the loss tan δ (= E'/E") of the curing composites. It is known [42] that during the processing the composite epoxy initially behaves as a viscous fluid, since its molecules are not crosslinked and molecular entanglement is the only impedance to flow. Its viscosity falls with increasing temperature until the start of the cure reaction, which corresponds to a maximum tan δ. Subsequently, the viscosity rapidly rises due to molecular mobility being inhibited by crosslinking of the molecules. This rapid change of phase toward solid state is known as gelation. As crosslinking proceeds, the material behaves more as an elastic medium, thus its E' increases while tan δ decreases until the fully cured state is reached.

As pointed out in Chapter 2, since the crosslinking reaction in thermosetting polymers is exothermic, the thermal DSC can monitor the exothermic flow of heat, and a characterization of the state of cure of composites is made. Traditionally, the "degree of cure" (α_{DOC}) of composites, measured by using the DSC technique, is used to assess the state of cure [17]. In our preliminary experiments in Chapter 2, several observations on the cure kinetics of AS4/3501-6 Gr/Ep prepregs have been made by using isothermal

DSC scanning. Figure 5-1, redrawn from Figure 2-8(b), shows the α_{DOC} as a function of cure time at different cure temperatures. As the cure temperature increases, the α_{DOC} increases, while the time for completion of the cure reaction decreases. At cure temperatures of 176°C and 186°C, the cure reaction is almost fully completed after one hour. However, even though the chemical reaction is nearly completed, the mechanical properties of composites may not be well developed because the α_{DOC} is a process parameter which gives information on the extent of the chemical cure reaction, while the extent of modulus is a parameter which gives information on the degree of mechanical property development [59]. The critical objective of the process engineer is to know when the material has been "fully processed", and the cure characterization should be reflective of the ultimate material application; thus, **the "end-of-cure" should be determined by the completion of the development of not only chemical but also mechanical properties of the composites.** As seen in Chapter 3, the ultrasonic technique is a very effective approach to evaluate the mechanical properties of the composites, and therefore to provide the possibility of *in-situ* monitoring the development of these properties in a curing composite.

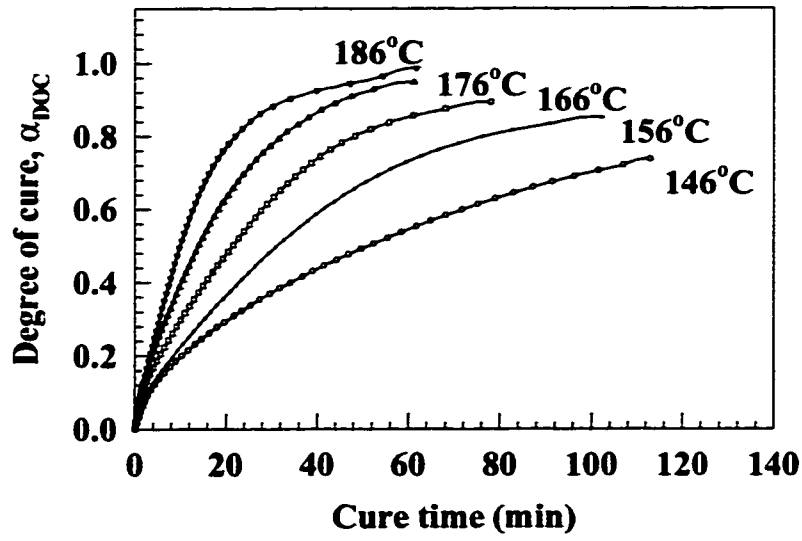

Figure 5-1 Degree of cure *vs.* cure process time for AS4/3501-6 Gr/Ep prepregs

The use of ultrasonics in cure monitoring of an epoxy was reported early in 1952 by Sofer and Hauser [50]. They found that the velocity increased monotonically with time, whereas ultrasonic attenuation peaked near the gel point. Since then, the ultrasonic technique for cure monitoring has been reported frequently in the literature [51-66] because it can provide a direct and nondestructive measurement of the viscoelastic properties of a curing composite, and information on the development of mechanical properties of the composite. There are a number of limitations, though; specifically, the commonly-used piezoelectric ultrasonic transducers (UTs) can only be operated continuously up to a temperature of about 60°C. This limitation presents difficulties when applying this technique in an actual processing environment which has, such as for Gr/Ep composites, a temperature of 176°C. Because it is not convenient to obtain high temperature piezoelectric UTs, one classic approach which uses buffer rods is still attractive, and is adopted here due to its simplicity and low cost [67-77]. The UT end of the buffer rod is air-cooled so that the high-performance room temperature UTs can be used, and the other (probing) end contacts the processed part. However, ultrasonic buffer rods can introduce spurious signals, due to wave diffraction and the finite rod diameter. These signals always arrive later than the directly transmitted or reflected echoes. Such echoes are unwanted because of their possible interference with the desired signals from the sample. Consequently, the length and diameter of buffer rods should be carefully chosen. On the other hand, clad buffer rods, composed of a central core and an outer cladding, have been shown to provide a good signal-to-noise ratio (S/R) when used in ultrasonic pulse-echo instruments, making many on-line processing monitoring applications feasible [75-77].

In this Chapter, ultrasonic sensors are investigated as potential candidates for *in-situ* cure monitoring of AS4/3501-6 Gr/Ep composite in an autoclave. The ultrasonic sensors are incorporated into the autoclave using a buffer rod and a cooling system. The evolution of viscoelastic properties of the curing composite is monitored by continuous recording of the time delay, attenuation and shear reflectivity of ultrasound waves. The EFPI sensors are concurrently used to detect local strain development in the composite caused by temperature variation, chemical shrinkage and process-induced stresses. The

results from the two techniques are compared in order to evaluate their suitability for *in-situ* cure processing monitoring of Gr/Ep composites in an autoclave. We also discuss using this technique to detect the "end-of-cure", in relation to using the DSC technique to determine the "end-of-cure" in terms of traditional "degree-of-cure".

5.2 Experimental setup

The *in-situ* cure monitoring system developed in this study consists of ultrasonic and/or fiber-optic sensors, and associated electronics. It is incorporated into an autoclave as shown in Figure 5-2. A special feedthrough is designed for the ultrasonic transducer cables and/or optical fibers, thermocouple wires and air-cooling Teflon tubes to pass through the autoclave, as indicated in Figure 5-3. This autoclave feedthrough can maintain a seal at 100 psi. Two aluminum (Al) plates 1 cm thick are used as the mold, and the monitored curing materials are AS4/3501-6 Gr/Ep prepregs.

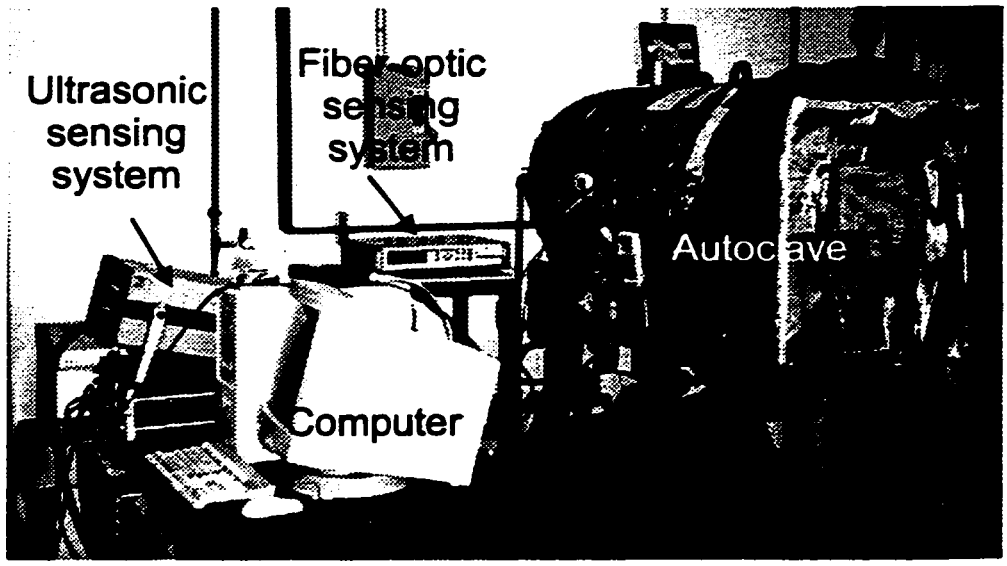

Figure 5-2 Actual *in-situ* fiber-optic and/or ultrasonic cure monitoring system

5.2.1 Ultrasonic sensor

The ultrasonic sensing system is composed of high-performance 5 MHz broadband longitudinal piezoelectric UTs, couplants, clad Al buffer rods [72, 73] (Figure

5-4), and air cooling systems which surround the UTs, as shown in Figure 5-5. This system can be operated in either pulse/echo and/or through-transmission mode. The clad buffer rods consist of an Al core and a thermally sprayed Al cladding. The length of each buffer rod is 17 cm, and the width is less than 1.5 cm. These buffer rods are screwed into the Al mold, with the end faces flush with the mold inner surface, as indicated in Figure 5-6. The principle of ultrasonic guidance in clad buffer rods is like clad optical fibers in which the energy is guided in the core, and thus the threading in the cladding region does not disturb the guided ultrasonic energy inside the core. The variation in amplitude of the reflected ultrasonic signals at the rod/composite interface, and those of the amplitude and time delay of signals traversing back and forth through the composite thickness, enable us to monitor the cure. The 100 psi compressed air cooling allows the cooling of the UTs from 190°C down to 60°C, which is the maximum allowable temperature for the UTs used. The 17 cm clad buffer rod length is chosen so that the temperature gradient is not large, and the thermal characteristics of the threaded buffer rod end are the same as those of the mold. Ultrasonic waveforms are recorded with a sampling rate of 100 MHz every 5 or 10 minutes during the entire cure process, using a computerized system consisting of an ultrasonic MP270 pulser/MR106 receiver (MetroTek, Inc., Kennewick, WA), LeCroy 9400 dual 125 MHz digital oscilloscope (LeCory, Co., Chestnut Right, NY) and a PC Pentium®. Data acquisition and signal processing are handled by computer programs written in LabVIEW ® software.

5.2.2 Panel processing

All panels of graphite fiber reinforced epoxy used in this study were laid up manually from the same lot of AS4/3501-6 Gr/Ep prepregs. The commercially recommended cure cycle is used to process the composites [110], as stated in Section 4.2.2 in Chapter 4. The temperature of the panel is monitored by a K-type thermocouple embedded into the panel, close to the location of ultrasonic and/or embedded fiber-optic sensors. For typical cases, effects of cycle conditions on the curing composite are examined by using the cure temperatures of 146°C and 156°C, or by extending cure time from 2 to 3 hours while maintaining 176°C.

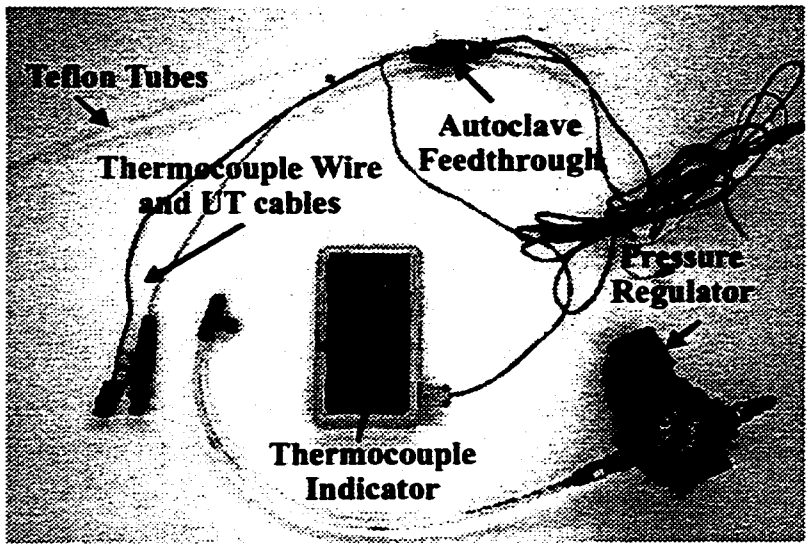

Figure 5-3 A special autoclave feedthrough

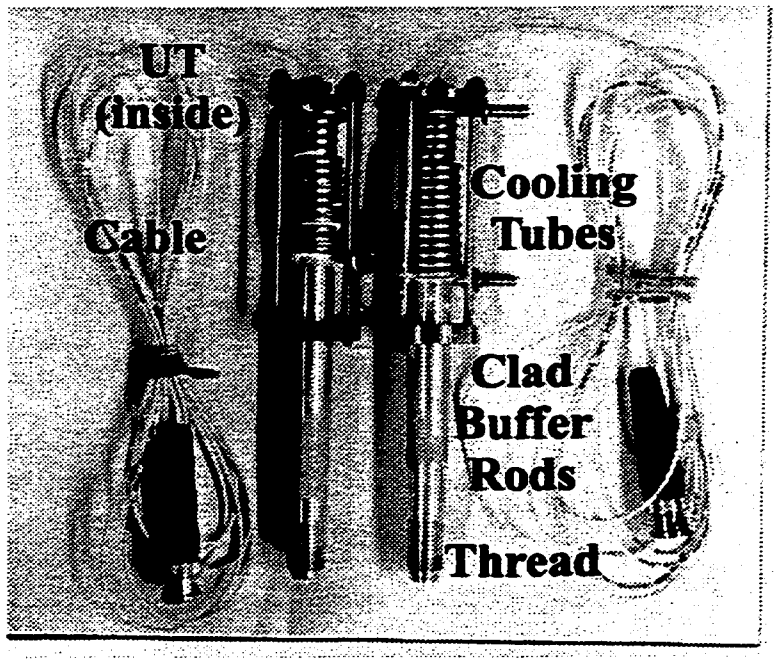

Figure 5-4 A pair of ultrasonic transducers with clad Al buffer rods

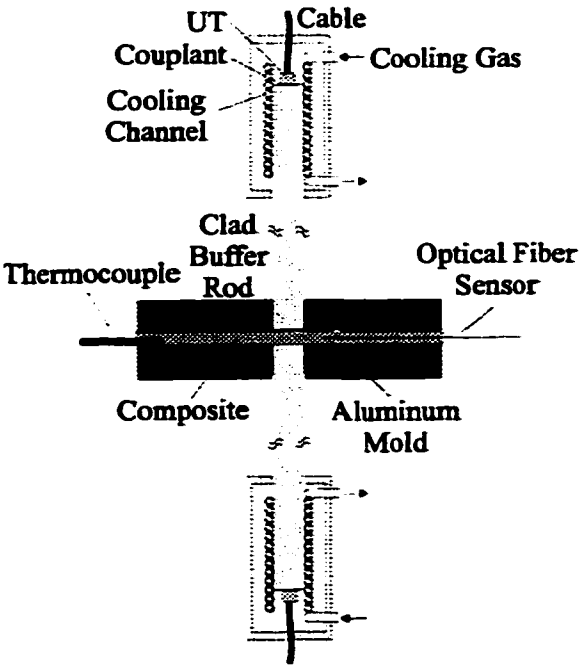

Figure 5-5 Illustration of cure monitoring using optic fiber and ultrasonic sensors simultaneously

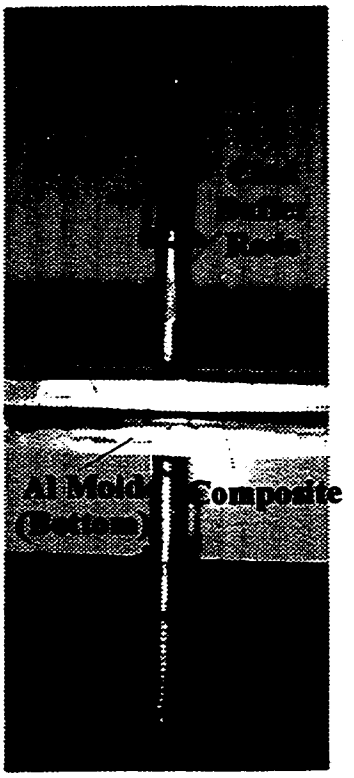

Figure 5-6 Clad Al buffer rods

5.3 Cure monitoring results using ultrasonics

5.3.1 Ultrasonic behavior in viscoelastic medium

The propagation of through-thickness ultrasonic waves in a viscoelastic medium can be expressed by

$$\frac{\partial^2 u_3}{\partial t^2} = \frac{C_{22}^*}{\rho}\frac{\partial^2 u_3}{\partial x_3^2} \tag{5-1}$$

where u_3 denotes the displacement in the direction x_3, and ρ is the density. The elastic stiffness component C_{22} is replaced by the complex quantity:

$$C_{22}^* = L' + jL'' \tag{5-2}$$

in which C_{22} can be called as the longitudinal modulus, and L' and L" are its real and imaginary parts, for a plane wave along x_3 in the form $e^{i(k^* x_3 - \omega t)}$, where k* is a complex wave-number, as defined as Equation (3-24) in Section 3.3.2 of Chapter 3. Rewriting (3-24)

$$k^* = \frac{\omega}{V} + j\alpha \tag{3-24}$$

Then solving the equation of wave motion (5-1) yields:

$$\omega^2 = \frac{C_{22}^*}{\rho}k^{*2} \tag{5-3}$$

thus the expressions of L' and L" can be obtained:

$$L' = \frac{\rho V^2 \omega^2(\omega^2 - \alpha^2 V^2)}{(\omega^2 + \alpha^2 V^2)^2} \tag{5-4}$$

and

$$L'' = \frac{2\rho\alpha V^3 \omega^3}{(\omega^2 + \alpha^2 V^2)^2} \tag{5-5}$$

For the longitudinal velocities and attenuation measured during cure, $\alpha^2V^2 << \omega^2$; then, to a good approximation

$$L' = \rho V^2 \text{ and } L'' = \frac{2\rho\alpha V^3}{\omega} \tag{5-6}$$

and so

$$\tan \delta = \frac{L''}{L'} = \frac{2\alpha V}{\omega} \tag{5-7}$$

Representing the resin with a simple viscoelastic response with a single relaxation time, Winfree [131] adequately explains the trends of resin's velocity and attenuation changes during cure. The shear K and compression G moduli thus can expressed as

$$M = M_0 + \frac{M_r \omega^2 \tau^2}{1+\omega^2 \tau^2} + i\frac{M_r \omega\tau}{1+\omega^2 \tau^2} \tag{5-8}$$

where M represents both K and G. G_0 and K_0 are static moduli, while G_r and K_r are the difference between the high frequency and static moduli called the relaxation moduli, and τ is the relaxation time. To a good approximation, the longitudinal velocity can be expressed [131] as

$$V_L \approx \left[\frac{1}{\rho}(K_0 + \frac{4}{3}G_0)\right]^{1/2} \tag{5-9}$$

Crosslinking between the polymer chains increases both K_0 and G_0, resulting in an increase in V_L. Moreover, the attenuation [131] is

$$\alpha_L = \frac{(K_r + \frac{4}{3}G_r)(\frac{\omega\tau}{1+\omega^2\tau^2})\omega\rho^{1/2}}{2(K_0 + \frac{4}{3}G_0)^{3/2}} \tag{5-10}$$

The relaxation time for a simple polymer chain is proportional to the length of the chain. As the cure progresses, crosslinking increases the effective length of the chain, increasing the relaxation time. If the original value for $\omega\tau$ is less than 1, then as the relaxation time increases, $\frac{\omega\tau}{(\omega^2\tau^2+1)}$ goes through a maximum at $\omega\tau$ equal to one.

Therefore, the above equations indicate that the variation of the viscoelastic properties of the curing composite can be monitored by measuring ultrasonic velocity (or time-delay $V = \frac{2h}{t}$) and attenuation.

5.3.2 Results and discussion

When using ultrasonics for cure monitoring, three parameters are typically employed to infer the state-of-cure of a material: the ultrasonic (1) velocity or time delay, (2) attenuation, and (3) shear reflectivity. The material properties which are useful for determining the state-of-cure, such as moduli and viscosity, can be subsequently deduced from this information by using a viscoelastic analytical model. By monitoring the evolution of the ultrasonic time delay, attenuation and shear reflectivity in a curing composite as a function of run time, we can understand the cure process qualitatively and quantitatively.

5.3.2.1 Pulse/echo mode

In pulse/echo mode, the ultrasonic wave traveling through the material is reflected from the back side of the laminate to the originating surface, where it is detected by the same UT that generates the pulses, as illustrated in Figure 5-7.

Figure 5-8(a) shows the ultrasonic waveform as a function of run time for the $[0_{16}]$ panel cured at 176°C for 2 hours, where L^1 represents the echo reflected from the probing end of the clad Al buffer rod/top surface of the panel interface, and L_2 the second echo reflected from the back surface of the panel. The recorded variations of process temperature and ultrasonic time delay between L^1 and L_2 are shown in Figure 5-8(b). For 176°C curing process, it is seen that, due to thermal expansion of the buffer rod, echo L^1 shifts toward a higher time delay before the constant cure temperature is reached; it comes to a standstill during the hold period at 176°C, and then gradually returns to its original position at the end of the cool-down stage. The second echo L_2, during the initial stage, is too weak to be recorded using the current setup until the gelation of the composite epoxy takes place. Although ultrasonic velocity dispersion induced by absorption and scattering losses causes the signals to have a slight distortion, the time delay between the first echo L^1 and the second echo L_2 can be determined using a cross-correlation algorithm. The sharp decrease in the time delay, in the temperature range after phase I, may be attributed to the gelation of the prepregs. The subsequent gradual

decrease of the time delay corresponds to the progressive crosslinking reaction of the composite after gelation period. Effects of the state of cure on the time delay can be, therefore, described as a continuous decrease of the time delay as the material changes from a liquid, through a gel, to a solid due to increasing stiffness of the composite. Then the panel starts to cool down, and the time delay further decreases. After a certain time, a sudden rise in the time delay is found. This discontinuity results from the sudden detachment of the panel from the Al mold plate at the sensed region. This interpretation is supported by the observation in Figure 5-8(a) of a sudden phase change of 180° and an increase in amplitude of the echo reflected from the back surface of the panel at that moment. This is confirmed by the change of the interface condition from "panel-mold plate" to "panel-air".

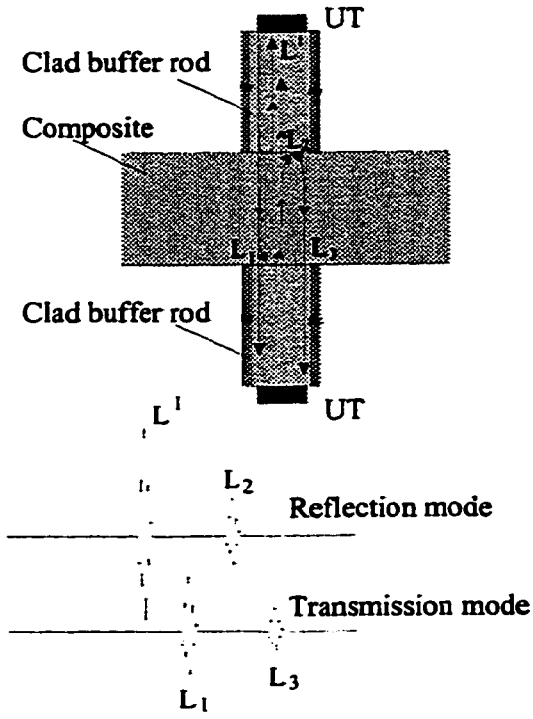

Figure 5-7 Illustration of reflection/transmission mode

Figure 5-8(b) also shows the time delay recorded from two other runs using cure temperatures of 146°C and 156°C, respectively. It is noted that increasing cure temperature shifts the curve of the time delay *vs.* run time to a distinctly lower value, which indicates that ultrasonic *in-situ* cure monitoring can monitor the change induced by different curing temperatures. Compared with Figure 5-1, it is not difficult to find some

similarity between the ultrasonic and isothermal DSC experimental results: the progress of the gelation and cure reaction of the composite epoxy at 146°C and 156°C is much slower than that at 176°C.

5.3.2.2 Transmission/reflection mode

In transmission mode, the ultrasonic wave passes through a laminate and is detected by another UT located at the opposite side of the mold. Meanwhile, these two UTs can still conduct reflection mode measurements individually, as illustrated in Figure 5-7. For these measurements of the $[0_{16}]$ panel cured at 176°C, the cure time is arbitrarily extended from 2 to 3 hours, in order to observe the end-of-cure. Figures 5-9(a) and (b) show the ultrasonic waveforms obtained by using simultaneous transmission and reflection modes. In reflection mode, Figure 5-9(a), the feature of the waveform is the same as that of Figure 5-8(a), while in transmission mode, Figure 5-9(b), the first echo L_1 has traveled through the panel thickness once and the second echo L_3 has made an additional round-trip. These two echoes can be used to evaluate through-thickness ultrasonic attenuation.

The variations of the time delay *vs.* run time from both top and bottom UTs exhibit the same trend, as shown in Figure 5-10. After curing for 2 hours at 176°C, the time delay reaches a plateau, suggesting that the end-of-cure, in the sense of the development of the stiffness of the composite, has been reached, and the extra hour of curing does not contribute to the further improvement of the stiffness of the composite. Here, again, as the panel cools down, the time delay decreases. After a certain time, because of detachment of the panel from the top Al mold plate at the sensed region, the signal from the top UT completely vanishes, while the time delay obtained from the bottom UT shows a discontinuity. For transmission mode, the shape of the time delay variation is the same as that obtained from reflection mode, as indicated in Figure 5-10. After the detachment of the panel from either side of the Al mold plates, the through-thickness transmission signal is totally lost.

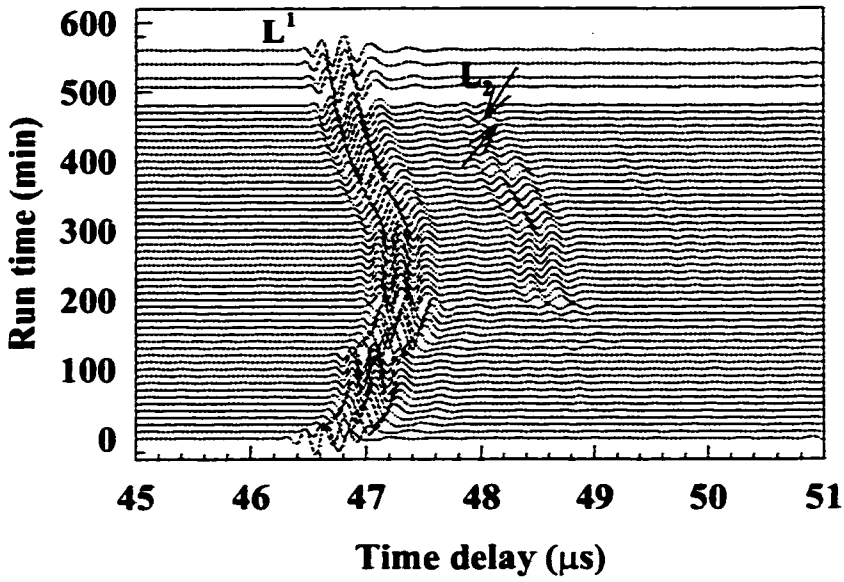

(a)

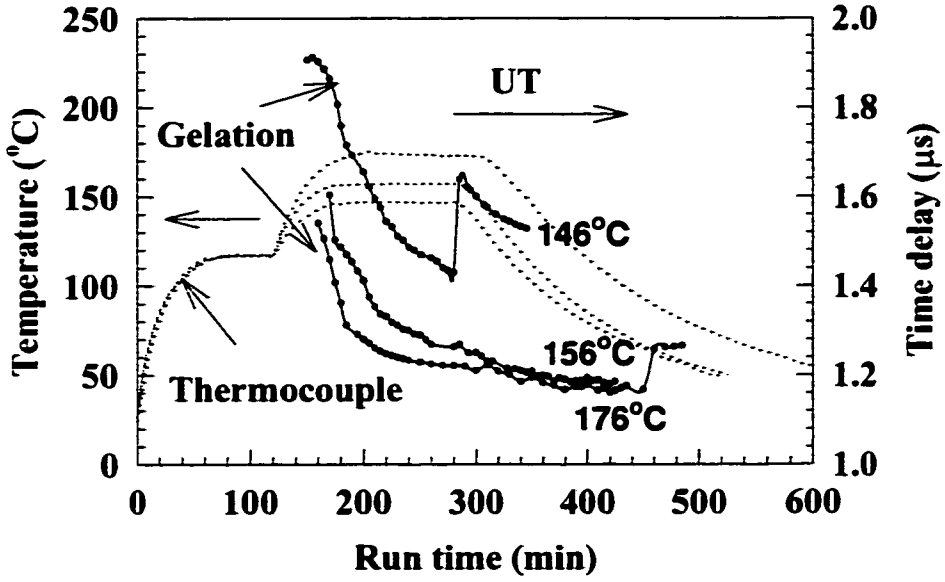

(b)

Figure 5-8 Ultrasonic cure monitoring by using reflection mode (a) Waveforms obtained from $[0_{16}]$ panel cured at 176°C for 2 hrs. (b) Variation of the time delay with cure temperature

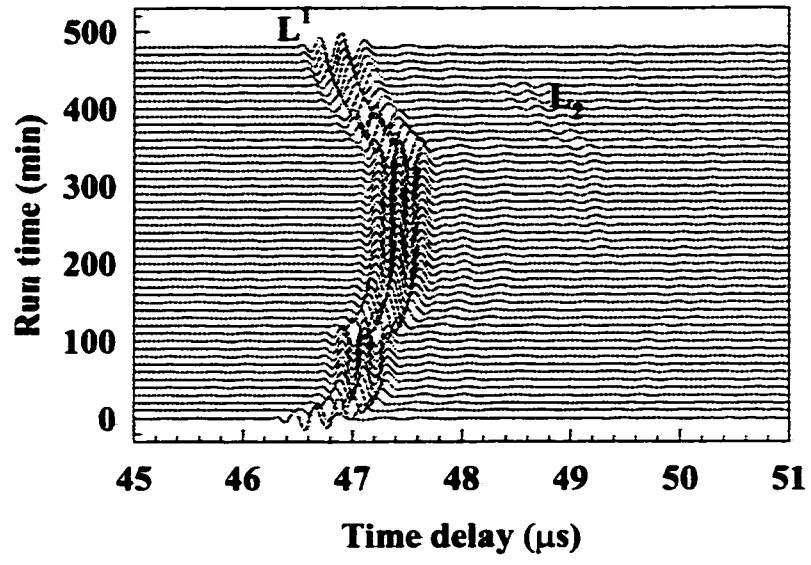

(a)

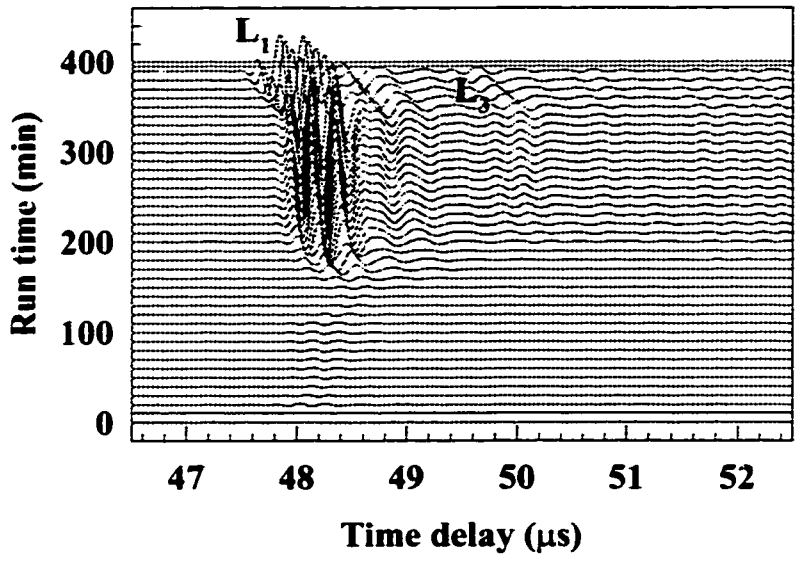

(b)

Figure 5-9 Ultrasonic waveforms obtained from (a) reflection and (b) transmission mode

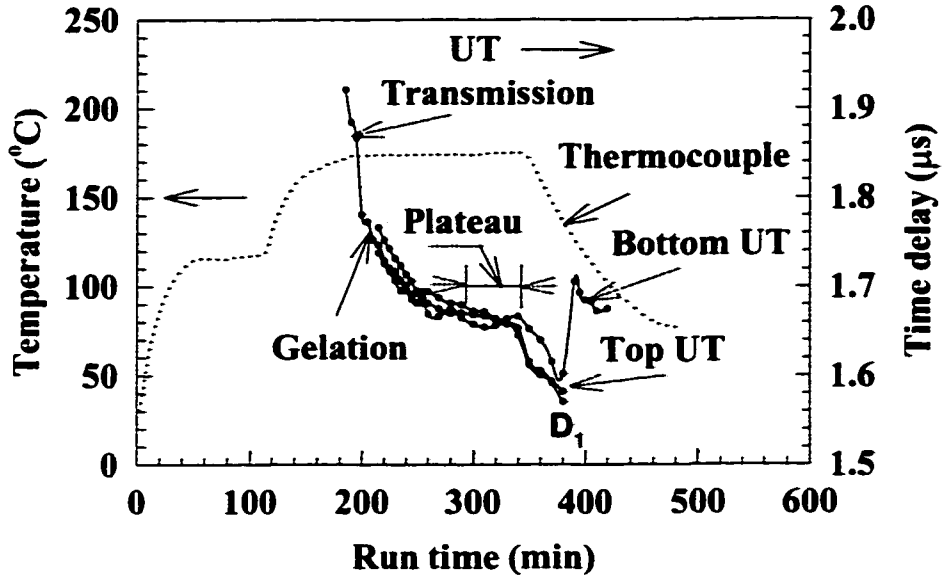

Figure 5-10 Time delay *vs.* run time obtained from reflection/transmission mode, where D_1 refers to the time when the detachment of the panel from the Al mold happens.

Figure 5-11, obtained from the same cure cycle as Figure 5-10, presents the variation of ultrasonic attenuation of the curing composite *vs.* run time during the cure, where ultrasonic attenuation α is defined as

$$\alpha = \frac{10}{h}\log\left(\frac{L_3}{L_1}\right) \tag{5-8}$$

In which L_1 and L_3 are the amplitudes of these pulses indicated in Figure 5-9(b), and h is the thickness of the panel. The variation in Figure 5-11 represents the basic features of the viscoelastic behavior of the epoxy resin as it cures. The attenuation reaches a maximum point, the gel point, and then drops dramatically during the development of gelation, indicating the rapid rise of the viscosity due to accelerated crosslinking at the early stage of the cure reaction. Then, the attenuation gradually decreases because, as crosslinking proceeds, the material behaves more as an elastic medium, with reduced absorption of ultrasonic energy. The plateau is reached when the constant viscoelastic properties of the composite have been developed at the end of cure. Finally, the attenuation further decreases as the material is cooled down. It has also been observed that thermoelastic damping of the cured composite, measured by Dynamic Mechanical

Analyzer (DMA) during this study, decreases with decreasing temperature (referred to in Section 2.4, Chapter 2).

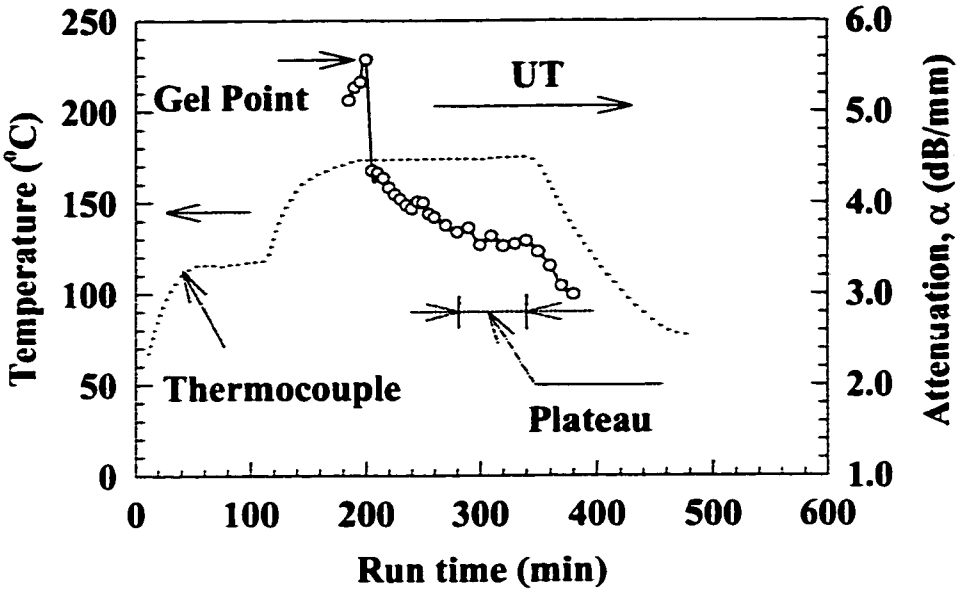

Figure 5-11 Ultrasonic attenuation *vs.* run time

5.4 Simultaneous ultrasonic and fiber-optic cure monitoring

In order to compare the cure monitoring capabilities of the ultrasonic and fiber-optic sensors, experiments are carried out on a [$90_6/0_2$/SG1, SG2/$0_2/90_6$] panel in which both techniques are operated simultaneously. Two fiber-optic strain gages are embedded at the mid-plane of the panel. The locations sensed by the fiber-optic and ultrasonic sensors are different but close to each other. The cure temperature and cure time are 176°C and 2 hours, respectively.

As shown in Figure 5-12, the two fiber-optic strain gages provide almost identical records of the cure process, before detachment of the panel from the Al mold plates occurs during the cooling stage. The strain gage-detected gelation period, as determined from the strain-temperature variation, agrees with the sharp drop of ultrasonic time delay which, as discussed earlier, corresponds to the rapid increase of the viscosity of the

composite epoxy at the early stage of the cure reaction. However, as observed earlier, the ultrasonic sensor is able to determine the end-of-cure, while the EFPI fiber-optic sensor is not. The end-of-cure happens as the ultrasonic time delay reaches a plateau.

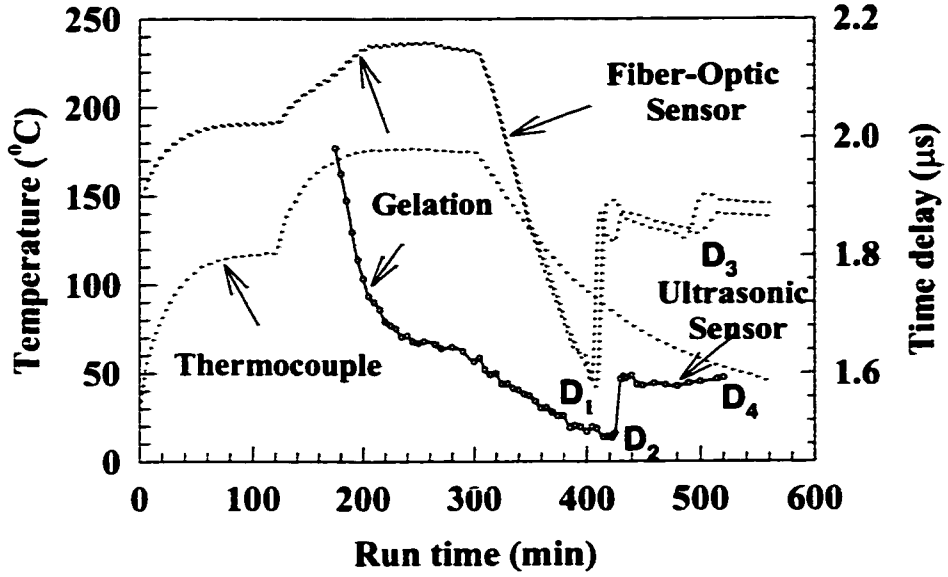

Figure 5-12 Results of simultaneous fiber-optic and ultrasonic cure monitoring

During the early cool-down stage, because the panel is attached to the Al mold plates, the free contraction of the panel is impeded, and the thermal strain detected by the fiber-optic sensors dramatically drops. After a certain time (D_1), the sudden detachment of one side of the panel from the Al mold plate happens, and its thermal strain sharply bounces back. This dip (D_1) is much larger than the dips indicated in Figures 4-6, 4-9 and 4-10 because in Figures 4-6, 4-9 and 4-10, we used the mold releasing agent at the bottom and accessories like peel ply, bleeder, *etc.* on top of the prepregs, while for simultaneous fiber-optic and ultrasonic monitoring, both sides of the panel are in direct contact with the mold releasing agent, leading to very different clinging force between the panel and the Al mold plates. Correspondingly, ultrasonic time delay appears as a discontinuity (D_2). Once more, when the detachment of the other side of the panel occurs, the readings from the fiber-optic sensor experience another small bounce (D_3), while the ultrasonic sensor totally loses its signal (D_4),

5.5 Ultrasonic impedance monitoring

It has been known for a long time that the shear reflectivity of ultrasonic waves from the interface between the probing end of the buffer rod and monitored curing resin is related to the viscoelastic properties of polymers [63,66,131,132]. This could lead to a direct evaluation of the complex shear modulus, dynamic (high frequency) viscosity, and even the relaxation times of the shear stresses. In this section, a shear reflectivity to evaluate the state-of-cure and viscoelastic behaviors of curing AS4/3501-6 Gr/Ep composites is presented.

5.5.1 Reduction of temperature effects

It is well known that piezoelectric UTs cannot function at elevated temperatures, and therefore a cooled buffer rod is required to convey the ultrasonic waves from the transducers to the processed materials and back. Cooling the buffer rods leads to simultaneous temperature, velocity and attenuation gradients, which are difficult to characterize. In order to significantly eliminate the adverse effects caused by the UT, couplant and buffer rod on the ultrasonic time delay and amplitude measurements, minor physical discontinuity "a" (*e.g.* a notch) near the probing end of the clad buffer rod is created to provide a reference signal, as indicated in Figure 5-13. Figure 5-14 shows the reflected 5 MHz shear waves from the curing composite. S^1 is the shear wave echo reflected from the probing end of the buffer rod, while S_a is the signal induced by the discontinuity "a". The latter signal is used for normalization. This distance between the discontinuity "a" and the end of the probe is around 16 mm, which is reasonably small to reduce the errors induced by the temperature gradient, but still large enough to allow the resolution, in time domain, of two signals. However, as seen in Figure 5-14, it is realized that the creation of the discontinuity "a" in the clad buffer rod does introduce slight spurious signals. Therefore S_a should be as small as possible; however, because one would like to reduce the digitization error, S_a should not be too small.

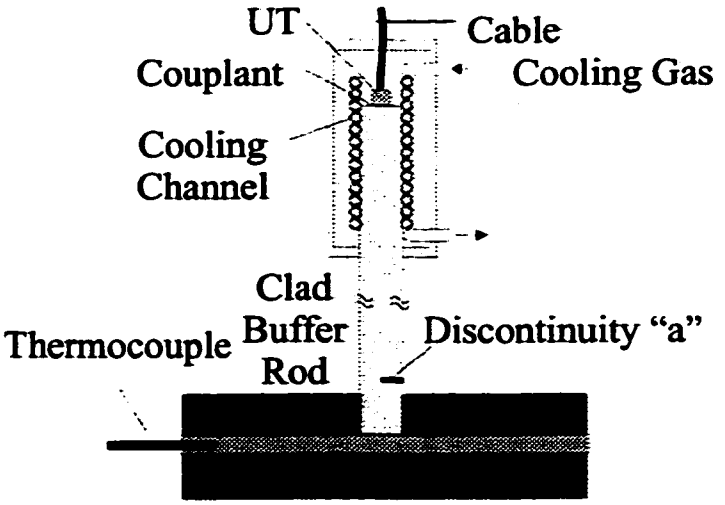

Figure 5-13 A clad buffer rod with one discontinuity, inside the Al mold

5.5.2 Shear impedance monitoring

The amplitude and phase of the reflected ultrasonic shear waves are correlated with the viscoelastic behaviors of the composite. Shear ultrasonic impedance Z_S is the product of the density (ρ) and shear wave (V_S) velocities, respectively. The reflection coefficient, Γ^*, at the buffer rod/process composite material interface is

$$\Gamma^* = \frac{(Z_B - Z_C^*)}{(Z_B + Z_C^*)} \tag{5-11}$$

where subscripts B and C refer to the buffer rod and processed composite material, respectively, and "*" denotes the complex number. Because the ultrasound in the polymer composite is highly attenuative, its velocity, V_C^*, and thus ultrasonic impedance, Z_C^*, are complex numbers, while since Al is a low-loss material, its ultrasonic impedance may be considered as a real number. By definition, $Z_C^* = \sqrt{\rho G_C^*}$, where G_C^* is the complex shear modulus of the composite, and ρ is its density. The complex shear modulus can then be calculated from the value of Γ*[132]:

$$G_C^* = \frac{Z_B^2}{\rho}\left(\frac{1-\Gamma^*}{1+\Gamma^*}\right)^2 \tag{5-12}$$

The evaluation of G_C^* leads to the calculation of the dynamic (high frequency) viscosity η, since this quantity is by definition the ratio of the imaginary part of the shear modulus to the angular frequency ω:

$$\eta = \frac{G_C^-}{\omega} \tag{5-13}$$

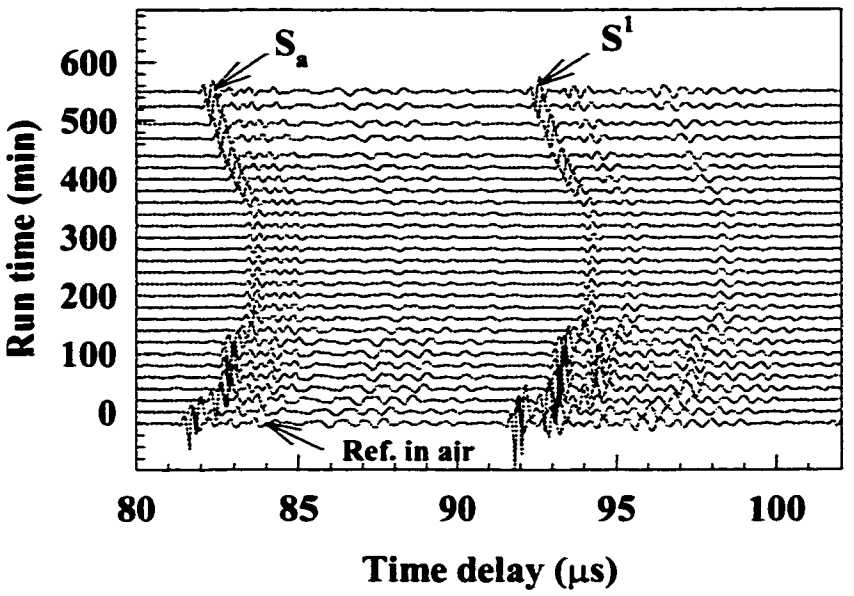

Figure 5-14 Ultrasonic waveforms obtained from 5 MHz shear UTs with one discontinuity "a"

On the other hand, let the Γ^* at the buffer rod/air (without processed composite) interface be unity, which means a total reflection at the interface; then the measured Γ_S^* can be expressed as [77]

$$\Gamma_S^* = \frac{S_C^1 / S_{a.C}}{S_{air}^1 / S_{a.air}} \tag{5-14}$$

where S is the amplitude of ultrasonic signals reflected from the notch or probing surface of the buffer rod. Subscript "C" denotes the buffer rod, which is in contact with the processed composite, while the subscript "air" denotes the buffer rod whose probing end is in contact with air. For simplicity, it is assumed that $S_{a,air}/S^1_{air}$ measured at elevated

temperature is approximately equal to that measured at ambient temperature. This approximation may not introduce significant errors in the magnitude of the shear reflectivity, but does induce phase errors.

The time delay between S^1 and S_a is related to the local average ambient temperature between the discontinuity "a" and the end of the buffer rod. This information may be used to evaluate the temperature of the Al mold and processed materials during cure processes. Figure 5-15 shows the time difference between the arrival of the echoes from the probe interface and the reference notch, plotted as a function of the process temperature. This time delay reflects the influence of temperature on the shear modulus, Poisson's ratio, density and length of the buffer rod material that is between the reference notch S_a and the probing surface S^1. If this temperature curve is well calibrated, it could be used for *in-situ* ultrasonic temperature monitoring during the cure processing of the composite.

Figure 5-16 shows the variation in shear reflectivity from the probing interface with the process temperature, indicating that during the gelation period of the composite epoxy, the reflectivity dramatically drops. Afterwards, the reflectivity decreases quite slowly as the cure reaction proceeds. During the cooling down stage, because of the influence of temperature, the reflectivity slowly increases. Then because of partial detachment of the panel from the Al mold, a sudden increase in reflectivity is observed. Obviously, the shear reflectivity of the curing composite is very sensitive to the development of gelation and the early stage of the cure reaction of the composite epoxy.

The evaluation of the phase information and the accuracy of Γ_S^* measurements is also of importance. However, because of the inherent defects in the present experiments, the phase information can not be accurately evaluated. In order to compensate for thermally-induced phase shift, two temperature runs are necessary. During the first one, in a temperature cycle similar to the one expected for the real cure, no composite is present. Then a run is made with the composite curing. However, it is still inevitable that a temperature difference between the recording of the two ultrasonic waveforms exists.

Furthermore, it is well known that because of the large difference between the Z_B of a clad Al buffer rod and Z_C^* of a polymer composite, a small error in Γ_S^* will lead large errors in Z_C^*. Thus, in order to obtain an accurate ultrasonic impedance of the processed material, Z_B should have low acoustic shear impedance and be as close as possible to Z_C^*.

5.6 Summary

The ultimate mechanical properties of composites are largely dependent upon the chemical and rheological events taking place during the manufacturing process. An *in-situ* measurement sensor is, therefore, essential for automated control of polymer composite fabrication. This Chapter presents a state-of-the-art cure processing monitoring system using thermally insulated ultrasonic transducers with clad Al buffer rods, and a specially designed autoclave feedthrough. This system has successfully monitored the entire cure process from semi-solid to a gel and solid. The major merits of the developed system can be summarized as: (1) workable at high temperature (up to 180°C) and gas pressure (up to 100 psi) inside an autoclave; (2) higher ultrasonic signal to spurious noise ratio (S/N), and high signal strength; (3) suitable for longitudinal and/or shear wave measurement in reflection and/or transmission mode.

By continuous recording of the velocity, attenuation and/or shear reflectivity of ultrasound waves, some important experimental features have been captured:

(1) Like the EFPI fiber-optic sensor, the ultrasonic sensor can sense the gelation period of AS4/3501-6 Gr/Ep composite, the start of cooling, and the detachment of the composite from the Al mold plates. In particular, the sudden decrease in ultrasonic time-delay and shear reflectivity, and the appearance of a peak in ultrasonic attenuation, give a clear indication of the gelation period of the curing composite epoxy. Also, the sudden phase change of ultrasonic pulses indicates the detachment of the composite part from Al mold during the cool-down period. The timing of the detachment from the Al mold plates may provide information concerning the development of thermal mismatch-induced strains.

However, the magnitude of developed residual stresses of the curing composite cannot be evaluated by the present ultrasonic technique alone.

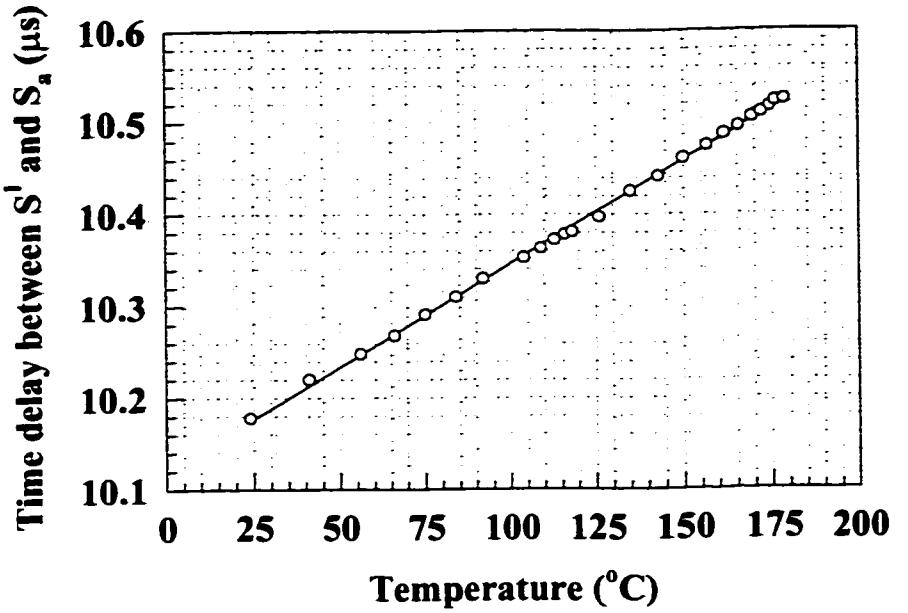

Figure 5-15 Temperature *vs.* time delay between S_a and S^I

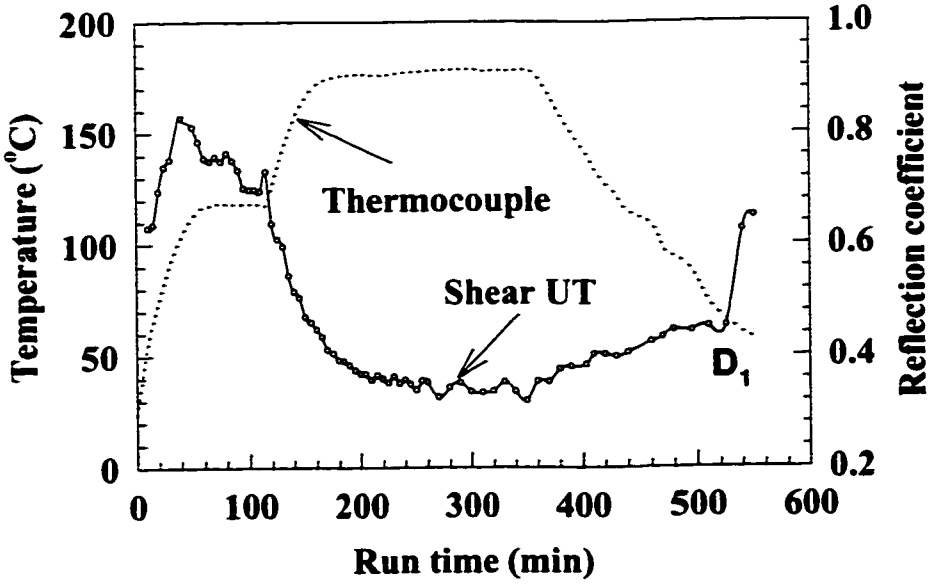

Figure 5-16 Reflection coefficient measurements for 5 MHz shear wave during cure

(2) *In-situ* ultrasonic cure process monitoring can sense the end-of-cure, in terms of the development of the viscoelastic properties of the composite, while the EFPI fiber-optic monitoring cannot. The end-of-cure is observed when the ultrasonic time delay or attenuation reaches a plateau during the second dwell stage of the cure reaction. In the case of AS4/3501-6 Gr/Ep composite, these results also agree with the commercially recommended cure process, which says that for 176°C cure temperature, two hours of cure time is enough to reach the end-of-cure. Moreover, for different cure temperatures from 146°C to 156°C and 176°C, increasing cure temperature significantly accelerates the development of the stiffness of the composites. This experimental research suggests that ultrasonic monitoring may be an effective way to *in-situ* assess the state-of-cure.

(3) The shear reflectivity from the probing end reflects the development of viscoelastic properties of the curing composite. The variation of the reflectivity is very sensitive to the development of gelation and early stages of cure reaction. Moreover, the variation in time delay (between the notch and the probing surface) with temperature implies that our system may also be used as a simultaneous temperature probe.

(4) It is also proved that the "degree of cure" measured by the DSC technique does not accurately reflect the mechanical property development during the cure. Significant changes in the stiffness of the composites still occur when the "degree of cure" indicated by DSC is almost fully developed.

Chapter 6

CONCLUSIONS AND FUTURE WORK

6.1 Claims of originality

The original experimental research contributions of this thesis have been mentioned in various locations of each chapter. However, for the convenience of the reader, they are outlined below:

In Chapter 2,

(1) The correlation between the process parameters such as cure temperature and cure time, and dynamic mechanical properties of AS4/3501-6 Gr/Ep has been systematically developed.

In Chapter 3,

(1) The correlation between elastic constants, ultrasonic velocity and dispersion and attenuation of AS4/3501-6 Gr/Ep composites and curing process conditions has been developed. The experimental results indicate that as process parameters, cure temperature significantly affect the development of the mechanical properties of curing composites.

In Chapter 4,

(1) An *in-situ* EFPI fiber-optic cure monitoring system has been developed. A special autoclave feedthrough for optical fibers and thermocouple wires to penetrate into an autoclave, which can still maintain a seal of 100 psi inside the autoclave, has been designed. Moreover, this feedthrough can be easily disassembled so that fiber-optic

sensors can be protected from damage, and reusable for in-service monitoring of the composite structures after the cure process. This system can be used to monitor local strain development in a composite resulting from temperature change, chemical shrinkage and process-induced stresses.

(2) By using this fiber-optic cure monitoring system, the gelation period and the build-up of residual strains in the curing composites, prior to and after the detachment from the Al molds, can be observed. The detachment of the curing composite from the Al mold during the cool-down phase indicates the magnitude of thermal mismatch between them. The importance of this finding is that thermal mismatch between the Al mold and the composite panel before detachment may result in micro-cracks during cool-down stage.

In Chapter 5,

(1) A state-of-the-art ultrasonic cure monitoring system for Gr/Ep composites has been developed, by using thermally insulated ultrasonic sensors with clad buffer rods. Moreover, a specially-designed autoclave feedthrough for optical fibers, thermocouple, ultrasonic transducer cables and air-cooling Teflon tubes makes the entire monitoring inside an autoclave possible. This system can monitor the evolution of viscoelastic properties of the composites by continuous recording of the velocity (time delay), attenuation and shear reflectivity of ultrasound waves.

(2) *In-situ* cure monitoring results of AS4/3501-6 Gr/Ep composites indicate that (i) ultrasonic sensors can sense the gelation period of the curing composite and the starting of the cooling stage; (ii) ultrasonic cure monitoring can sense the end-of-cure of the composites in terms of the development of stiffness of the curing composite, when ultrasonic time delay and attenuation reach a plateau. This strongly suggests that ultrasonic monitoring may be an effective way for *in-situ* assessment of the state-of-cure; (iii) ultrasonic sensors can clearly observe the detachment of cured panels from the Al mold during the cool-down period; (iv) by using clad buffer rods with a discontinuity, variations in shear reflectivity during the cure process can be measured,

and the potential simultaneous temperature measurement by this technique is also demonstrated.

The above thesis work has led to one published refereed journal paper (for the contents of Chapters 2 and 3): Journal of Polymer Composites; one submitted refereed journal paper (for the contents of Chapters 4 and 5): Journal of Composite Materials; one journal paper which is in preparation (for the content of Chapters 4), and two published international conference papers (for the contents of Chapters 2, 3, 4 and 5): 1996 ICCE/3 and 1997 Annual Conference of America Society for Composites. The work related with ultrasonic cure monitoring system led to a professional service from Institute for Aerospace Research, National Research Council of Canada under Contract No. CS7-253552-00 for implementation of our *in-situ* ultrasonic cure monitoring system for graphite/epoxy composite processing in an autoclave.

6.2 Conclusions

The current experimental research on cure processing monitoring and characterization of AS4/3501-6 Gr/Ep composites using fiber-optics and ultrasonics can be summarized as

- **Characterization of viscoelastic properties**

(1) Thermal characterization

DSC analysis is used to characterize the chemical kinetic behavior of Hercules 3501-6 epoxy and AS4/3501-6 Gr/Ep prepreg, while DMA tests are carried out to characterize the viscoelastic properties of the composites by measuring their complex modulus E^*, loss tan δ and apparent glass transition temperature T_g.

The results indicate that cure processing parameters significantly affect the final properties of the materials. As cure temperature increases, the degree of cure increases, while the time for the completion of the cure reaction significantly decreases. For example, at cure temperatures of 176°C and 186°C, the cure reaction is almost fully

completed after 60 minutes cure reaction, while after curing for 120 minutes at 146°C, the degree of cure of the composite only reaches around 70%. The features of cure kinetic behaviors of the present Hercules 3501-6 epoxy can be captured by modified Springer's equations.

Meanwhile, increasing cure temperature in the range from 146°C and 186°C results in a noticeable decrease in loss tan δ, and a profound increase in the T_g of the epoxy and composite by around 55°C and 74°C, respectively. At the same time after being cured for 60 minutes at 176°C, the T_gs of the epoxy and composite are still increased by around 21°C and 6°C by another hour's curing, respectively, although at that period the cure reaction is almost fully completed in terms of the development of degree of cure.

(2) Ultrasonic characterization

Effects of cure process parameters on the viscoelastic properties of AS4/3501-6 Gr/Ep composites have been investigated by using the velocities of elastic waves which propagate in various directions in composites, along with density, attenuation, and velocity dispersion. The results show that the moduli of Hercules 3501-6 epoxy monotonically increase with increasing cure temperature from 146°C to 176°C, whereas the moduli of the corresponding composite cured at 186°C for 120 minutes have a drop. Also, the moduli of the composite monotonically increase with increasing cure time at 176°C, whereas the moduli of the epoxy, after being cured for 80 minutes at 176°C, exhibit no change. The ultrasonic through-thickness dispersion and attenuation of the epoxy and composite are less sensitive to variations in cure conditions in the present range of measured frequencies.

In short, ultrasonic testing is an effective technique to evaluate viscoelastic properties of composites processed by different cure conditions. The sensitivity of the measurement is much higher than the conventional static mechanical technique. However, ultrasonic dispersion and attenuation may not be suited to characterize the

variation of mechanical properties of the composites caused by different cure conditions, because of their low sensitivity in this case.

• *In-situ* cure processing monitoring

(1) *In-situ* fiber-optic cure processing monitoring

The EFPI fiber-optic sensor has been investigated as a potential candidate for *in-situ* cure monitoring of AS4/3501-6 Gr/Ep composites. The *in-situ* cure monitoring system developed in this study is comprised of optical fibers, a K-type thermocouple, and the associated signal process instruments. A special feedthrough is designed for the optical fibers and thermocouple wires to penetrate the autoclave, which can maintain a seal at 100 psi. Moreover, the fiber-optic gages can also be kept in good condition during the period of cure processing, and be re-used for future in-service monitoring of composites after the cure process.

The real-time experimental research indicates that (1) the optical fiber can sense the gelation period, the start of cooling and the build-up of residual strains during cure; (2) the information on detachment during the cool-down period may help to evaluate the development and magnitude of thermal mismatch strains between the Al mold and the composite panel. The importance of this finding is that thermal mismatch between the Al mold and the composite panel before detachment may result in micro-cracks.

In short, this technique is particularly suited for non-destructive, real-time *in-situ* monitoring of the development of residual stress in curing composites. Moreover, this technique has been shown to possess a clear potential for further monitoring the structural integrity of the composite during part qualification, and throughout its service life. However, the EFPI fiber-optic gages cannot sense the end-of-cure without the assistance of other sensors. This technique, in combination with other types of sensors including ultrasonics, holds promise for alleviating some of the problems associated with the manufacture of advanced materials.

(2) *In-situ* ultrasonic cure processing monitoring

A state-of-the-art cure processing monitoring system has been established by using thermally-insulated ultrasonic transducers with clad buffer rods and a specially designed autoclave feedthrough. This system has successfully monitored the entire cure process from semi-solid to a gel and solid. The major merits of the developed system can be summarized as (1) workable in an autoclave at high temperature (up to 180°C) and gas pressure (up to 100 psi); (2) high signal to spurious ultrasonic noise ratio (S/N), and high signal strength; (3) suitable for longitudinal and/or shear wave measurement in reflection and/or transmission mode.

By monitoring the evolution of viscoelastic properties of AS4/3501-6 Gr/Ep composites by continuous recording of the velocity (time delay), attenuation and/or shear reflectivity of ultrasound waves, some important features have been captured: (1) ultrasonic sensors can sense the development of the gelation of composites, the start of cooling, and the detachment of the composites from the Al mold plates. In particular, the sudden decrease in ultrasonic time-delay and shear reflectivity, and the appearance of a peak in ultrasonic attenuation give a clear indication of gelation period of the curing composite. Also, the timing of the detachment from the Al mold may provide information concerning the development of thermal mismatch strains during the cool-down phase. (2) *In-situ* ultrasonic cure process monitoring can sense the end-of-cure, in terms of the development of the viscoelastic properties of the composite. The end-of-cure is observed when the ultrasonic time delay or attenuation reaches a plateau during the cure reaction dwelling stage. In the case of AS4/3501-6 Gr/Ep composites, these results also agree with the commercially recommended cure process, which stipulates that at 176°C cure temperature, two hours of cure time is enough to reach the end-of-cure. Moreover, for different cure temperatures of 146°C, 156°C and 176°C, increasing cure temperature significantly accelerates the development of the stiffness of the composites. (3) The shear reflectivity from the probing end reflects the development of viscoelastic behavior of the curing composite. The variation of the reflectivity is very sensitive to the gelation period and early stage of cure reaction since the viscosity of the curing composite dramatically

increases. Moreover, the variation of time delay between the notch and the probing surface of a buffer rod with temperature implies that the cure monitoring system may also be used as a simultaneous temperature probe during the cure.

Furthermore, simultaneous *in-situ* fiber-optic and ultrasonic monitoring indicates that extra information about the build-up of residual stresses during processing may be obtained by this technique. These monitors could be integrated into decision-making of an expert system to control the final quality of composites at any stage of the cure process.

6.3 Suggested future experimental research

Our preliminary experimental research has attracted the attention from two Canadian institutions: Institute for Aerospace Research, NRC and Bell Helicopter Textron. On the basis of wide investigation and discussion, our near future work will be the following:

- To transfer the present technology from the laboratory bench to the factory environment (in industrial autoclaves)
- To characterize the properties of composite during the cure processing, not at room temperature which is well below T_g
- To study effects of the geometry of composites and process parameters on ultrasonic cure processing monitoring (these factors affect the sensitivity of monitored parameters during the cure.)
- To investigate effects of mold materials and releasing agents on the detachment of the composite component from the mold
- To correlate the ultrasonic measurement results with desired material properties, such as degree of cure, porosity, delamination and glass transition temperature
- To establish intelligent composite cure expert system with our "smart" sensors

Much development is still required to transfer the present technology from the laboratory bench to the factory environment; however, with the potential financial savings

offered by better control and lower component rejection, intelligent composite cure expert system with "smart" sensors are likely to become a reality.

Appendix I:

Alignment procedure for through-transmission measurement in a water immersion tank at IMI

The precision of ultrasonic measurements of the anisotropic elastic constants is very sensitive to the alignments among the ultrasonic transducers (UTs), sample and positioners. In order to achieve a good alignment, the following procedure is carried out. At first, the turntable is aligned in the reference XY plane by using both optical and ultrasonic techniques which guarantee flatness. The center of the turntable is then used as the reference point. Then the X, Y, Z and two rotational axes of the positioner controlled by stepping motors are calibrated.

The remaining critical steps of the alignment in the measurements are that two UTs, the transmitter UT_T and the receiver UT_R and the center of the turntable must be aligned collinearly, and the alignment line should be in parallel with the Y axis of the positioner, as shown in Figure I-1(a). Also the front faces of the UTs and the sample surfaces should be parallel to the XZ plane, as shown in Figure I-1(b). The details are described below:

A. The UT_R attached to the scanner of the postioner is firstly aligned to the flat part of the turntable (*i.e.* XY plane) by adjusting UT_R and making sure that the reflected echo from the flat turntable reaches the maximum. This ensures that the axis of the UT_R is parallel to the Z axis. Then the UT_R is rotated 90°, thus the axis of the UT_R is parallel to the XY plane.

B. In order to accurately align the axis of UT_R parallel to the X or Y axis, as a first step, we operate the UT_R in the reflection mode and align the UT_R so that the reflection echo from the flat wall which is nearly parallel to the YZ plane is maximized. Then we scan the UT_R along the YZ plane, using the time delay of the received ultrasonic signal to evaluate the parallelism between the YZ plane and the flat wall. It is found that the deviation is 0.06°. Thus it can be assumed that the axis of the UT_R is parallel to the X axis within a 0.06° error bound. We then rotate the UT_R 90° in the XY plane, and the UT_R now points to the Y axis.

C. The UT_R is further operated in the reflection mode, and scanned along the X direction through a cylindrical reflector located at the center of the turntable (XY plane). The location of maximum reflection echo indicates that the UT_R is aligned with the center of the turntable, and also parallel to the Y axis.

D. In order to align the other transducer UT_T, the cylindrical reflector is firstly removed from the turntable. We then move the UT_R along the Y axis from one side of the turntable across the center point, and reach the other side. The UT_T is later installed with an optimum distance described in Section E below, away from the UT_R. Since the UT_T is fixed to a jig having three-dimensional freedom of movement, it is adjusted to have the maximum reflection echo from the reflector, which is the front surface of the UT_R. Now we consider that the axis of the UT_T is aligned along the Y axis.

E. The distance y between the UTs and the sample as shown in Figure I-1(a) should be in the far field regime. This means that $S = y\lambda/a^2 \geq 2$, where S is dimensionless distance factor, y is the distance, λ is the acoustic wavelength in water, and a is the radius of the transducer.

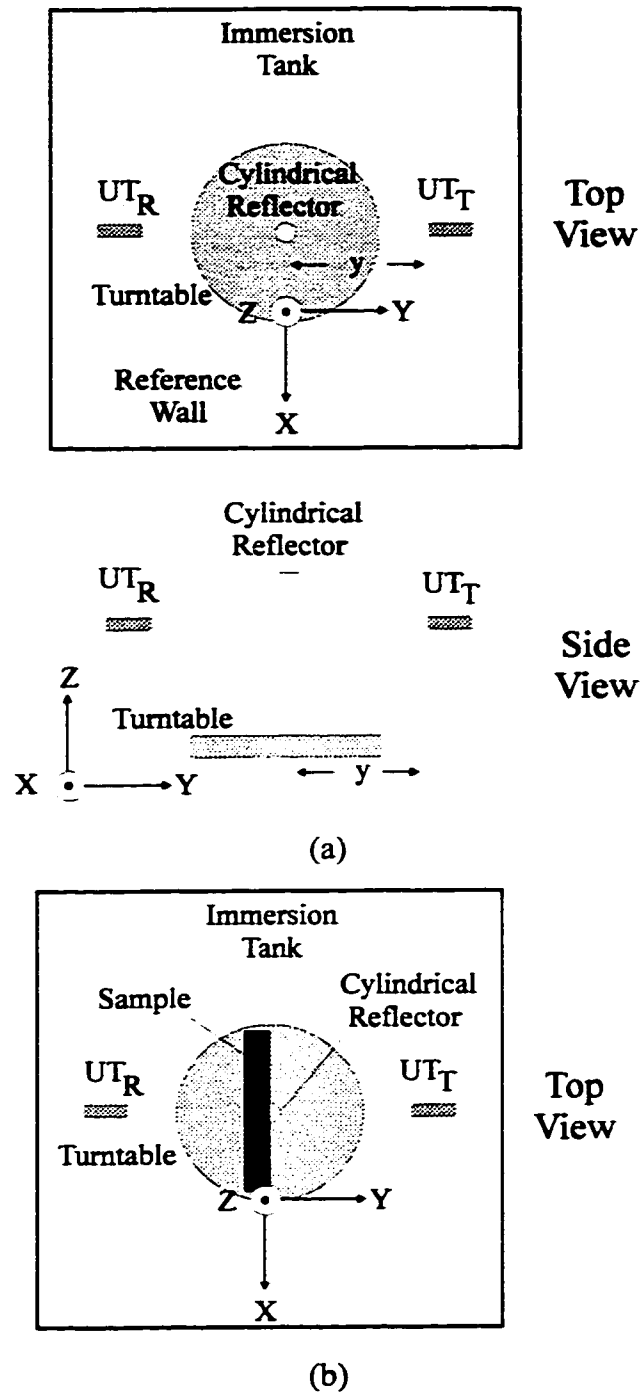

Figure I-1 Alignment configuration for (a) transducers, and (b) the sample

Case A:

let f = 5 MHz; then λ (in water) = 0.3 mm.

let a = 0.125" = 3.175 mm; then ka = $(2\pi a)/\lambda$ = 66 (>10, which is a requirement)

let S = 3; then y = 100 mm.

Case B:

let f = 2.25 MHz; then λ (in water) = 0.667 mm.

let a = 0.25" = 6.35 mm; then ka= $(2\pi a)/\lambda$ = 59.8 (>10, which is a requirement)

let S = 3; then y = 181 mm.

F. The front surface of the sample should be parallel to the XZ plane and at the center of the turntable, as shown in Figure I-1(b).

Now it can be said that the system is aligned.

References

[1] Schwartz, M.M. (ed.), Fabrication of Composite Materials: Source Book, American Society for Metals, Metal Park, OH, 1985

[2] Schwartz, M.M. (ed.), Composite Materials Handbook, McGraw-Hill, New York, 1984

[3] Ciriscioli, P.R., G.S. Springer, and W.I. Lee, *An expert system for autoclave curing of composites*, J. Composite Materials, **25**, 1991:1542-1587

[4] Hull, D., Introduction to Composite Materials, Cambridge University Press, 1981

[5] Loos, A.C. and G.S. Springer, *Curing of epoxy matrix composites*, J. Composite Materials, **17**, 1983:135-169

[6] Sih, G.C., *Toward decision making in knowledge-based systems for composite cure*, in Advanced Technology for Design and Fabrication of Composite Materials and Structure, G.C.Sih, A.Carpenteri, and C.Surace (eds.), Kluwer Academic Publishers, Netherlands, 1994: 1-14

[7] Purslow, D. and P. Childs, *Autoclave moulding of carbon fiber-reinforced epoxies*, Composites, **17**(2), 1986:127-136

[8] Huang, H.T., *Process-property relationships in autoclave cured graphite/epoxy resin composites*, Ph.D. Thesis, Polytechnic University, 1988

[9] Donnellan, T.M., P.A. Mehrkam, A. Yen, R. Jurek, and R.J. Morgan, *Structure-property relationships in high temperature resin and composites*, Proc. Am. Soc. Composites, Sixth Technical Conf., Albany, NY, Technomic, Lancaster, PA, 1991:3-12

[10] Hoa, S.V., Computer-Aided Design of Polymer-Matrix Composite Structures, Marcel Dekker, New York, 1995

[11] Tsai, S.W., Composites Design, 4th edtion, Think Composites, Dayton, 1988

[12] Tsai, S.W and H.T. Hahn, Introduction to Composite Materials, Technomic, Lancaster, PA, 1980

[13] Hollaway, L., Handbook of Polymer Composites for Engineers, Woodhead Publishing Ltd., Cambridge, England, 1994

[14] Design and Manufacturing of Advanced Composites, Proc. 5th ASM/ESD Advanced Composites Conf., Dearborn, MI, ASM International, Metals Park, OH, 1989

[15] Hoa, S.V. and H. Hamada, (eds.), Design and Manufacturing of Composites: Proc. Joint Canada-Japan Workshop on Composites, Kyoto, Japan, 1996, Technomic, Lancaster, PA, 1997

[16] Carlsson, L.A. and R.B. Pipes, *Experimental characterization of advanced composite materials*, Prentice-Hall, Inc., Englewood Cliffs, NJ, 1987

[17] Lee, W.I., A.L. Loos, and G.S. Springer, *Heat of reaction, degree of cure, and viscosity of Hercules 3501-6 resin*, J. Composite Materials, **16**, 1982:510-520

[18] Loos, A.C., *Modeling the curing process of thermosetting resin matrix composites*, in Review of Progress in QNDE, **5B**, 1986: 1001-1013

[19] Loos, A.C. and G.S. Springer, *Calculation of cure process variables during cure of graphite/epoxy composite*, in Composite Materials: Quality Assurance and Process, **STP 797**, C.E. Browning (ed.), ASTM, 1983:110-118

[20] White, S.R. and H.T. Hahn, *Process modeling of composite materials: residual stress development during cure, part I. model formulation*, J. Composite Materials, **26**(16), 1992: 2402-2422

[21] White, S.R. and H.T. Hahn, *Process modeling of composite materials: residual stress development during cure, part II. experimental validation*, J. Composite Materials, **26**(16), 1992:2423-2453

[22] Mallow, A.R., F.R. Muncaster, and F.C. Campbell, *Science based cure model for composites*, in Proc. Am. Soc. Composites, First Technical Conf., Dayton, OH, Technomic, Lancaster, PA, 1986:171-186

[23] Ciriscioli, P.R., Q. Wang, and G.S. Springer, *Autoclave curing - comparisons of model and test results*, J. Composite Materials, **26**(1), 1992:90-102

[24] Jang, B.Z., Advanced Polymer Composites, ASM International, Matels Park, OH, 1994

[25] Chiao, L. and R.E. Lyon, *A fundamental approach to resin cure kinetics*, J. Composite Materials, **24**(7), 1990: 739-752

[26] Mantell, S.C., P.R. Ciriscioli, and G. Almen, *Cure kinetics and rheology models for ICI Fiberite 977-3 and 977-2 thermosetting resins*, J. Reinforced Plastics & Composites, **14**(8), 1995:847-865

[27] Nielsen, L.E., Mechanical Properties of Polymers and Composites, **1**, Marcel Dekker, Inc., New York, 1974

[28] Murayama, T., Dynamic Mechanical Analysis of Polymeric Material, Elsevier Scientific Publishing, Co., New York, 1978

[29] Kim, Y.K. and S.R. White, *Process-induced stress relaxation analysis of AS4/3501-6 laminate*, J. Composite Materials, **16**(1), 1997:2-16

[30] J.-Y. Chen, S.V. Hoa, C.-K. Jen, D. Levesque, and J.-P. Monchalin, *The studies of dynamic mechanical properties of AS4/3501-6 composites with different curing conditions*, ICCE/3, New Orleans, LA, 1996:155-156

[31] Day, D.R. and D.D. Shepard, *Correlation of dielectric cure index to degree of cure for 3501-6 graphite epoxy*, in Design and Manufacturing of Advanced Composites, ASM International, Metal Park, OH, 1989:147-151

[32] Kranbuehl, D.E., S.E. Delos, M.S. Hoff, M.E. Whitharn, and L.W. Weller, *Dynamic dielectric analysis for nondestructive cure monitoring and process control*, in Advanced Composites: the Latest Development, ASM International, Metal Park, OH, 1986:61-67

[33] Sanford, W.M. and R.L. McCullough, *Modelling the viscosity and dielectric behavior during the cure of epoxy matrix composites*, in Proc. Am. Soc. Composites, First Technical Conf., Dayton, OH, Technomic, Lancaster, PA, 1986: 129-136

[34] Kim, J.S. and D.G. Lee, *Measurement of the degree of cure of carbon fiber epoxy composite materials*, J. Composite Materials, **30**(13), 1996:1436-1457

[35] Mopsik, F.I., S.-S. Chang, and D.L. Hunston, *Dielectric measurements for cure monitoring*, Materials Evaluation, **47**, 1989:448-465

[36] Ciriscioli, P.R. and G.S. Springer, *Dielectric cure monitoring - a critical review*, SAMPE Journal, **25**(3), 1989:35-42

[37] Steenkiste, R.J.V. and G.S. Springer, Strain and Temperature Measurement with Fiber Optic Sensors, Technomic, Lancaster, PA, 1997

[38] Roberts, S.S. and R. Davidson, *Cure and fabrication monitoring of composite materials with fiber-optic sensors*, Composites Science and Technology, **49**, 1993:265-276

[39] Crosby, P.A., G.R. Powell, G.F. Fernando, C.M. France, R.C. Spooncer, and D.N. Waters, *In situ cure monitoring of epoxy resin using optic fiber sensors*, Smart Mater. Struct., **8**, 1996:415-428

[40] Lawrence, C.M., D.V. Nelson, J.R. Spingarn, and T.E. Bennett, *Measurement of process-induced strains in composite materials using embedded fiber optic sensors*, Proc.SPIE, **2718**, 1996:60-68

[41] Milkovich, S.M., R.I. Altkorn, R.H. Haidle, M.J. Neatrour, and J.M. Fildes, *In situ sensors for intelligent process control for fabrication of polymer-matrix composite materials*, Proc. SPIE, **2191**,1994:349-360

[42] May, R.G. and R.O. Claus, *In-situ optic sensor for composite cure monitoring through characterization of resin viscoelasticity*, Proc. SPIE, **2948**, 1996:24-34

[43] Dorighi, J., S. Krishnawamy, and J. Achenbach, *A fiber-optic ultrasonic system to monitor the cure of epoxy*, Res. Nondestr. Eval., **9**, 1997:13-24

[44] May, R.G, J.M. Sanderson, and R.O. Claus, *Combined fiber optic strain sensor and composite cure monitor for smart structure applications*, Proc. SPIE, **2191**, 1994:46-57

[45] Drug, M.A., L. Elandjian, W.A. Stevenson, R.D. Driver, G.M. Leskowitz, and L.E. Curitiss, *Fourier Transform Infrared (FTIR) fiber-optic monitoring of composites during cure in an autoclave*, Proc. SPIE, **1170**, 1989:

[46] Liu, Y.M., C. Ganesh, J.P.H. Steele, and J.E. Jones, *Fiber optic sensor development for real-time in-situ epoxy cure monitoring*, J. Composite Materials, **31**(1), 1997:87-102

[47] Myrick, M.L., S.M. Angel, R.E. Lyon, and T.M. Vess, *Epoxy cure monitoring using fiber-optic Raman spectroscopy*, SAMPE Journal, **28**(4), 1992:37-42

[48] Leka, G.L. and E. Bayo, *A close look at the embedment of optical fibers into composite structures*, J. Composites Technology & Research, **11**(3), 1989:106-112

[49] Chiou, S., P. Kukuchek, D. Echternach, G. Carman, and L. Lai, *Processing monitoring of carbon/phenolic composites using smart sensors*, Proc. SPIE, **2191**, 1994:338-348

[50] Sofer, G.A. and E.A. Hauser, *A new tool for determination of the stage of polymerization of thermosetting polymers*, J. Polymer Science, **8**(6), 1952:611-620

[51] Papadakis, E.P., *Monitoring the moduli of polymers with ultrasound*, J. Appl. Phys., **45**(3), 1974:1218-1222

[52] Lindrose, A.M., *Ultrasonic wave and moduli change in a curing epoxy resin*, Experimental Mechanics, July, 1978:227

[53] Rokhlin, S.I., D.K. Lewis, K.F. Graff, and L. Adler, *Real-time study of frequency dependence of attenuation and velocity of ultrasonic waves during the curing reaction of epoxy resin*, J. Acoust. Soc. Am., **76**(9), 1986:1786-1793

[54] Whitney, T.M and R.E. Green, Jr., *Cure monitoring of carbon epoxy composites: an application of resonant ultrasound spectroscopy*, Ultrasonics, **34**, 1996:347-353

[55] Winfree, W.P. and F.R. Parker, *Measurement of the degree of cure in epoxies with ultrasonic velocity*, Preview of Progress in QNDE, **5B**, 1986:1055-1060

[56] Parker, F.R. and W.F. Winfree, *Acoustic characterization of composite cure*, Review of Progress in QNDE, **5B**, 1986:1063-1067

[57] Veronesi, W.A, *In-process cure monitoring of fiber-reinforced polymer composites using ultrasound*, Proc. Sagamore Conf., 1994:333-341

[58] Chow, A.W. and J.L. Bellin, *Simultaneous acoustic wave propagation and dynamic mechanical analysis of curing of thermoset resins*, Polymer Engineering and Science, **32**(3), 1992:182-190

[59] White, S.R. and P.T. Mather, *Ultrasonic and thermal cure monitor of an epoxy resin*, 36th International SAMPE Symposium, 1991:15-18

[60] Saliba, T, S. Saliba, J. Lanzafame, and L. Gudeman, *In-situ cure monitoring of advanced composite materials*, 37th International SAMPE Symposium, 1992:1445-1454

[61] Biermann, P.J., J.H. Carnmer, C.A. Lebowitz, and L.M. Brown, *End-of-cure sensing using ultrasonics for autoclave fabrication of composites*, Proc. SPIE, **2948**, 1996:72-83

[62] Tuegel, E.J. and H.T. Hahn, *Ultrasonic cure characterization of epoxy resin: constitutive modeling*, in Proc. Am. Soc. Composites, First Technical. Conf., Dayton, OH, Technomic, Lancaster, PA, 1986: 129-136

[63] Yen, C.E. and B.R. Tittmann, *Guided wave sensor for in-situ high temperature process monitoring*, Proc. 1995 IEEE Ultrasonics Symposium, Seattle, WA, 1995:799-802

[64] Piche, L., P. Massines, G. Lessard, and A. Hamel, *Ultrasonic characterization of polymer as function of temperature, pressure and frequency*, Proc. 1987 IEEE Ultrasonics Symposium, Denver, CO, 1987:1125-1130

[65] Sahnoune, A., L. Piche, A. Hamel, R. Gendron, and L.E. Daigneault, *Ultrasonic monitoring of forming in polymer*, ANTEC'97, 1997:2259-2263

[66] Shah, V., K. Balasubramaniam, R.-D. Costley, and J.P. Singh, *Sensor development for high temperature viscosity measurement*, in Review of Progress in QNDE, San Diego, CA, 1997

[67] Jen, C-K., C. Neron, E.L. Adler, G.W. Farnell, J. Kushibiki, and K. Abe, *Long acoustic imaging probe*, Proc. 1990 IEEE Ultrasonics Symposium, Honolulu, HI, 1990:875-880

[68] Jen, C.-K., Z. Wang, C. Neron, A. Miri, and K. Abe, *Tapered acoustic buffer rods*, Electronic Letters, **27**(20), 1991:1877-1879

[69] Jen, C.-K., Z. Wang, A. Nicolle, J.F. Bussiere, E.L. Adler, and K. Abe, *Acoustic waveguiding rods of graded velocity profiles*, Ultrasonics, **30**, 1992:91-94

[70] Jen, C.-K., C. Neron, A. Miri, H. Soda, A. Ohno, and A. McLean, *Fabrication and characterization of continuously cast clad metallic buffer rods*, J. Acoust. Soc. Am., **91**, 1992:3565-3570

[71] Soda, H., C.-K. Jen, G. Motoyasu, S. Okumura, A. Ohno, and A. McLean, *Fabrication and characterisation of aluminium clad aluminium-copper alloy cored rods, Materials Science and Technology*, **11**, 1995:1174-1179

[72] Jen, C.-K. and J.-G. Legoux, *High performance clad metallic buffer rods*, Proc. IEEE Ultrasonics Symposium, San Antonio, TX, 1996:771-776

[73] Legoux, J.-G. and C.-K. Jen, *Ultrasonic applications of thick metallic coatings*, Proc.ITSC '96, Cincinati, OH, 1996:65-72

[74] Marple, B.R., C.-K. Jen, and J. Voyer, *Ceramic-clad ceramic system for ultrasonic wave guidance*, Proc. ITSC '98, Nice, France, 1998

[75] Jen, C.-K., B. Cao, K.T. Nguyen, C.A. Loong, and J.-G. Legoux, *On-line ultrasonic monitoring of a die-casting process using buffer rods*, Ultrasonics, **35**, 1997:335-344

[76] Chen, J.-Y., S.V. Hoa, C.-K. Jen, and H. Wang, *In-situ monitoring of graphite/epoxy cure using optical fiber and ultrasonic sensors*, submitted to J. Composite Materials, 1997

[77] C.-K. Jen, J.-Y. Chen, S.V. Hoa, K.T. Nguyen, J.-G. Legoux, and H. Hebert, *Clad buffer rods for in-situ process monitoring*, Proc. 1997 IEEE Ultrasonics Symposium, Toronto, ON, 1997

[78] Lee, S.Y. and G.S. Springer, *Effects of cure on the mechanical properties of composites*, J. Composite Materials, **22**(1), 1988:15-29

[79] Rokhlin, S.I. and W. Wang, *Critical angle measurement of elastic constants in composite material*, J. Acoust. Soc. Am., **86**(5), 1989:1876-1882

[80] Rokhlin, S.I. and W. Wang, *Double through-transmission bulk wave method for ultrasonic phase velocity measurement and determination of elastic constants of composite materials*, J. Acoust. Soc. Am., **91**(6), 1992:3303-3312

[81] Chu, Y.C. and S.I. Rokhlin, *Stability of determination of composite moduli from velocity data in planes of symmetry for weak and strong anisotropies*, J. Acoust. Soc. Am., **95**(1), 1994:213-225

[82] Chu, Y.C. and S.I. Rokhlin, *Comparative analysis of through-transmission ultrasonic bulk wave methods for phase velocity measurements in anisotropic materials*, J. Acoust. Soc. Am., **95**(6), 1994:3204-3212

[83] Chu, Y.C., A.D. Degtyar, and S.I. Rokhlin, *On determination of orthotropic material moduli from ultrasonic velocity data in nonsymmetry planes*, J. Acoust. Soc. Am., **95**(6), 1994:3191-3203

[84] Chu, Y.C. and S.I. Rokhlin, *A method for determination of elastic constants of a unidirectional lamina from ultrasonic bulk velocity measurements on [0/90] cross-ply composites*, J. Acoust. Soc. Am., **96**(1), 1994:342-352

[85] Wooh, S.-C. and I.M. Daniel, *Mechanical characterization of a unidirectional composite by ultrasonic methods*, J. Acoust. Soc. Am., **90**(6), 1991:3248-3253

[86] Kline, R.A., *Wave propagation in fiber reinforced composites for oblique incidence*, J. Composite Materials, **22**, 1988:287-303

[87] Kline, R.A. and Z.T. Chen, *Ultrasonic technique for global anisotropic property measurement in composite materials*, Material Evaluation, **46**, 1988:986-992

[88] Kim, K.Y., *Analytic relations between the elastic constants and the group velocity in an arbitrary direction of symmetry planes of media with orthorhombic or higher symmetry*, Physical Review B, **49**(6), 1994:3713-3724

[89] Kim, K.Y., T. Ohtani, A.R. Baker, and W. Sachse, *Determination of all elastic constants of orthotropic plate specimens from group velocity Data*, Res. Nondestr. Eval, 7, 1995:13-29

[90] Kim, K.Y., R. Sribar, and W. Sachse, *Analytical and optimization procedures for determination of all elastic constants of anisotropic solids from group velocity data measured in symmetry planes*, J. Appl. Phys., **77**(11), 1995:5589-5600

[91] Every, A.G., *Determination of the elastic constants of anisotropic solids*, NDT & E International, **27**(1), 1994:3-10

[92] Veidt, M. and W. Sachse, *Ultrasonic evaluation of thin, fiber-reinforced laminates*, J. Composite Materials, **28**(4), 1994:329-342

[93] Veidt, M. and W. Sachse, *Ultrasonic point-source/point-receiver measurements in thin specimens*, J. Acoust. Soc. Am., **96**(4), 1994:2318-2326

[94] Levesque, D., N. Legros, and A. Ajii, *Ultrasonic determination of mechanical moduli of oriented semi-crystalline polymer*, Polymer Engineering & Science, **37**(11), 1997:1833-1844

[95] Minachi, A., D.K. Hsu, and R.B. Thompson, *Single-sided determination of elastic constants of thick composites using acousto-ultrasonic technique*, J. Acoust. Soc. Am., **96**(1), 1994:353-362

[96] Hosten, B., M. Deschamps, and B.R. Tittmann, *Inhomogeneous wave generation and propagation in lossy anisotropic solids. Application to the characterization of viscoelastic composite materials*, J. Acoust. Soc. Am., **82**(5), 1987:1763-1770

[97] Baudouin, S. and B. Hosten, *Immersion ultrasonic method to measure elastic constants and anisotropic attenuation in polymer-matrix and fiber-reinforced composite materials*, Ultrasonics, **34**, 1996:379-382

[98] Rose, J.L., J.J. Ditti, Y. Huang, D.P. Dandekar, and S. Chin, *One-sided ultrasonic inspection technique for the elastic constant determination of advanced anisotropic materials*, J. Nondestructive Evaluation, **10**(4), 1991:159-166

[99] Kushibiki, J.I. and N. Chubachi, *Material characterization by line-focus-beam acoustic microscope*, IEEE Trans. Sonics. Ultrasonics, **SU-32**(2), 1985:189-212

[100] Xiang, D., N.N. Hsu, and G.V. Blessing, *The design, construction and application of a large aperture lens-less line-focus PVDF transducer*, Ultrasonics, **34**, 1996:641-647

[101] Chan, K.H. and H.L. Bertoni, *Ray representation of longitudinal waves in acoustic microscopy*, IEEE Trans. Ultrason. Ferroelect. Freq. Cont., **38**(1), 1991:27

[102] Williams, J.H.Jr., H. Nayeb-Hashemi, and S.S. Lee, *Ultrasonic attenuation and velocity in AS/3501-6 graphite fiber composite*, J. Nondestructive Evaluation, **1**(2), 1980:137-148

[103] Williams, J.H.Jr., S.S. Lee, and H. Nayeb-Hashemi, *Ultrasonic wave propagation loss factor in composite in terms of constituent properties*, J. Nondestructive Evaluation, **1**(3), 1980:191-199

[104] Fecko, D.L, K.V. Steiner, and J.W. Gillespie, Jr., *Attenuation of ultrasonic energy in composite materials due to scattering*, Review of Progress QNDE, **13**, Thompson, D.O. and D.E. Chimenti, (eds.), Plenum Press, New York, 1994:1189-1195

[105] Huang, H.A., C.E. Bakis, and H.T. Hahn, *Prediction of ultrasonic wave attenuation in fiber reinforced composite laminates*, in Review of Progress in QNDE, 13, Thompson, D.O. and D.E.Chimenti, Plenum Press, New York, 1994:1181-1188

[106] Lhermitte, T.D., S.M. Handley, M.R. Holland, and J.G. Miller, *Anisotropy of the frequency-dependent ultrasonic attenuation in unidirectional graphite/epoxy composite material*, Proc. 1991 IEEE Ultrasonics Symposium, Lake Buena Vista, FL, 1991:819-823

[107] Muratore, J.F. and H.R. Carleton, *Phase spectroscopy in loss media*, Proc. 1985 IEEE Ultrasonics Symposium, San Francisco, CA, 1985:1047-1051

[108] O'Donnell, M., E.T. Jaynes, and J.G. Miller, *General relationships between ultrasonic attenuation and dispersion,* J. Acoust. Soc. Am., **63**(6), 1978:1935-1937

[109] O'Donnell, M., E.T. Jaynes, and J.G. Miller, *Kramers-Kronig relationship between ultrasonic attenuation and phase velocity*, J. Acoust. Soc. Am., **69**(3), 1981:696-701

[110] Hercules® Carbon Prepreg Tape AS4/3501-6 Product Data Sheet (No.843-3), Hercules Inc., Magna, UT

[111] McCarvill, W., Personal Communication, Hercules Inc., Magna, UT, 1996

[112] White, S.R. and H.T. Hahn, *Cure cycle optimization for the reduction of processing-induced residual stresses in composite materials*, J. Composite Materials, **27**(14), 1993:1352-1377

[113] Operator's Manual of DSC Analysis, TA Instruments, Inc., New Castle, DE

[114] J.D. Ferry, Viscoelastic Properties of Polymers, (3rd edition), John Wiley & Sons, Inc., New York, 1980

[115] DMA Time-Temperature Superposition Data Analysis Program, Operator's Manual (Ver.4.0), TA Instruments, Inc., New Castle, DE, 1993

[116] Auld, B.A., Acoustic Fields and Waves in Solids, John Wiley & Sons, New York, 1973

[117] Lee, S., M. Plamondon and P.C. Gaudert, *The effect of elevated temperature spikes on the mechanical properties of carbon fiber epoxy composites*, 38th International SAMPE Sym., 1993:1582-1593

[118] Jeong, H. and D.K. Hsu, *Experimental analysis of porosity-induced ultrasonic attenuation and velocity change in carbon composites*, Ultrasonics, **33**(3), 1995:195-203

[119] Pialucha, T., C.C.H. Guyott, and P. Cawley, *Amplitude spectrum method for the measurement of phase velocity*, Ultrasonics, **27**, 1989:270-279

[120] Krautkramer, J. and H. Krautkramer, Ultrasonic Testing of Materials, 4th ed., Springer-Verlag, Berlin, 1990

[121] Rogers, P.H. and A.L.Van Buren, *An exact expression for the Lommel diffraction correction integral*, J. Acoust. Soc. Am., **55**(4), 1974:724-728

[122] Butter, C.D. and G.B. Hocker, *Fiber optics strain gauge*, Applied Optics, **17**(18), 1978:2867-2869

[123] Belleville, C. and G. Duplain, *White-light interferometric multimode fiber-optic strain sensor*, Optics Letters, **18**, 1993:78-80

[124] Hahn, H.T. and N.J. Pagano, *Curing stresses in composite laminates*, J. Composite Materials, **9**, 1975:91-107

[125] Wang, T.-M., I.M. Daniel and J.T. Gotro, *Thermoviscoelastic analysis of residual stresses and warpage in composite laminates*, J. Composite Materials, **26**(6), 1992:883-899

[126] Kim, Y.K. and S.R. White, *Process-induced stress relaxation analysis of AS4/3501-6 laminates*, J. Reinforced Plastics & Composites, **16**(1), 1997:2-16

[127] Lawrence, C.M., D.V. Nelson, T.E. Bennett and J.R. Spingarn, *Determination of process-induced residual stress in composite materials using embedded fiber optic sensors*, to be published, 1998

[128] Belleville, C., FISO Technologies, Inc., Private Communication, May, 1997

[129] Faupel, J.H and F.E. Fisher, Engineering Design, 2nd ed., John Wiley & Sons, Inc., New York, 1981:897

[130] Crasto, A.S. and R.Y. Kim, *On determination of residual stress in fiber-reinforced thermoset composites*, J. Reinforced Plastics & Composites, **12**(5), 1993.:545-558

[131] Winfree, W.P., *Ultrasonic characterization of change in viscoelastic properties of epoxy during cure*, Proc. 1983 IEEE Ultrasonic Symposium, Atlanta, GA, 1983:866-869

[132] Cohen-Tenoudji, F., W.J. Pardee, B.R. Tittmann, L.A. Ahlberg, and R.K. Elsley, *A shear wave rheology sensor*, IEEE Transactions on Ultrasonics, Ferroelectrics, and Frequency Control, **UFFC-34**(2), 1987:263-269